AN INVESTIGATION OF THE DRYING PROCESS IN PICKERING FOAMS

by

OMER S. ALABIDALKREEM

A dissertation submitted to the

School of Graduate Studies

Rutgers, The State University of New Jersey

In partial fulfillment of the requirements

For the degree of

Doctor Philosophy

Graduate Program in Mechanical and Aerospace Engineering

Written under the direction of

Dr. Shahab Shojaei-Zadeh

And approved by

_____

_____

_____

_____

New Brunswick, New Jersey
May, 2018

ABSTRACT OF THE DISSERATATION

An Investigation of the Drying Process in Pickering Foams

By OMER S. ALABIDALKREEM

Dissertation Director:

Dr. Shahab Shojaei-Zadeh

Pickering foams, aqueous foams stabilized by solid particles, can be used as a precursor to fabricate solid porous polymers, ceramics, and composite materials. The fabrication process usually comprises of two subsequent steps of drying and solidification (*e.g.* sintering) after foam is prepared. Drying (or aging) in aqueous Pickering foams is a complex transport process which involves evaporation and drainage (induced by gravity) of the excess liquid along with deformation of the foam and possible formation of cracks caused by capillary-induced stresses. Crack formation is therefore depended on the drying conditions and the mechanical properties of sample. A comprehensive understanding of the drying process can provide us with predictive tools to select efficient process parameters (*e.g.* required drying time prior to sintering) as well as providing input prameters for developing numerical models.

In this thesis, we first provide experimental data (end of drying time, average moisture content, and effective moisture diffusivity) on drying of Pickering foams stabilized by polymer particles under controlled conditions (*i.e.* relative humidity and

temperature). Drying curves are presented for samples of various initial thicknesses and shapes on substrates of different hydrophobicity and temperatures. Moisture transport is represented via calculating the effective moisture diffusivity coefficients using *method of slope*. Also, we investigate drying for a bi-component Pickering foam prepared using Multi-walled Carbon Nanotubes (MWCNTs) and polymer particles. We show that the effective moisture diffusivity increases as the average moisture content decreases for all trials and that all data can be collapsed on a *master curve*. Also, effective moisture diffusivity increased as initial sample thickness as well as substrate temperature increase. On the other hand, effective moisture diffusivity does not depend strongly on the sample shape and MWCNTs concentration.

In next part, we explore the effect of initial sample thickness and shape, substrate temperature and wettability, as well as MWCNTs concentration on the crack formations in the samples. We demonstrate that substrate wettability, initial sample thickness, and MWCNTs concentration have a strong influence on the formation and propagation of cracks. We found that decreasing the wettability of the substrate reduces crack formation. Also, increasing the initial sample thickness reduces crack formation. On the contrary, increasing the MWCNTs concentration increases crack formation for all types of substrates. We demonstrate that substrate temperature and sample shape do not seem to influence crack formation but these parameters influence the crack patterns. Such information can be beneficial in using these foams as a precursor to fabricate porous composite porous materials.

Acknowledgments

Praise is to Allah for everything.

At the beginning I would like to thank God for his great help and guidance.

I am very grateful to my advisor Dr. Shahab Shojaei-Zadeh for his continuous encouragement, generous efforts, and valuable supervision. Also, I want to thank my thesis committee members, Dr. Nina Shapley, Dr. Kimberly Cook Chennault, and Dr. German Drazer for the time they spent to review my thesis.

Many thank go to John Petrowski and Paul Pickard for their help to complete the setup.

I would like to take sincerely this opportunity to thank my parents for their support, prayer and encouragement to overcome the difficulties in my work. Also, I would like to thank my brothers, my sisters, and my kids. Also, I would like to thank my wife, Zenaa Gader for her love and her encouragement and endurance through these challenging time. If it wasn't because of her presence, I would have never been able to take this long journey and accomplish this degree.

Finally, my special thanks to my lab-mates and my friends for their always help: Isabel Liberis, Abhay Srinivas, David Cunningham, Rick Schieni, Hassan Alsaraj, Mustafa Mozael, and Arab Hammadi.

Without the financial support of the College of Engineering, University of Mosul, Mosul, Ninawa, Iraq, this work never have been started.

Omer S. Alabidalkreem
Mechanical and Aerospace Engineering
Rutgers, The State University of New Jersey
April 11, 2018

Table of Contents

List of Illustrations

Chapter 1

Introduction

1.1 Overview

1.1.1 Pickering Foams

Fine solid particles with proper size and hydrophobicity are known to irreversibly adsorb at liquid/fluid interfaces (*i.e.* being surface active) [1-10]. Similar to surfactants (or surface active agents) molecules, such solid particles can stabilize interfaces forming particle-stabilized (aka Pickering) liquid/gas foams or liquid/liquid emulsions as shown in Figure 1. 1.

When adsorbed, the required energy needed to remove a particle (*or* molecule) from the interface, known as the *detachment energy*, is significantly higher than the thermal energy *"kT"* which explains their irreversible adsorption unlike the fast adsorption/desorption dynamics of surfactant molecules of similar size. The detachment energy of surfactant can be *1-3 kT*, while for solid particle the detachment energy can be 10^3-10^5 *kT*, where k is the *Boltzmann constant* (k = 1.38064852×10^{-23} J/K) and T is the temperature (K), [1, 8, 11].

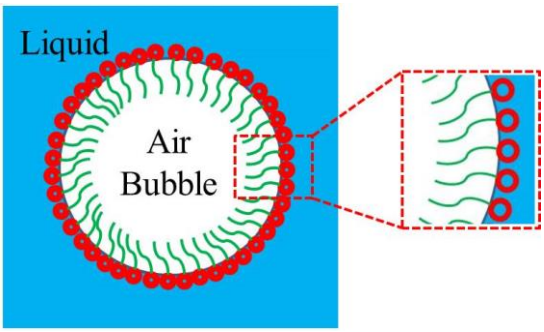

(a)

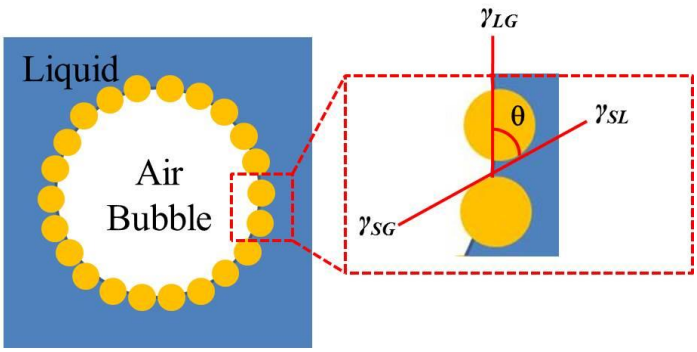

(b)

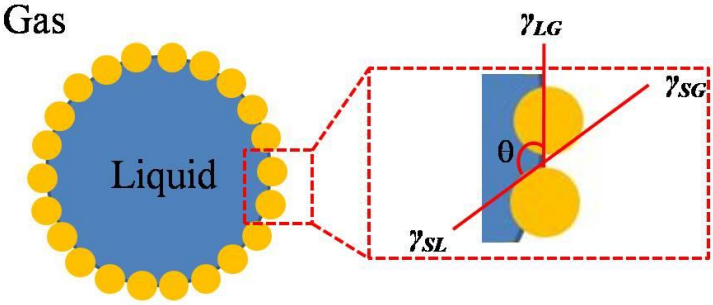

(c)

Figure 1. 1 (a) Surfactants (molecule contains hydrophilic head (polar) and hydrophobic tail (non-polar)) at a liquid-gas interface, **(b)** colloidal particles at a liquid-gas interface with $0 < \theta < 90$) (Pickering foams), and **(c)** colloidal particles at a liquid-gas interface with $90 < \theta < 180$ (Liquid marbles). These figures are not drawn to scale.

The detachment energy for a spherical particle at flat liquid/fluid interface can be calculated as [12]:

$$\Delta G_{particle} = \pi r^2 \gamma_{LG}(1 - cos\theta) \quad (1.\ 1)$$

where;

$$cos\theta = \frac{\gamma_{SG} - \gamma_{SL}}{\gamma_{LG}} \quad (1.\ 2)$$

here $\Delta G_{particle}$ is the detachment energy required to remove a particle from the interface, r is the radius of particle, γ_{LG} is the interfacial tension between the gas and liquid, γ_{SG} is the interfacial tension between the solid and gas, γ_{SL} is the interfacial tension between the solid and liquid, and θ is the particle three phase contact angle at the solid-liquid-gas interface (see Figure 1. 1).

The detachment energy is scaled with square of the particle radius, bigger particle provide higher detachment energy, while smaller particles provide foams with stronger stability, more nanoparticles adsorbe at the liquid/fluid interface [2, 7, 13]. To get higher value of detachment energy, the contact angle of solid particle should be near $90°$, see equation (1. 1). The contact angle of colloidal particles at a liquid/gas interface is too important to create a Pickering foams system. If contact angle is greater than $90°$ then the air will be around the liquid (*i.e.* Liquid marbles), the particles encapsulated the liquid. On the contrary, if contact angle is less than $90°$, then the liquid will be around the gas (*i.e.* Pickering foams), the particles encapsulated the air (see Figure 1. 1).

Based on the previous information, to prepare Pickering foams system, the contact angle of colloidal particles should be between 0° and 90°, hydrophilic powder (or colloidal particles) [14-17].

Owing to the high detachment energy, particles can decorate bubble interfaces in foams (or droplets in emulsions) and slow down the mechanisms that make Pickering systems *unstable* such as gravity-induced liquid *drainage* and bubble-bubble *coalescence* and *disproportionation* (Ostwald ripening) [18-20]. A stable Pickering foams system (see Figure 1. 2) can be then further processed, by a combination of drying and solidification, to make solid porous structures (or solid composite porous structure) with tunable morphology and properties. Of interest in this regard is then to develop a comprehensive understanding on how particle-stabilized foams undergo drying.

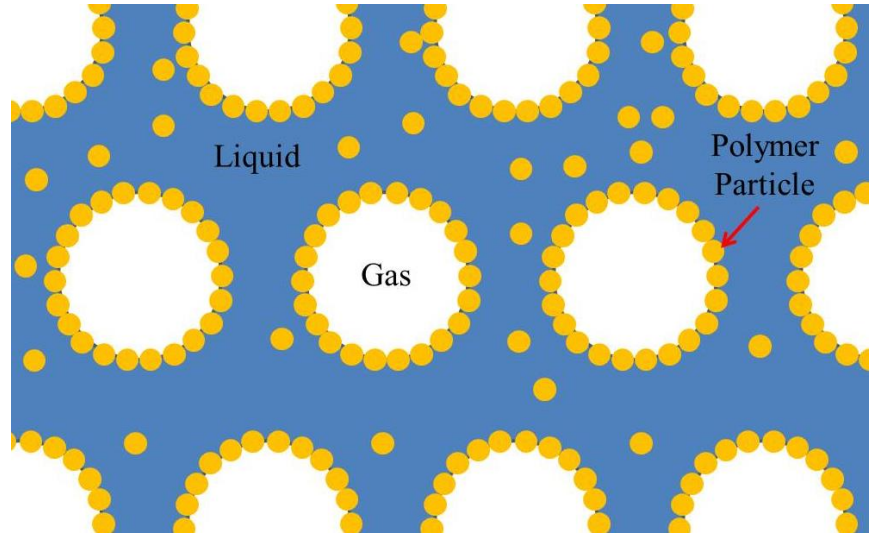

(a)

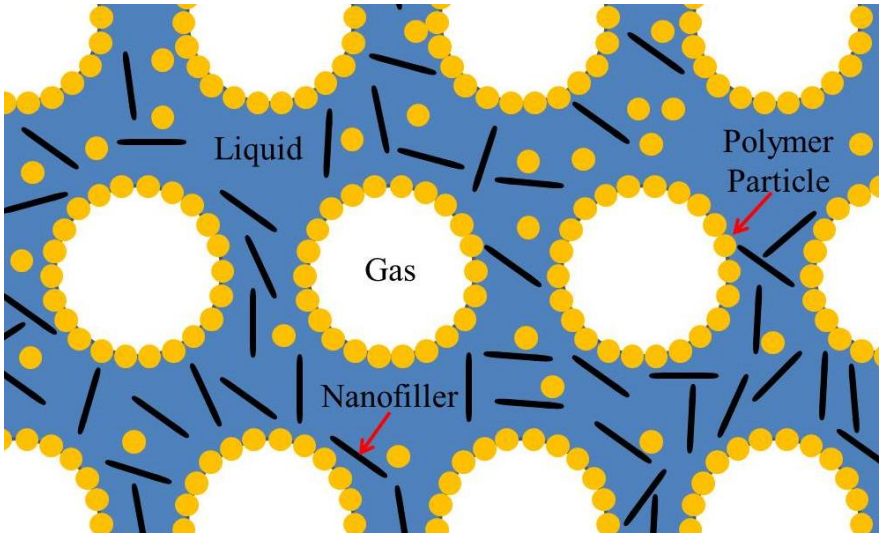

(b)

Figure 1. 2 Pickering foams stabilized by polymer particles **(a)** without Multi-walled Carbon Nanotubes and **(b)** with Multi-walled Carbon Nanotubes. These figures are not drawn to scale.

1.1.2 Drying Dynamics

Drying is a complex and dynamic transport process, where the liquid inside the wet foam leaves through a combination of surface evaporation (induced by diffusion) and drainage (induced by gravity), causing the foam to undergo dimensional reduction (*i.e.* shrinkage) as shown in Figure 1. 3. Also, liquid evaporation leads to morphology change (*i.e.* porosity) due to the capillary stress that occurs between the particles [3, 6, 9, 21-23].

One of the common transport properties used to describe the drying process in wet porous materials (*e.g.* Pickering foams) is effective moisture diffusivity. The effective moisture diffusivity includes moisture gradient (caused by evaporation and drainage), temperature gradient (change in sample temperature during drying), and porosity gradient (change in sample volume) [24-33].

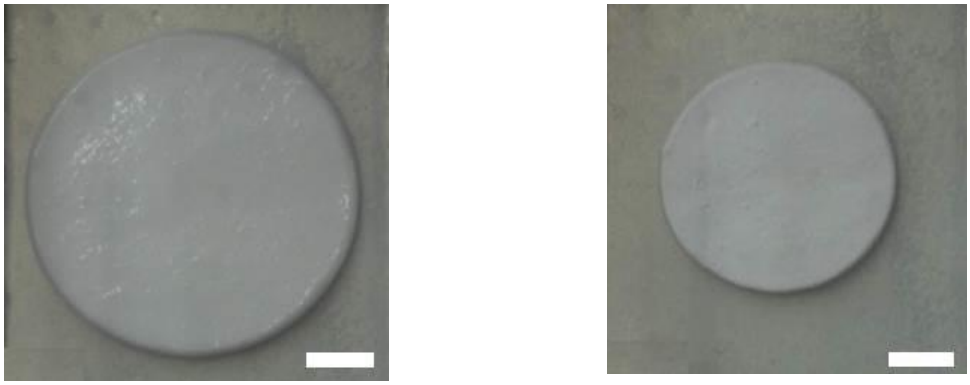

(a) **(b)**

Figure 1. 3 (a) An as-prepared wet foams and **(b)** crack-free dried foams. Scale bar is 10 mm.

The moisture transport can be described by the *Fick's second law* equation of unsteady state diffusion, which for the case of drying relates the spatial and temporal changes of the moisture content X (kg liquid/ kg dry solid) via moisture-dependent diffusivity D_{eff} (m^2/s) [34]. The diffusivity can be estimated by analysis of the drying data and applying the *method of slope* [35-39]. This method is described in more details in chapter three and we utilize it in this thesis to calculate the effective moisture diffusivity (D_{eff}) of the drying Pickering foams. As mentioned, change in sample volume due to shrinkage influences moisture diffusivity and should be included in calculation of effective moisture diffusivity. However, this may be neglected for certain conditions [40-46]. In this study, we first neglected and then included effect of samples shrinkage when calculating the effective moisture diffusivity and evaluate the appropriateness of each approach in certain situations.

Theoretical prediction of moisture diffusivity in such a complex system is not straight forward thus arising need for experimental measurements including the analysis of the drying data (*i.e.* moisture vs. time), and *X-ray* computed tomography to determine the sorption kinetics [47, 48]. In this thesis, we investigate the drying dynamics of Pickering foams and report the influence of several control parameters such as substrate wettability (*i.e.* contact angle), substrate temperature (*i.e.* drying rate), initial foams thickness, foams shape, and Multi-walled Carbon Nanotubes concentration (C_{MWCNTs}) in the foams on end of drying, change in dimensions, average moisture content, and effective moisture diffusivity of the samples.

1.1.3 Crack Formation

Pickering foams whose intrinsic phase properties are affected by the formation of cracks, cracked foam has a much different set to regular un-cracked foam. Because fractures compromise the integrity of porous materials, the cracking phenomenon can invite failure of devices or products (see Figure 1. 4).

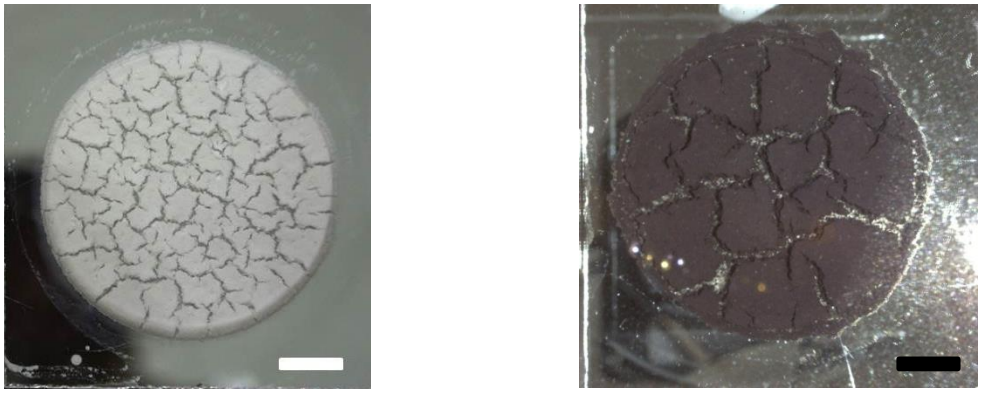

(a) **(b)**

Figure 1. 4 Crack formation in Pickering foams during the drying processes **(a)** dried PVDF foams and **(b)** dried PVDF/MWCNTs composite foams. Scale bar is 10 mm.

Accordingly, several trials and investigations have been conducted by researchers in the past to gather more information about crack formation on Pickering foams but very limited studies try to solve this challenging problem [6, 49, 50]. Moreover, the shrinkage maybe accompanied by cracks (or defects) formation which may render the structure unusable. Therefore, developing strategies to predict and control the drying as well as preventing crack formation and propagation seems to be necessary for successful fabrication of solid porous structures (or composite solid porous structure) using particle-

stabilized foams as precursor. It is worth noting that drying (*i.e.* aging) and crack formation are also relevant in other system such as in drying of particulate suspensions, gel, building materials (*e.g.* porous bricks and wood), pharmaceutical manufacturing (*e.g.* foam drying of vaccines), and in drying of food products and significant efforts have been placed to study such systems [51-59].

Common approaches proposed to obtain dry, crack-free structures in such systems include slow drying under controlled conditions (*e.g.* relative humidity, air velocity, pressure, and temperature), unidirectional drying, freezing drying, drying by chemical additives, and drying on superhydrophobic as well as flexible substrates [60-70].

In this thesis, we elimenated crack formation in Pickering foams by using low-adhesion substrates with high contact angles (*i.e.* superhydrophobic substrate), as well as large initial sample thickness both of which have been found to reduce the formation of cracks. Also, for samples located on glass substrate, we found that the probability of samples cracking depends strongly on the drying rate or substrate temperature (it decreases as substrate temperature increases, but the crack still occurs). On the contrary, this does not deppen for samples on PDMS substrates. In addition, as MWCNTs concentration in the composite Pickering foams increases the formation of cracks increases for the all types of substrates.

1.2 Scope of the Present Work

Overall, the aims of this work can be stated as follows:

(1) Determining the drying curves and the change in sample dimensions of Pickering foams under different drying conditions such as varying substrate wettability (*i.e.* contact angle) and temperature, sample shape and initial thickness, as well as concentration of MWCNTs. Three different substrates were used: hydrophilic glass with a contact angle (measured through DI-water) of $\theta \approx 30°$, hydrophobic poly(dimethylsiloxane) (PDMS) with $\theta \approx 95°$, and superhydrophobic modified glass with $\theta \approx 160°$. Also, five different temperatures were selected $T = 24, 30, 40, 50,$ and $60\ ℃$. In addition, three shapes of samples were examined (circle, square, and equilateral triangle). For circular case, samples with initial thicknesses of $Z_0 = 2.5, 3.25, 5, 7.5, 10,$ and $12.5\ mm$ and initial diameter of $D_0 = 34$ and $52\ mm$ were considered. For square shape, samples with initial thicknesses of $Z_0 = 5\ mm$ and initial *length* of $L_0 = 30.13\ mm$ is selected. For equilateral triangle case, samples with initial thicknesses of $Z_0 = 5\ mm$, initial height of $H_0 = 39.66\ mm$, and initial base of $B_0 = 45.79\ mm$ is selected. The concentration of MWCNTs varied between $0 – 0.5\ \%\ v/v$.

(2) Estimating the change in Pickering foams characterization such as porosity, volume, and density (bulk density and relative density) during drying.

(3) Calculting the effective moisture diffusivity of Pickering foams under all drying conditions by using the drying curves. *Method of slope* is employed to estimate the effective moisture diffusivity. Two approaches were used to determine the

effective moisture diffusivity. In the first approach, the effect of sample shrinkage is neglected while sample shrinkage is included in the second approach.

(4) Investegating the influence of all drying conditions on the probability of crack formation and pattern of Pickering foams during the drying processe.

1.3 Outline

In what follows, in chapter two, we first describe the material and methods used to conduct the experiments. Then, drying curves and change in samples dimension as well as sample characterization under all drying conditions are presented. The theoretical description to calculate the effective diffusivity is discussed in chapter three. In chapter four, the effect of drying conditions such as substrate wettability and temperature, initial sample thickness, sample shape, as well as MWCNTs concentration on crack formation in samples is discussed in detailes. Finally, the conclusion of all results and the future work are presented in chapter five.

Chapter 2

Drying Kinetics

2.1 Introduction

Drying of porous materials (or composite porous material) is an important subject both from engineering and fundamental point of views. One such system is foams stabilized by solid particles (*i.e.* Pickering foams). An understanding of drying process in Pickering foams will provide information on fabrication of solid porous materials (or composite solid porous material) using such foams as precursor. Several recent studies have been conducted on drying of Pickering foams. Lesov *et al.* studied the change in Pickering foams size during drying process. They clarified the mechanism of shrinkage of Pickering foams and he described the quantitatively the relation between the properties of foams suspension and the dry porous materials obtained from this suspensions [22]. In other work, Lesov *et al.* investigated the effect of foams porosity (air fraction) on the probability of cracking during drying processes [6]. Wong *et al.* investigate the effect of particles size, concentration, and wettability on the manufacture of Pickering foams. Where, macroporous materials with porosities between 33 and 95% and median pore sizes between 13 and 634 μm were obtained [10]. Rezvantalab *et. al.* demonstrate the fabrication of composite solid porous materials based on foaming of aqueous desperation of suspension particles and Multi-walled Carbon Nanotubes with varies concentration. They study the mechanical, morphological, as well as thermal and electrical transport

properties of the fabric (*i.e.* PVDF/MWCNTs porous composite). They found that the concentration of Multi-walled Carbon Nanotubes results in changing in the characterization of the dry composite foams [71].

Here, we are investigating drying kinetics by focusing on parameters such as end of drying, drying rate, average moisture content, and effective moisture diffusivity. Also, the change in foams dimensions, density, and porosity during drying process is explained.

In this work, natural convection was used to remove liquid via evaporation and drainage from wet Pickering foams. The drying process involves the application of heat to materials; the heat is transferred from the surroundings to the surface of the sample or it can transfer from substrate to the samples (*e.g.* heating from below). As a result of the applied heat, liquid leaves the sample to the surroundings via evaporation.

Fundamental Questions

(1) What is the effect of substrate wettability and temperature on the drying kinetices?

(2) What is the influence of sample shape and thickness as well as MWCNTs concentration on the drying kinetics?

(3) How is foam characterization change during drying under different drying conditions?

2.2 Materials and Methods

In this section, the materials used in this work are presented. Also, the method of preparing the Pickering foams (or composite Pickering foams) as well as the description of the experimental setup is explained with details.

2.2.1 Materials

We use commercially available poly(vinylidene fluoride) (PVDF) nanoparticles (Polysciences Inc.) with the primary particle size of $D_{50} = 250 \pm 30\ nm$ and a contact angle of $\sim 90°$, density of $1.76\ g/cm^3$, and melting point of $\sim 160\ °C$. The contact angle of the PVDF is close to the value that gives maximum detachment energy to the particles adsorbing at liquid/gas interfaces (*i.e.* $\theta \approx 90°$), see equation (1. 1). Also, we used Multi-walled Carbon Nanotubes (Sigma-Aldrich) as nanofillers. The average outer diameter of the MWCNTs is around *10 - 20 nm* and length of 5-9 μm.

Ethanol was added to lower the surface tension and facilitate foaming and adsorption of particles at liquid/gas (bubble) interfaces. Previous studies have demonstrated that *9 v/v %* aqueous ethanol solutions maybe used to produce stable PVDF foams, on the one hand and to reduce the three-phase contact angle of the solid particle to around *70°*, on the other hand [10, 23].

2.2.2 Methods

Beforehand, mold and substrate were hand cleaned by using DI-water then ethanol after that compressed nitrogen was applied to dry them. Details of the foam production process is described elsewhere [71]. Briefly, aqueous foams are prepared through direct foaming of PVDF and liquid (Deionized water and ethanol) suspensions. A specified mass of PVDF (*4 v/v %*) is added to a test tube along with adequate amount of ethanol (*9 v/v %*) and DI water (Millipore) and the mixture is sonicated for *one minute* with a probe sonicator (Qsonica, Q500) to uniformly disperse the particles in the suspension. The test tube was then capped and vigorously hand shaken for *five minutes* to foam the suspension. The resulting aqueous foam was then scooped into molds and the top surface was shaved with a blade to ensure constant volume across all trials.

In the case of composite foams (*i.e.* MWCNTs/PVDF), composite foams are prepared through direct foaming of PVDF and suspension of MWCNTs (Deionized water, MWCNTs and ethanol). A specified mass of MWCNTs with different concentrations (C_{MWCNTs} *= 0, 0.1, 0.3, and 0.5 v/v %*) is added to a test tube along with DI water and the mixture is sonicated for *two minutes* with a probe sonicator to uniformly disperse the MWCNTs in the suspension. Then, a specific amount of ethanol (*9 v/v %*) is added to the suspension and the suspension is hand shaken for *half minute*. Next, a specified mass of PVDF (*4 v/v %*) is added to the suspension and the mixture is sonicated again for *two minutes*. The test tube was then capped and vigorously hand shaken for *five minutes* to foam the suspension.

Three molds with different shapes are used:

(1) Circle.

(2) Square.

(3) Triangle (equilateral).

In the case of circle shape, the molds are cut from poly(vinylchloride) (PVC) tubes, forming rings with two different inner diameter of *52* and 34varying thickness of *2.5, 3.25, 5, 7.5, 10,* and *12.5 mm.*

In the case of square shape, the molds are cut from plastic sheet (Acrylic) using laser cutter, forming molds with inner dimension length of *30.13 mm* and thickness of *5 mm*.

In the case of triangle (equilateral) shape, the mold are cut also from plastic (Acrylic) sheet using laser cutter, forming molds with inner dimension of base of *45.79 mm,* height of *39.66 mm,* and thickness of *5 mm*.

Three substrates with different wettability are used:

(1) Hydrophilic glass substrate with contact angle of $\theta \approx 30^{\circ}$;

(2) Hydrophobic polydimethylsiloxane (PDMS) substrate with $\theta \approx 95^{\circ}$;

(3) Superhydrophobic modified glass substrate with $\theta \approx 160^{\circ}$.

The contact angles of all the substrates are measured using an in-house goniometer as shown in Figure 2. 1.

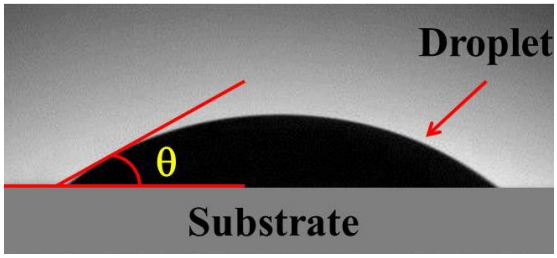

(a)

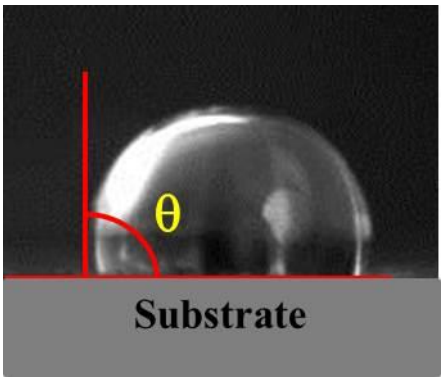

(b)

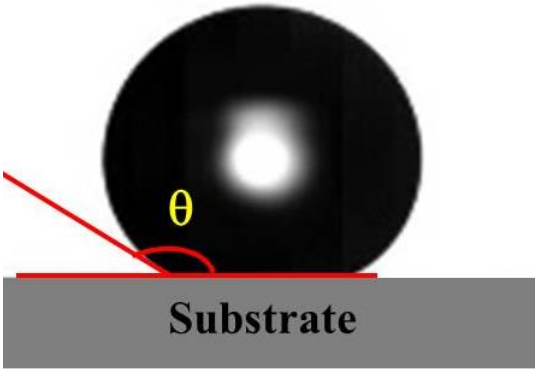

(c)

Figure 2. 1 Contact angle (θ) between droplet (DI-Water) and substrate at: **(a)** glass (hydrophilic with $\theta \approx 30°$), **(b)** PDMS (hydrophobic with $\theta \approx 95°$), and **(c)** modified glass (superhydrophobic with $\theta \approx 160°$).

PDMS substrates (~ *2 mm* thick) are prepared by thoroughly mixing a *10:1* ratio of silicone base (Sylgard 184, Dow Corning) to cross-linking agent and subsequent curing at *60 ℃* in an oven. Superhydrophobic substrates are prepared by spraying glass substrates with a thin non-stick coating agent (Rust-Oleum). We determined that the coated surface remains superhydrophobic for the duration of the experiments. To ensure use superhydrophobic substrate with high contact angle for each test, a new superhydrophobic substrate is used for each trial (*i.e.* used substrate is not reused for next trial)

Immediately after scooping the foam into PVC molds, they are placed on one of the substrates and the combination is placed on a digital scale (Mettler Toledo, PB303-SRS) that is confined in a transparent air-tight acrylic chamber with dimensions (*depth = 15 cm, width = 17 cm,* and *length = 18 cm*). The scale is interfaced with a data logger (RS232, Eltima) to record sample mass over time. A digital thermometer and a digital hygrometer (Inkbird) are placed near the sample to continuously record the temperature and relative humidity of the chamber.

We remove the PVC and plastic molds after short period to eliminate the effect of mold contact surface on sample shrinkage as well as crack formation. The following points shows the period for each case:

1- *One hour* for samples dried at room temperature;

2- *Half hour* for samples dried at heated substrate;

3- *Immediately* for samples of different shapes and those with PVDF/MWCNTs (*i.e.* composite porous foams).

All trials are carried out at laboratory conditions (temperature, pressure, and relative humidity).

To keep the relative humidity constant during drying, containers of silica gel are placed inside the chamber. To determine changes in dimension, top- and side-view images of samples are recorded at regular intervals using a digital camera (Infinity, Lumenera) as shown in Figure 2. 2.

When samples are completely dried, an air convection oven (Tuttlingen/Germany) was used to sintering the dried samples. The samples were placed on an aluminum plate, and then they heated gradually. The initial temperature inside the oven was *65 ℃* with *10 ℃* increments every *10 min*, till *165 ℃*. The samples were kept at this temperature (above polymers melting point) for *3 hours*, after which consolidated porous structures were formed. To reuse the used silica gel with *black color* (*i.e.* fully wet silica) for next trial, they dried using the oven at temperature of $T = 180$ ℃ for around $t = 12$ *h*. Later on, a dry silica gel with an *orange color* (*i.e.* fully dry silica) is ready to use for next trials.

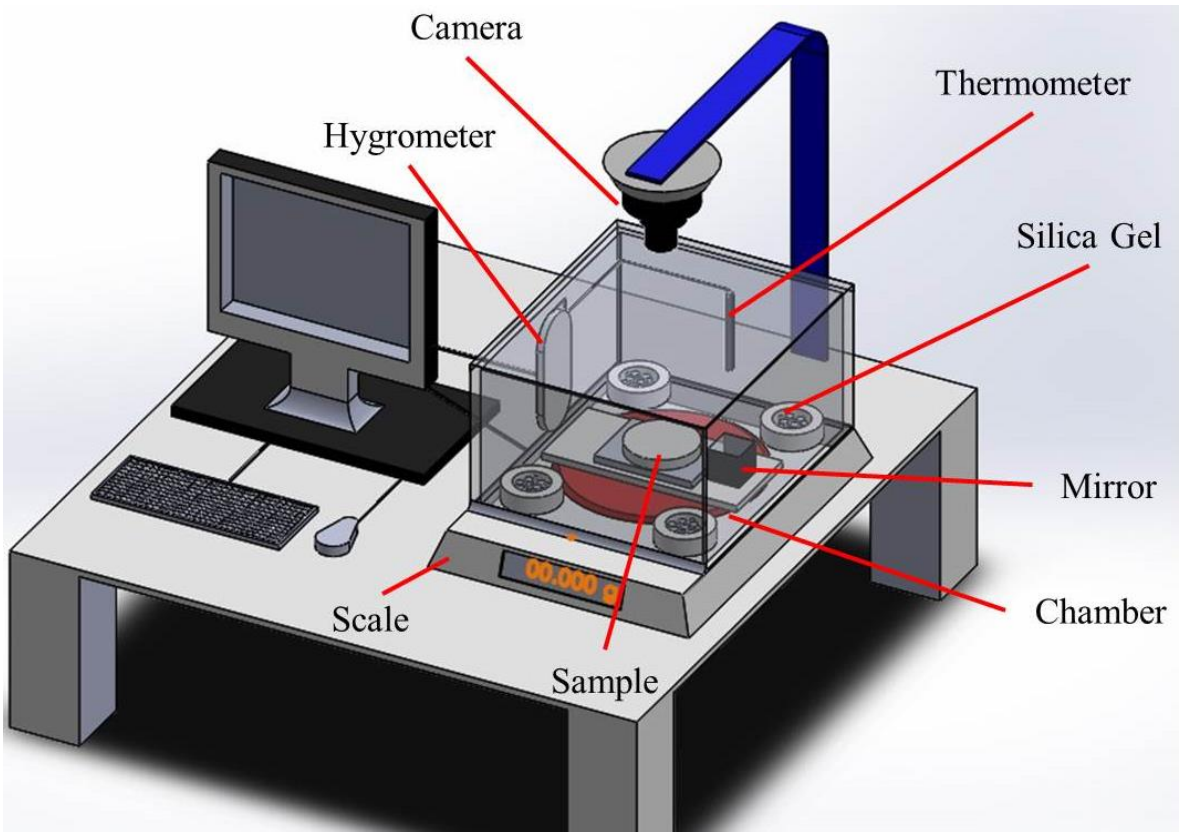

Figure 2. 2 Experimental setup.

2.3 Aging of Pickering Foams

The change in sample mass and dimensions (*i.e.* shrinkage) as well as the effect of substrate temperature and wettability, sample thickness and shape, and the effect of MWCNTs concentration on the samples are presented and discussed with details in this section.

2.3.1 Drying Curve

The change in sample mass over time is shown in Figure 2. 3 (a) for an initial foam thickness of *5 mm* and initial diameter of *52 mm* as it dries out on three different substrates ($\theta \approx 30°$, $95°$, and $160°$). As expected, the sample mass decreases as the liquid content leaves due to a combination of surface evaporation and gravity-induced drainage, eventually reaching a plateau which indicates the end of drying point (t_e) as highlighted in Figure 2. 3 (a), see appendix A to see the drying conditions over time.

The end of drying point, defined as the point after which the change in sample mass is negligible, is plotted in Figure 2. 3 (b) for samples of various initial thickness undergoing drying on three different substrates, obviously thin samples dry faster as expected. Moreover, at a fixed initial thickness, the drying takes longer on superhydrophobic substrates. This is possible due to two factors:

(1) As the substrate contact angle increases, drained liquid is forced to stay within the sample making the surface evaporation the only drying mechanism;

(2) Decreasing the wettability (*i.e.* increase the contact angle value) of the substrate results in crack-free dried samples. Formation of cracks on the other hand, maybe considered as added pathways for liquid evaporation, lack of which may

lengthening sample drying time. Crack formation is presented and discussed in chapter four.

Using the presented data, MATLAB is used to find the relationship between the end of drying time and initial sample thickness (*i.e.* curve fitting) for un-cracked samples with initial thickness of $Z = 2.5 - 12.5$ and initial diameter of $D_0 = 52\ mm$ as well as substrate with $\theta \approx 160°$ (*i.e.* superhydrophobic substrate) as shown in equation (2. 1). The unit of the end of drying time (t_e) is *hour* and initial sample thickness (Z_0) is *mm*. Clearly, the end of drying time is increased linearly as initial sample thickness increases.

$$t_e = 1.97Z_0 + 7.13 \qquad (2.\ 1)$$

By employing the following equation and by using the presented data in Figure 2. 3 (a), the drying rate (*DR*) for samples over time can be estimated [26, 28, 72], see Figure 2. 4.

$$DR = \frac{m_{i+1} - m_i}{\Delta t} \qquad (2.\ 2)$$

Where, m_i is the sample mass at any time (t_i), m_{i+1} is the sample mass at $t_{i+\Delta t}$, and Δt is period of drying step.

We can see from Figure 2. 4, during the drying process for foam samples, drying rate is not depended strongly on the drying conditions such substrate wettability. Also, drying rate under different drying conditions decreased continuously as drying time increases. We can report that falling rate period is the main stage in this system (*i.e.* Pickering foams), the constant rate period is absence during the drying process in this system which usual occurs at the beginning of drying in different system [57].

.

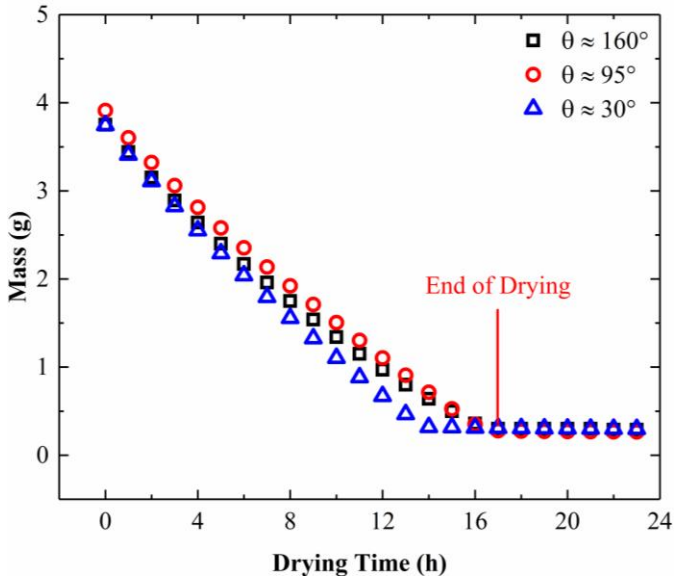

(a)

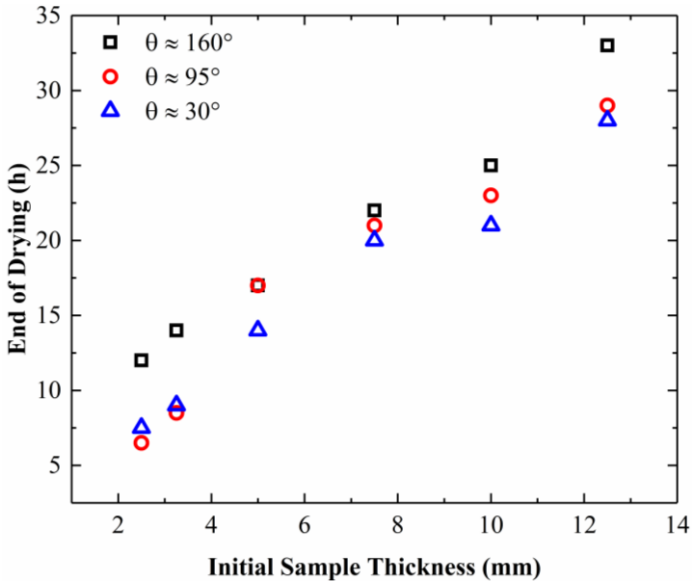

(b)

Figure 2. 3 (a) Mass change during drying for samples with initial thickness of $Z_0 = 5$ *mm* and initial diameter of $D_0 = 52$ *mm* as well as substrates with $\theta \approx 30°, 95°$, and $160°$ and **(b)** end of drying time for samples with initial thickness ranging between *2.5* and *12.5 mm* and initial diameter of $D_0 = 52$ *mm* on three different types of substrates.

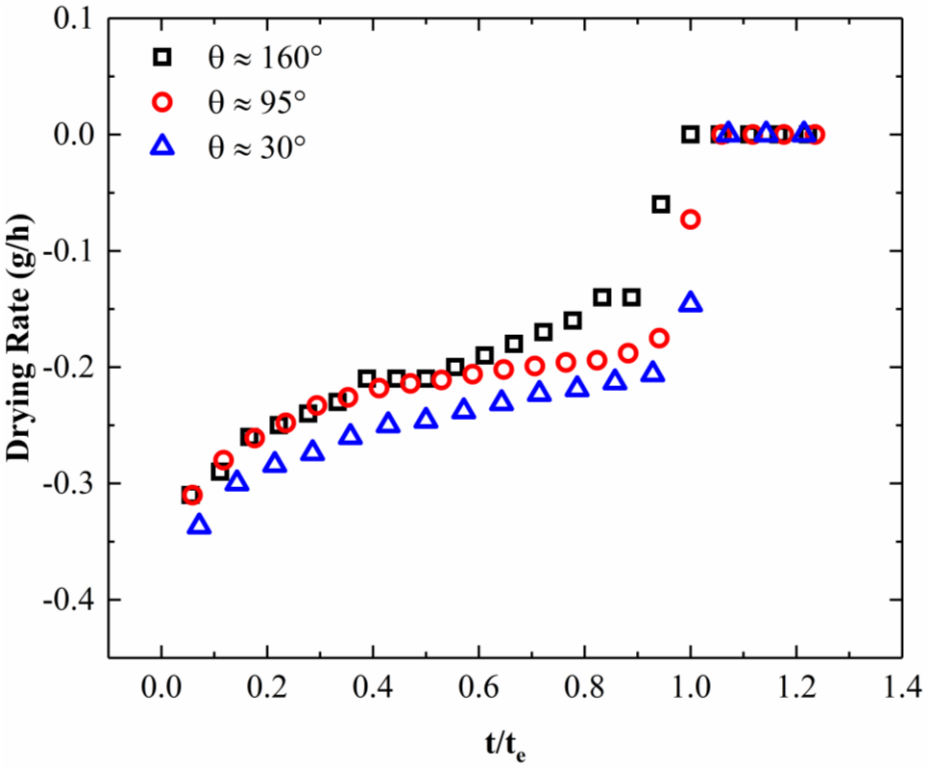

Figure 2. 4 Drying rate during drying for samples with initial thickness of $Z_0 = 5\ mm$ and initial diameter of $D_0 = 52\ mm$ as well as substrates with $\theta \approx 30°, 95°$, and $160°$. t_e is the end of drying time.

2.3.2 Dimensional Variation and Shrinkage

As samples undergo drying and lose their moisture content, their dimension changes resulting in shrinkage in all directions (*i.e.* radial and vertical) as demonstrated in Figure 2. 5. Drying-induced shrinkage is caused by capillary-induced stresses and is a well-known phenomenon in drying of wet porous materials and thin coating of nano-particle suspensions [73, 74]. We notice that diameter reduction (*i.e.* shrinkage) is larger for the sample on the superhydrophobic substrate. This is because of the low adhesion between the sample and the substrate as opposed to the hydrophilic and partially hydrophobic substrates.

Assuming constant final volume for the samples, larger reduction in radial direction may translate into smaller reduction in sample thickness, see Figure 2. 5 (b), samples located on superhydrophobic substrate. This however seems not to be the case for the other two substrates which may be an indication of change in local sample porosity during aging. Shrinkage in diameter or thickness for all un-cracked samples follows two distinct slopes before reaching a constant plateau. However, two-linear slopes trend are less pronounced for the shrinkage in sample thickness.

Obviously, as initial sample thickness increase, the change in sample dimensions is closer as shown in this figure. This is due to the free crack in foams samples. In other words, the difference in the change in sample dimension is dependent strongly on the probability of crack formation during drying process.

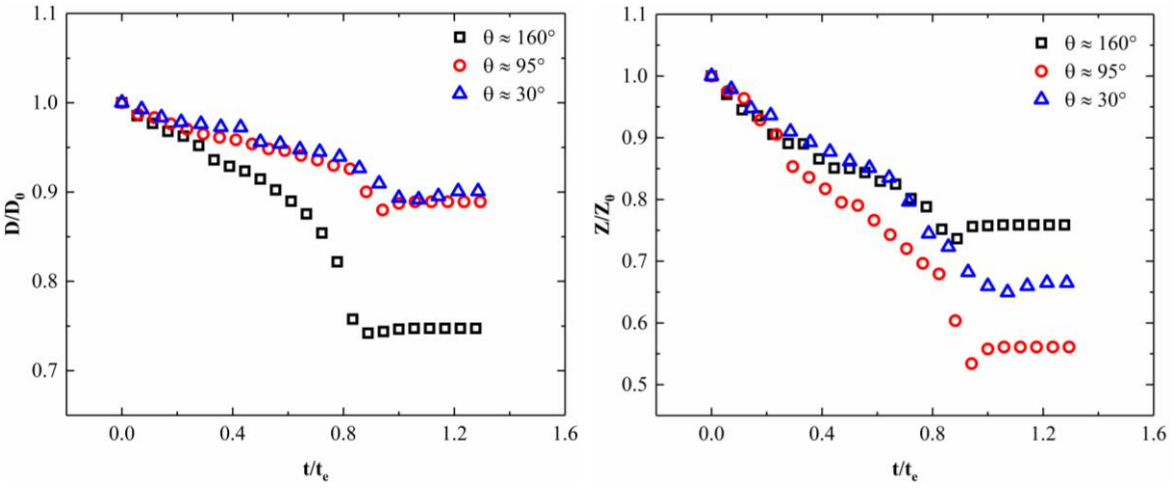

(a)

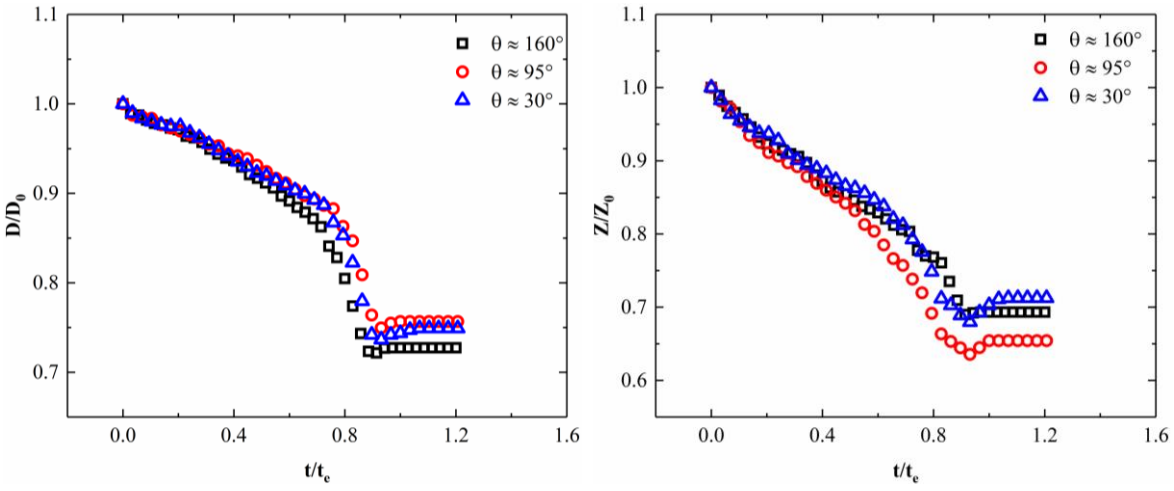

(b)

Figure 2. 5 Change in diameter and thickness during drying for samples with initial thickness of **(a)** $Z_0 = 5\ mm$ and **(b)** $Z_0 = 12.5\ mm$, and initial diameter of $D_0 = 52\ mm$ as well as substrates with $\theta \approx 30°, 95°,$ and $160°$. t_e is the end of drying time.

Figure 2. 6 shows the change in samples volume versus drying time, where V_0 is the initial foam volume and t_e is the end of drying time.

The behavior of sample in first step is discussed earlier in this section. In the next section, the increased in sample volume (*i.e.* swilling) over time is discussed in details. In the last step, the drying is stopped (*i.e.* fully dry sample) so there is no change in sample dimensions.

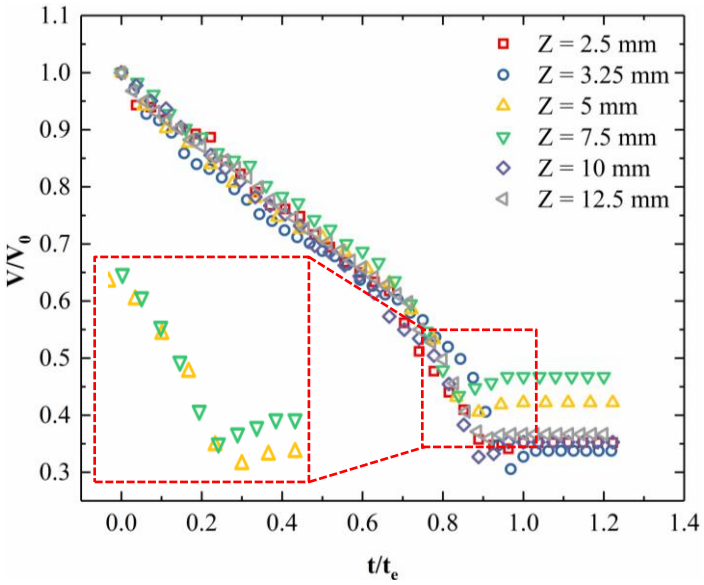

Figure 2. 6 Change in volume during drying for un-cracked samples with initial thickness ranging between *2.5* and *12.5 mm* on substrate with $\theta \approx 160°$. The curves in the box show the expansion in foams volume through the end of drying. V_0 and t_e is the initial foam volume and the end of drying time, respectively.

Using the data in Figure 2. 5, we have calculated radial shrinkage ratio as demonstrated in Figure 2. 7 (a) [22] as:

$$K_r = 100 * \left(1 - \frac{D}{D_0}\right) \qquad (2.\ 3)$$

where, K_r is the shrinkage ratio in radial direction, D is sample diameter at any time, and D_0 is the initial sample diameter. Also, the vertical shrinkage ratio using the following equation is demonstrated in Figure 2. 7 (b).

$$K_Z = 100 * \left(1 - \frac{Z}{Z_0}\right) \quad (2.\ 4)$$

where, K_Z is the shrinkage ratio in vertical direction, Z is sample thickness at any time, and Z_0 is the initial sample thickness.

The degree of sample shrinkage in both directions depended on the substrate type and initial sample thickness. Where for samples with initial thickness of $Z_0 = 5\ mm$ and initial iameter of $D_0 = 52\ mm$ on substrate with $\theta \approx 160°$ as well as $Z_0 = 12.5\ mm$ and initial iameter of $D_0 = 52\ mm$ on substrate with $\theta \approx 30° - 160°$, the vertical and horizontal shrinkage trend two slopes, the second slope is higher than the first slope. On the contrary, for sample with initial thickness of $Z_0 = 5\ mm$ and initial iameter of $D_0 = 52\ mm$ on substrate with $\theta \approx 95°$ and $30°$, the vertical and horizontal shrinkage trend one slope. The reason is the crack free in samples with $Z_0 = 5\ mm$ and initial iameter of $D_0 = 52\ mm$ on substrate with $\theta \approx 160°$ and $Z_0 = 12.5\ mm$ and initial iameter of $D_0 = 52\ mm$ on substrate with $\theta \approx 30° - 160°$. During the second slope, the capillary pressure is higher than for the first period, more details about the crack and capillary pressure is discussed in chapter four.

For all un-cracked samples, the shrinkage ratio in vertical and horizontal direction are seem equivalent. While for cracked samples, the shrinkage in vertical direction is higher than the shrinkage in vertical direction due to the crack formation. More details about the crack formation is discuused with detail in chapter four.

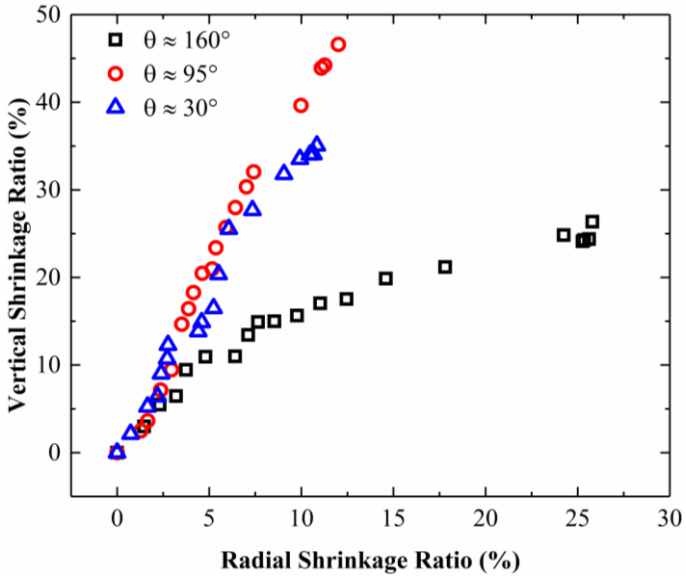

(a)

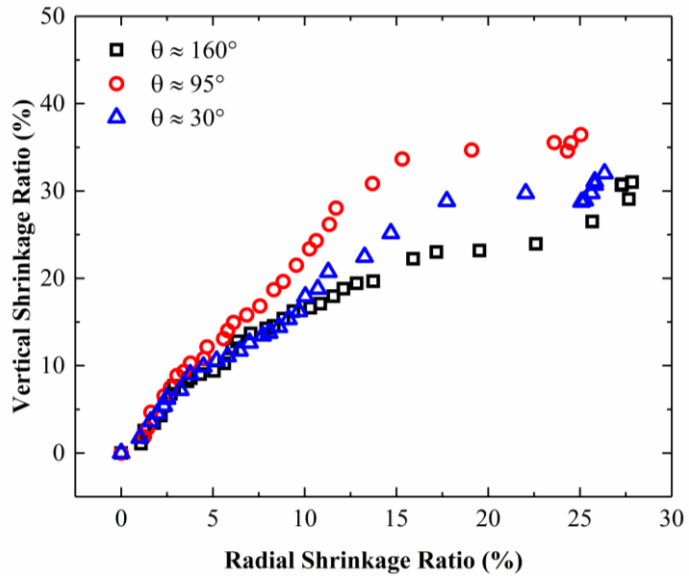

(b)

Figure 2. 7 Shrinkage ratio in diameter and thickness during drying for samples with initial thickness of **(a)** $Z_0 = 5\ mm$ and **(b)** $Z_0 = 12.5\ mm$ and initial diameter of $D_0 = 52\ mm$ as well as substrates with $\theta \approx 30°, 95°,$ and $160°$.

To investigate the sample expansion during drying, we have measured the sample temperature and we plotted diameter, mass, and temperature over time for initial sample thickness ($Z_0 = 5\ mm$) and initial iameter ($D_0 = 52\ mm$) as well as superhydrophobic substrate ($\theta \approx 160°$) as shown in Figure 2. 8. We note from this figure that the sample size (*i.e.* diameter) follow the change in mass and temperature of the sample. By focusing on the end of drying (see Figure 2. 8), we observe that as sample temperature increase, there seems to be an expansion in sample diameter.

The temperature of the ambient is around *24 ℃* (*i.e.* dry bulb temperature), while the sample temperature is around *20 ℃* (*i.e.* wet bulb temperature) Other researchers have observed similar behavior in temperature although for different system [57]. We would like to point out that this behavior has not been observed or reported in other studies and we believe this is the first time that such expansion is reported. This behavior however requires further investigation.

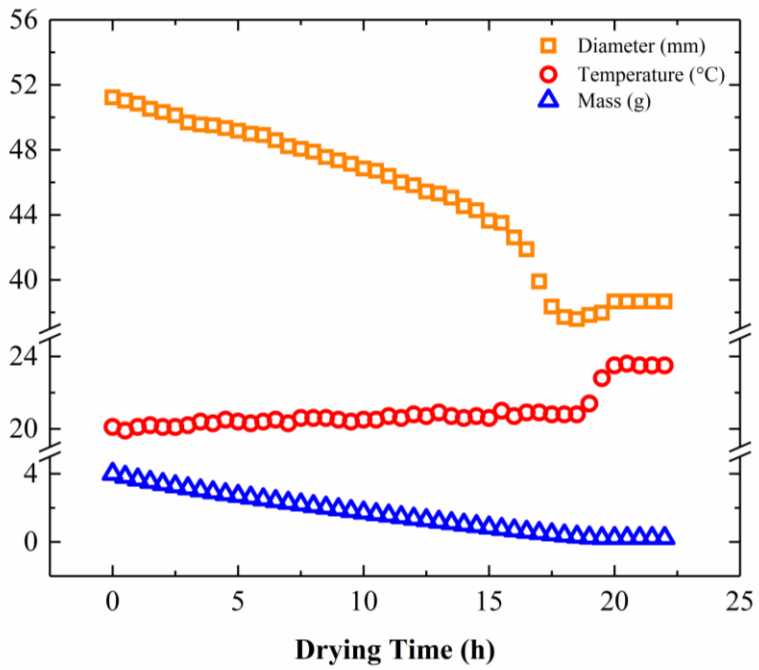

Figure 2. 8 Change in sample size, temperature, and mass during drying for sample with initial thickness of $Z_0 = 5\ mm$ and initial diameter of $D_0 = 52\ mm$ as well as substrate with $\theta \approx 160°$. Sample diameter shows a slight expansion teward the end of drying.

2.3.3 Substrate Temperature

The effect of substrate temperature on the samples drying curves is discussed in this section. As substrate temperature increased, the drying time decreased exponentially in all cases due to increase in the evaporation rate as shown in Figure 2. 9. For samples dried on superhydrophobic substrate, the end of drying time is around *21 h* at laboratory conditions, while it is around *1.5 h* for substrate at *60 ℃, 90 %* reduction. Also, one can note from this figure that the end of drying of samples located on the superhydrophobic substrate is more than the sample located on hydrophobic and hydrophilic substrates due to the crack free of these samples (more detail is presented and discussed in chapter four).

The result presented in Figure 2. 9 (b) are fitted to find the relationship between the end of drying and substrate temperature for un-cracked samples as shown in equation (2. 5). The unit of the end of drying time (t_e) is h and substrate temperature (T) is °C.

$$t_e = 0.41e^{(-3.07T)} + 3.26e^{(-0.6T)} \qquad (2.\ 5)$$

We can assume a linear decreases in mass over time, for samples located over superhydrophobic substrate, the drying rate increased from around (*-0.19 g/h*) for substrate tuned at laboratory temperature (*T = 24 ℃*) to around (*-2.07 g/h*) for substrate tuned at higher temperature (*T = 60).* Clearly, the substrate temperature played a positive rule to increase the drying rate during drying.

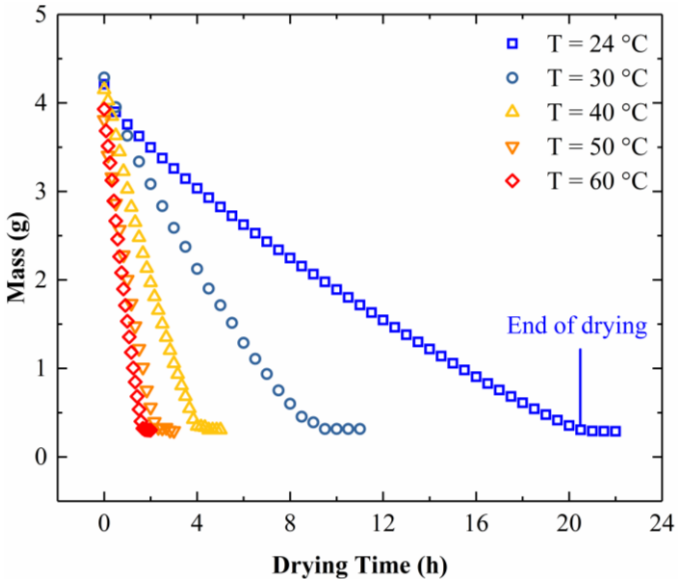

(a)

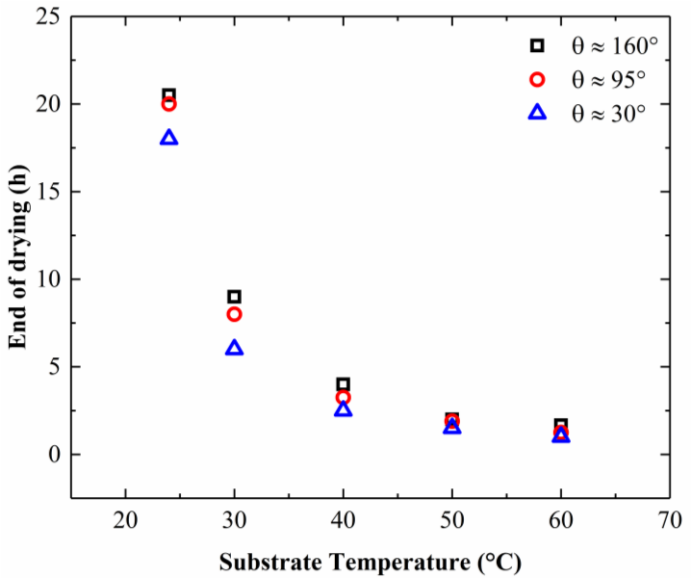

(b)

Figure 2. 9 (a) Mass change during drying for sample with initial thickness of $Z_0 = 5\ mm$ and initial diameter of $D_0 = 52\ mm$ as well as substrates with $\theta \approx 160°$ and **(b)** end of drying time for samples with initial thickness $Z_0 = 5\ mm$ and initial diameter of $D_0 = 52\ mm$, substrate temperature of $T = 24 - 60\ ℃$, as well as substrates with $\theta \approx 30°, 95°$, and $160°$.

2.3.4 Sample Shape

The effect of sample shape on the drying curves is showed and discussed in this section. Three shapes with equal surface area are selected here in this work (circle, square, and triangle). The initial dimension of samples are: circle with diameter of $D_0 = 34\ mm$, square with length of $L_0 = 30.13\ mm$, and triangle with base of $B_0 = 45.79\ mm$ and height of $H_0 = 39.66\ mm$. As shown in Figure 2. 10, for samples with different shapes and initial thickness of $Z_0 = 5\ mm$ on superhydrophobic substrate, the sample shape has no strong effect on the drying curve.

The end of drying time for all shapes is ranged between *13* and *17 h* due to the equal surface area of all samples. The end of drying time is estimated for all samples under different drying conditions as shown in Figure 2. 10 (b). All samples dried at laboratory conditions ($T = 22\ ℃$ *and* $\phi = 25 \pm 5\ \%$). In conclusion, for samples with same surface area, the drying curves is not depend strongly on the samples shape.

By using equation (2. 2) and by using the presented data in Figure 2. 10 (a), the drying rate (*DR*) for samples with different shapes over time can be estimated as shown in Figure 2. 11. Obeviosly, during the drying period time, there are only one drying period (*i.e.* falling rate period), same behavior is reported in the case of samples dried at different substrate, see Figure 2. 4. For samples with different shapes and same surface area, the drying rate is seems similar during drying process. If we assumed linear decreases in sample mass during drying process, the drying rate (*DR*) for samples located over superhydrophobic substrate with different shapes is around (*-0.12 g/h*).

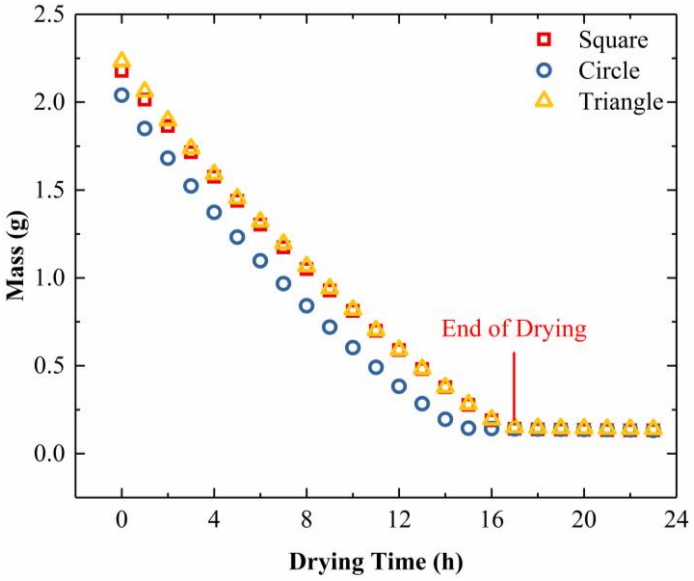

(a)

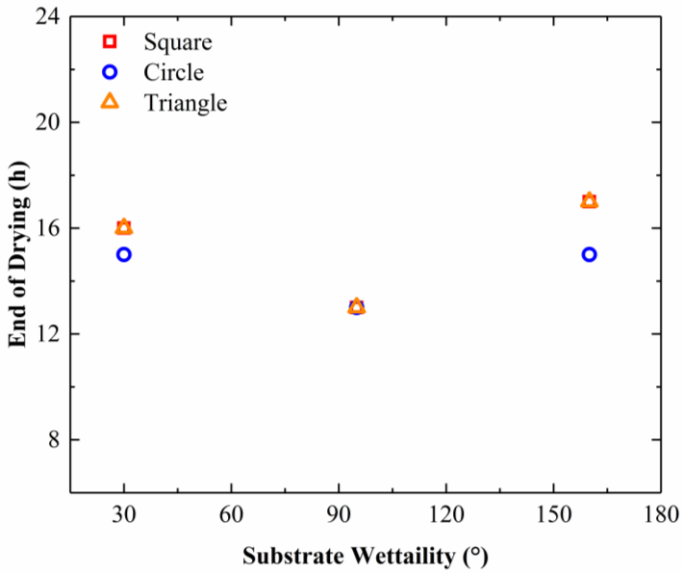

(b)

Figure 2. 10 (a) Mass change during drying for sample with three different shapes of samples and initial thickness of $Z_0 = 5\ mm$ and substrate with $\theta \approx 160°$ and **(b)** end of drying time for samples with three different shapes and initial thickness of $Z_0 = 5\ mm$ on three different types of substrate**.** The surface area of all samples is equal. The initial dimension of samples are: circle with diameter of $D_0 = 34\ mm$, square with length of $L_0 = 30.13\ mm$, and triangle with base of $B_0 = 45.79\ mm$ and height of $H_0 = 39.66\ mm$.

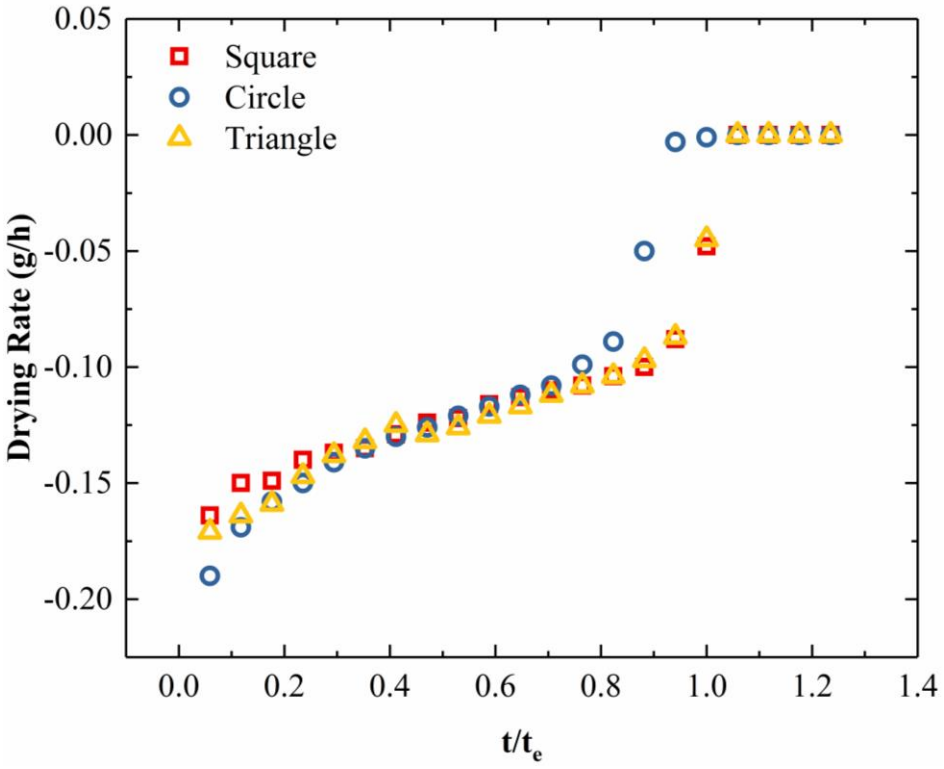

Figure 2. 11 Drying rate during drying for samples with three different shapes and initial thickness of $Z_0 = 5\ mm$ as well as substrates with $\theta \approx 160°$. t_e is the end of drying time.

2.3.5 Composite PVDF/MWCNTs Foam

The effect of MWCNTs concentration (C_{MWCNTs}) loaded in foams on the drying curves is discussed in this section. For a fixed PVDF volume fraction, we note the drying time needed to remove the liquid from the sample (*i.e.* end of drying time) increases linearly as the concentration of MWCNTs increases for all cases (*i.e*. three different substrates). The reasons for this increase maybe due to the change in sample morphology (*i.e* bubble size) as well as the increases in the initial mass of the sample as shown in Figure 2. 12(a), more details about the sample morphology is shown and discussed in next section. For samples dried on superhydrophobic substrate, the end of drying time is increased from *16 h* for sample with *0 % v/v* concentration to *30 h* for sample with *0.5 % v/v* concentration, which show a two-fold increase. In this section, all samples are dried at laboratory conditions, $T = 22 \pm 1$ ℃ and $\phi = 25 \pm 5$ %.

By employing equation (2. 2) and by using the presented data in Figure 2. 12 (a), the drying rate (*DR*) for samples over time can be estimated, see Figure 2. 13.

We can see from this figure , in the case of $C_{MWCNTs} = 0.1$ *and* 0.3 *v/v %* and during the drying period time, there are two drying period. In the first period, drying rate is increased. While, drying rate is decreased in the second period (*i.e.* falling rate period).

In the case of $C_{MWCNTs} = 0$ *and* 5 *v/v %,* during the drying period time, there are just one drying period (*i.e.* falling rate period), same behavior is reported in the case of samples dried at different substrate, see Figure 2. 4.

We can report, for composite PVDF/MWCNTs foams, there is no constatnt rate period which usual appear in another sustem [57].

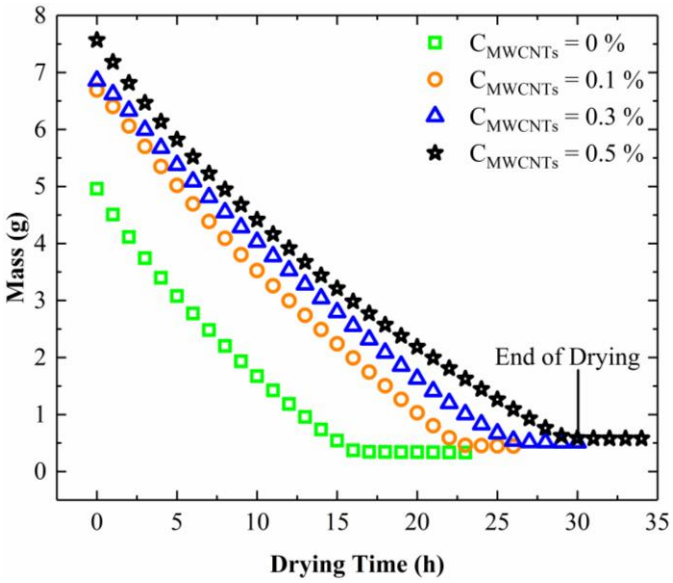

(a)

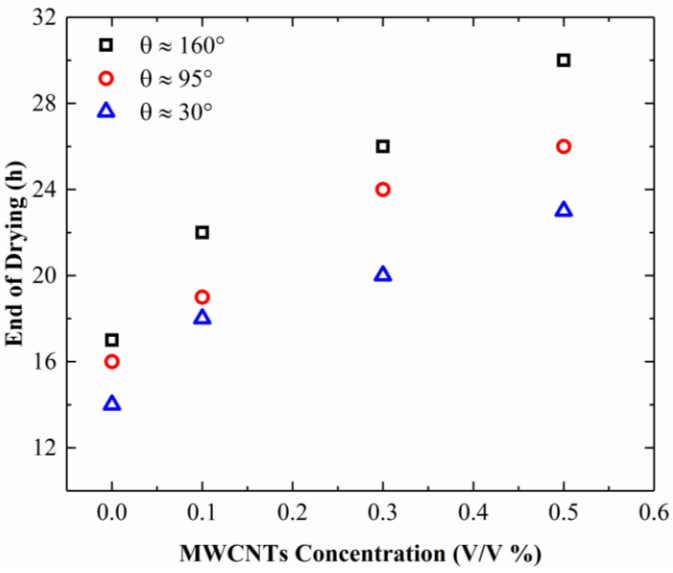

(b)

Figure 2. 12 (a) Mass change during drying for sample with initial thickness of Z_0 = *5 mm* and initial diameter of D_0 = *52 mm* as well as substrate with $\theta \approx 160°$ and **(b)** end of drying time for samples with initial thickness of Z_0 = *5 mm* and initial diameter of D_0 = *52 mm*, multi walled carbon nanotubes concentration of C_{MWCNTs} = *0 - 0.5 % v/v*, and substrates with $\theta \approx 30°$, *95°*, and *160°*. All samples dried at laboratory conditions.

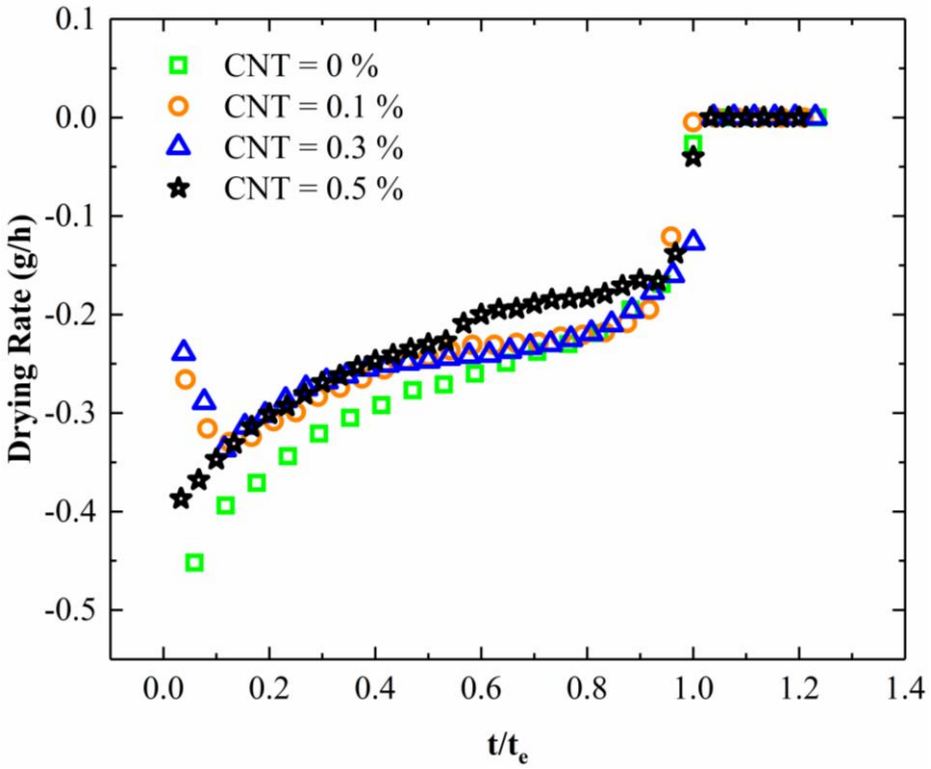

Figure 2. 13 Drying rate during drying for samples with initial thickness of $Z_0 = 5\ mm$ and initial diameter of $D_0 = 52\ mm$, multi-walled carbon nanotubes concentration of $C_{MWCNTs} = 0 - 0.5\ \%\ v/v$ as well as substrates with $\theta \approx 160°$. All samples dried at laboratory conditions. t_e is the end of drying.

2.4 Characterization of Pickering Foams

In this section, the change in foams characterization such as volume reduction, porosity, and density (bulk density and relative density) during drying is studied in details. The effect of the drying conditions (initial sample thickness as well as substarte wettability and temperature) on foams characterization is investigated.

As mentioned before, the composition of Pickering foams can be divided into three phases:

(1) Solid (PVDF or PVDF/MWCNTs);

(2) Liquid (DI-water and ethanol);

(3) Gas (occurs during foaming process).

Solid mass (or volume) stays constant during drying process, while liquid and air mass (or volume) are continue to change. For the liquid phase, the whole liquid inside sample is vanished due to drainage and evaporation. On the contrary, the air volume is increased due to the the fact that the evaporated liquid is replaced partially by air, if we assume there is change in sample size (*i.e.* shrinkage).

2.4.1 Volume reduction

The volume of foam changes during drying due to shrinkage induced by capillary stresses. The ratio of volume change is depends on the volume of liquid that leaves the sample by evaporation and drainage. In this study, the entire liquid is totally evaporated and drainaged. If the volume of evaporated and draianged liquid are replaced by air, collapse or shrinkage does not occur during drying and the size of foam remains constant.

However, if the volume of the evaporated and drainaged liquid are partially replaced partially by the air, the foam under go shrinkage (*i.e.* shrink).

To show the change in sample characterization during drying process, the sample dimensions are collected in real time using a digital camera. Utilizing the collected data (*e.g.* diameter and thickness), sample volume is calculated, assuming a cylindrical shapes.

Figure 2. 14 shows the change in foam volume for un-cracked sample under different drying conditions, the foams dimension change (*i.e.* shrink) over time. We can see the foam volume reduces over drying time. The decrease in foam volume is not depends on the drying condition (*i.e.* initial sample thickness as well as substrate temperature and wettability), see Figure 2. 14 (a) and Figure 2. 14 (b). The final volume (V_e) of all un-cracked samples is around 0.37 of the initial sample volume (V_0).

Generally, for Pickering foams system, the reduction in foams volume toward the end of drying is linear with two slopes. The second slope is higher than the first slope due to the increases in capillary pressure over time. More details about the evoluation of capillary pressure in Pickering foams during drying process is discussed in chapter four.

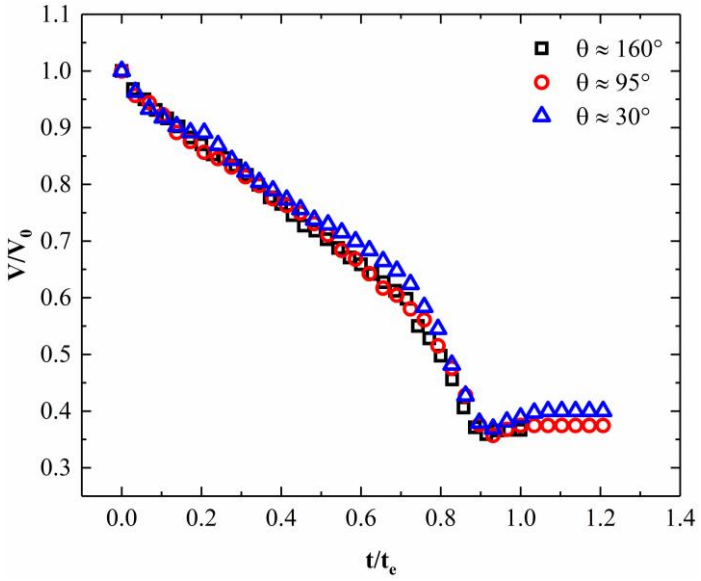

(a)

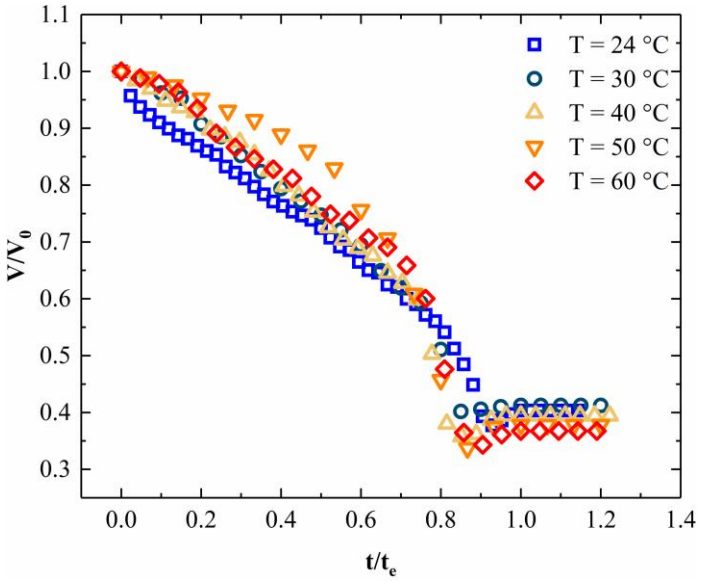

(b)

Figure 2. 14 Volume change during drying for **(a)** samples with initial thickness of Z_0 = *12.5 mm* initial diameter of D_0 = *52 mm* and substrates with $\theta \approx 160°$, *95°*,and *30°* and **(b)** samples with initial thickness of Z_0 = *5 mm* and substrates with $\theta \approx 160°$ and temperature of *T = 24* to *60 ℃*. V_0 and t_e is the initial sample volume and the end of drying time, respectively.

2.4.2 Porosity

Porosity (or void fraction) has important effect on mass and heat transfer during drying. In addition, it has a significant affect on the mechanical properties and quality of solid foam products. Porosity (P) is the ratio of gas (or air) volume (V_g) inside the sample to the whole sample volume (V). By studying the change in porosity over time, we may inter some information about the moisture migration behavior duting drying.

Scanning electron micrograph (SEM) images are taken to examine the microstructure for the sintered un-cracked solid foams as shown in Figure 2. 15. These images showe the morphology of the dried foams (distribution of pores or bubbles) and the high porosity of the solid samples.

Sample porosity during drying is calculated using the following equation [75, 76]:

$$P = \frac{V_g}{V} \tag{2. 6}$$

The sample volume over time (V) is measured experimentally, see Figure 2. 14. We use equation (2. 7) to calculate the air volume over time:

$$V_g = V - (V_s + V_l) \tag{2. 7}$$

here V_s is the volume of solid matrix (or solid particles used to prepare sample). We calculate V_s from the mass of fully dried foam sample (with neglecting the mass of air).

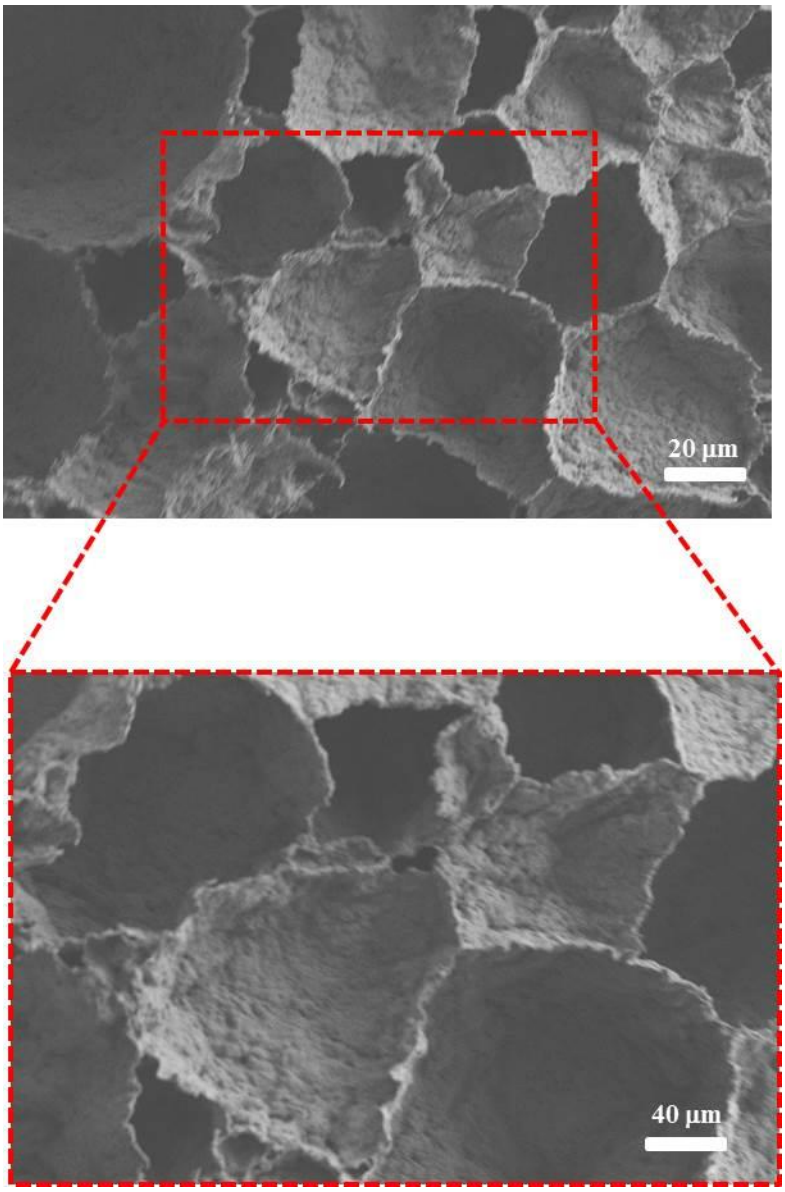

Figure 2. 15 Scanning electron micrograph (SEM) images of the sintered un-cracked solid foams produced after drying the aqueous foams precursor for *24 h* and then sintered at *165 ℃*.

To calculate the volume of solid matrix inside the sample, we use:

$$V_s = m_s/\rho_s \qquad (2.\ 8)$$

where m_s is the mass of the sample at the end of drying (*i.e.* fully dried) and ρ_s is the density of solid material (*e.g.* PVDF particles, *1.76 g/cm*^{3}).

Furthermore, V_l is the volume of liquid (DI-Water and ethanol) used to prepare aqueos foams. By measuring total sample mass over time, the liquid volume is calculated as:

$$V_l = m_l/\rho_l \qquad (2.\ 9)$$

here m_l is the mass and ρ_l is the density of the liquid (DI-water and ethanol). Note that the liquid mass over time is:

$$m_l = m - m_s \qquad (2.\ 10)$$

As mentioned before, m is the sample mass in real time which measured experimentally.

The sample porosity is increased over time due to the evaporation and drainage of liquid as shown in Figure 2. 16. For example, the porosity of sample located over superhydrophobic substrate is changed from *43 %* at the begging (*i.e.* wet sample) to *79 %* at the end (*i.e.* dry sample). For all un-cracked samples, the final porosity for dry

sample is around two times the initial porosity under different drying conditions, see Figure 2. 16.(a) and Figure 2. 16. (b).

Generally, for all uncracked samples, the sample porosity depends on two parameters;

(1) The amount of air that is replaced by the liquid inside the sample (induced due to the liquid evaporation).

(2) Ratio of sample shrinkage during drying induced by capillary stresses.

There are four periods marked on Figure 2. 16 (a)**.** In the first period shows linear increase in sample porosity that means the change in air volume inside the sample is equivalent to the change in sample size (*i.e.* shrinkage). In the second period, the sample porosity stays constant due to the domination of sample shrinkage (*i.e.* change in sample size in this period is greater than the change in air volume). In the third period, the porosity is increased sharply due to the expansion phenomenon that occurs in this period (*i.e.* the sample is swelling during this period). Lastly, the porosity stays constant due to the end of drying (*i.e.* fully dry sample during this period).

Generally, the change in sample porosity over time is not depends on the drying conditions (*i.e.* initial sample thickness as well as substrate wettability and temperature) as shown in Figure 2. 16 (a) and Figure 2. 16 (b). The results presented in these figures show the high porosity of the dry foams that fabricated using foaming method. For all un-cracked samples, the final porosity is around 0.83, which show a two-fold increase.

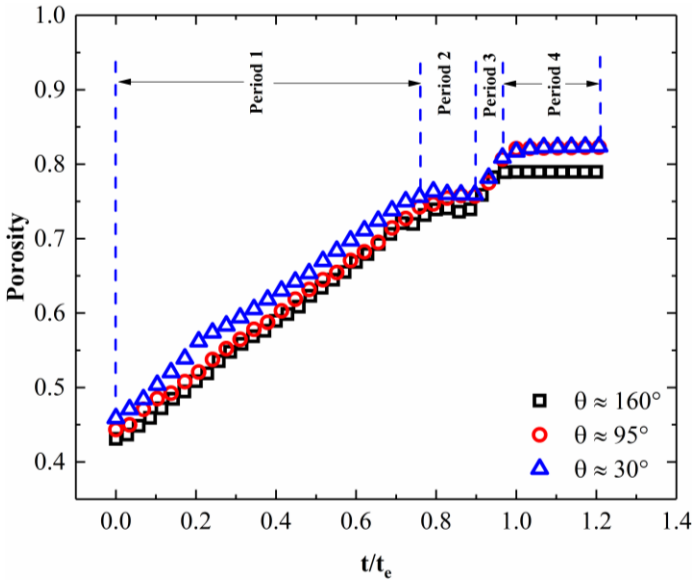

(a)

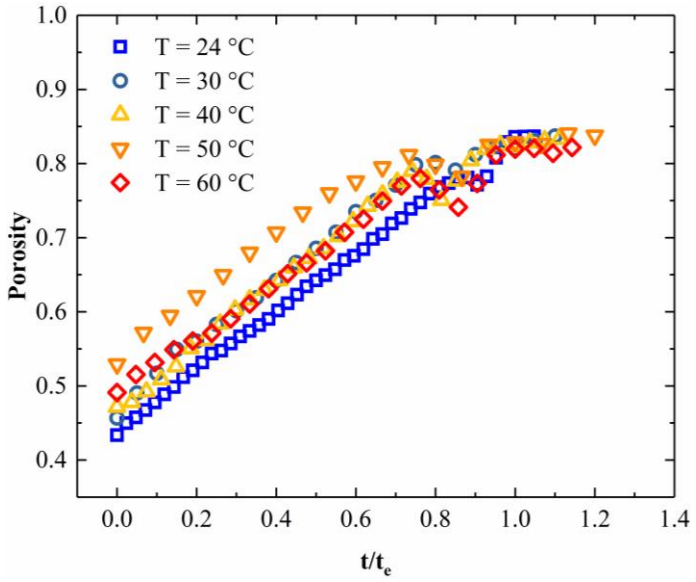

(b)

Figure 2. 16 Porosity change during drying for **(a)** samples with initial thickness of Z_0 = *12.5 mm* and initial diameter of D_0 = *52 mm* as well as substrates with $\theta \approx 160°$, *95°*, and *30°* and **(b)** samples with initial thickness of Z_0 = *5 mm* and initial diameter of D_0 = *52 mm* as well as substrates with $\theta \approx 160°$ and temperature of *T = 24 to 60 ℃*. t_e is the end of drying time.

2.4.3 Density

In this section, both bulk density and relative density are defined and studied in details. The bulk density (ρ_b) or apparent density is defined as the ratio of sample mass to the sample volume and it can calculate as:

$$\rho_b = \frac{m}{V} \tag{2. 11}$$

where;

$$m = m_g + m_l + m_s \tag{2. 12}$$

$$V = V_g + V_l + V_s \tag{2. 13}$$

The air mass can be neglectedin compared to the solid and liquid fractions ($m_a = 0$). The bulk density is then:

$$\rho_b = \frac{m_l + m_s}{V_g + V_l + V_s} \tag{2. 14}$$

The relative density (ρ_r) is the ratio of the foam density/bulk density (ρ_b) to that of the solid matrix (ρ_s), it is calculated as [71]:

$$\rho_r = \frac{\rho_b}{\rho_s} \tag{2. 15}$$

This parameter provides information about the air content of porous structures.

The bulk density and relative density for sample located over superhydrophobic substrate are changed from *1.47 g/cm*^{3} and *0.82* for wet Pickering foams to *0.1 g/cm*^{3} and *0.07* , respectively for fully dry Pickering foams as shown in Figure 2. 17 (a). Moreover, for the un-cracked sample, the final bulk density and relative density are around *0.1 g/cm*^{3} and *0.07,* respectively as shown in Figure 2. 17 and Figure 2. 18.

We can report from these figures that neither the sample size (*i.e.* sample thickness) nor the substrate temperature and wettability influance the final density (*i.e.* bulk density and relative density) of dry Pickering foams samples.

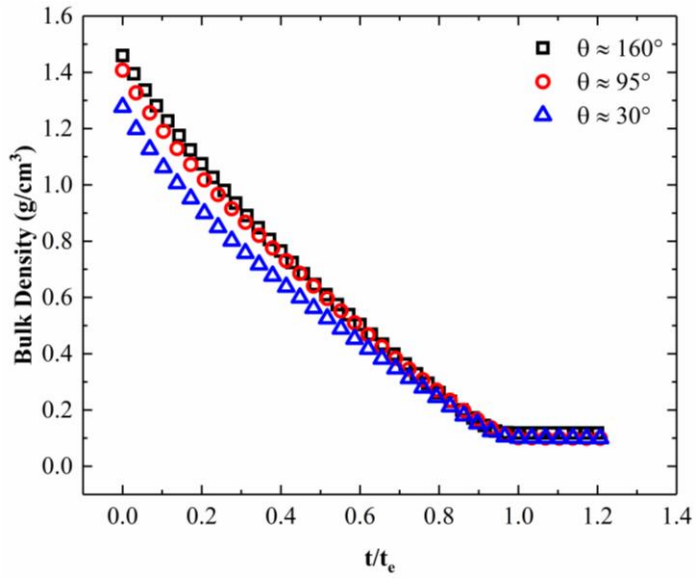

(a)

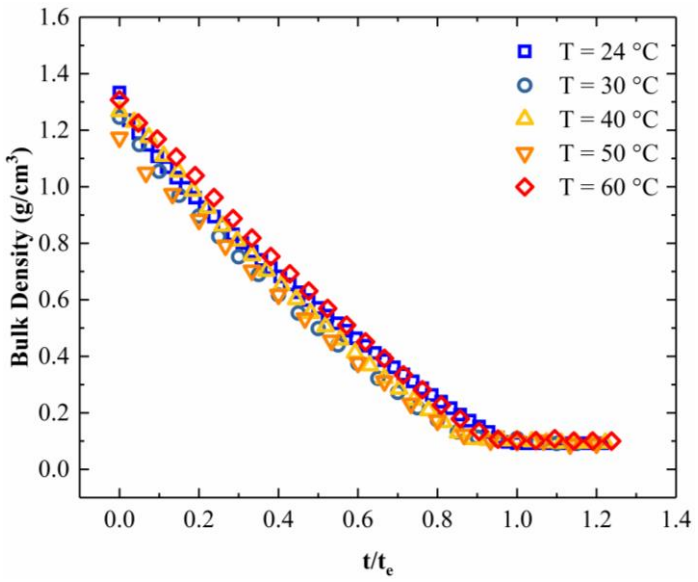

(b)

Figure 2. 17 Bulk density change during drying for **(a)** samples with initial thickness of $Z_0 = 12.5\ mm$ and initial diameter of $D_0 = 52\ mm$ as well as substrates with $\theta \approx 160°$, $95°$, and $30°$ and **(b)** samples with initial thickness of $Z_0 = 5\ mm$ and initial diameter of $D_0 = 52\ mm$ as well as substrates with $\theta \approx 160°$ and temperature of $T = 24$ to $60\ ℃$. t_e is the end of drying time.

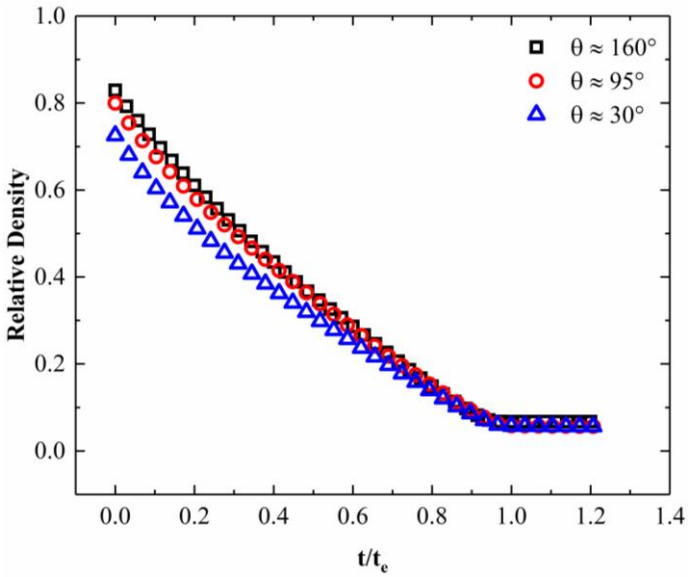

(a)

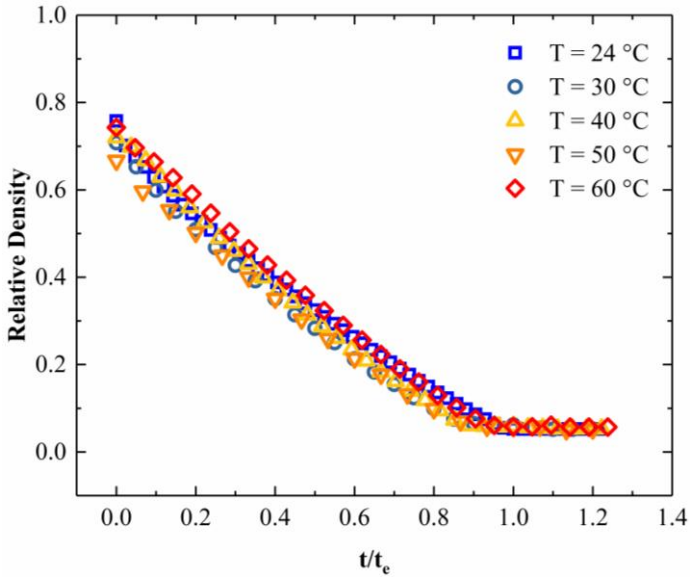

(b)

Figure 2. 18 Relative density change during drying for **(a)** samples with initial thickness of $Z_0 = 12.5\ mm$ and initial diameter of $D_0 = 52\ mm$ as well as substrates with $\theta \approx 160°$, $95°$, and $30°$ and **(b)** samples with initial thickness of $Z_0 = 5\ mm$ and initial diameter of $D_0 = 52\ mm$ as well as substrates with $\theta \approx 160°$ and temperature of $T = 24$ to $60\ ℃$. t_e is the end of drying time.

2.5 Piezoelectric Coefficient

One of the most important properties of the Poly(vinylidene fluoride) porous material is the piezoelectric properties [77-79]. Poly(vinylidene fluoride) (PVDF) is a type of polymer that has wide applications in biomedical, chemical, electronic industries due to the great properties of this polymer. PVDF has low density, high elasticity, fine thermal stability and chemical resistance, on one hand as well as it is commercially available with low cost. Furthermore, It is semi crystalline thermoplastic and electroactive polymer and exists in the five different phases (ε, α, δ, γ, and β) [80]. PVDF in β phase has fined piezoelectric and dielectric constant due to its biocompatibility and high flexibility makes it an interesting material [77-79].

Based on these properties, PVDF has more technical important; used as smart materials (*i.e.* convert the mechanical energy to mechanical energy and vice versa) such as actuator, transducers and sensors [79, 81, 82]. There are many methods used to form PVDF in β phase, one method is formed by adding nanofillers such as multi-walled carbon nanotubes (MWCNTs) and the other method is by mechanical stretching [80, 83, 84].

In this section, the piezoelectric coefficients of the sintered un-cracked samples are measured and discussed.

The sintered un-cracked samples with different thickness are tested in this work. A layer of 0.025 mm thick stainless steel foil tape was applied to each side to prevent short circuits through the sample. A high electrical poling field is applied to the samples by using a high voltage generator. The value of the voltage depends on the sample thickness. The voltage is varied between 11 kV for the thinner sample to 18.5 kV for the

thicker sample. Samples are polled under the following conditions: substrate temperature of (T_{sb} = 80 °C), Frequency of (Freq = 110 Hz), dynamic force of (F_{dy} = 0.25 N), and pooling time of (t_p = 30 min).

Figure 2. 19 shows the Piezoelectric coefficients of samples before and after poling, longitudinal piezoelectric coefficient (d_{33}) and transverse piezoelectric coefficient (d_{31}). The piezoelectric coefficient of theun-poled sampes are seem similar. While, the piezoelectric coefficient of the poled samples can be significantly higher than of the un-poled samples. Also, we can see the the piezoelectric coefficient is dependent on the pooling voltage.

For the longitudinal piezoelectric coefficient (d_{33}), the increase in the piezoelectric coefficient for lower pooling voltage is higher than the higher pooling voltage. While, for the transverse piezoelectric coefficient (d_{31}), the increase in the piezoelectric coefficient for higher pooling voltage is higher than the lower pooling voltage. The difference in the piezoelectric coefficients may due to the difference in the voltage applied that used to pole the samples. Lastly, for all samples, the piezoelectric coefficients for poled samples are increased if we compare with unpoled samples.

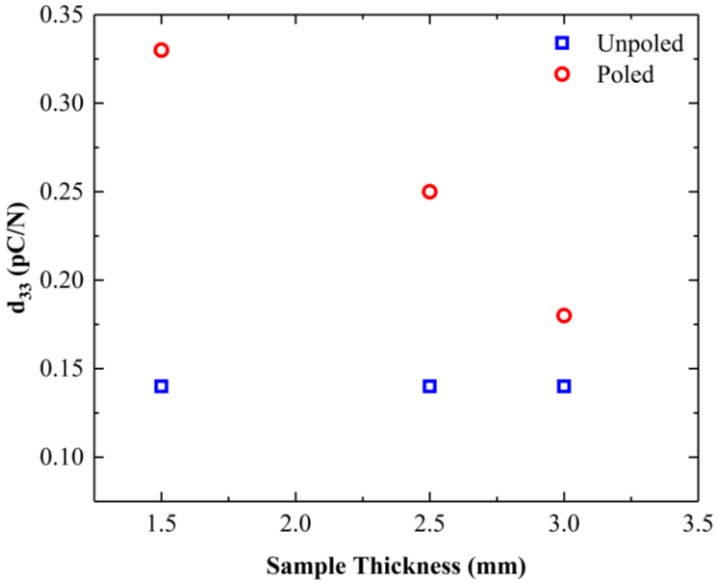

(a)

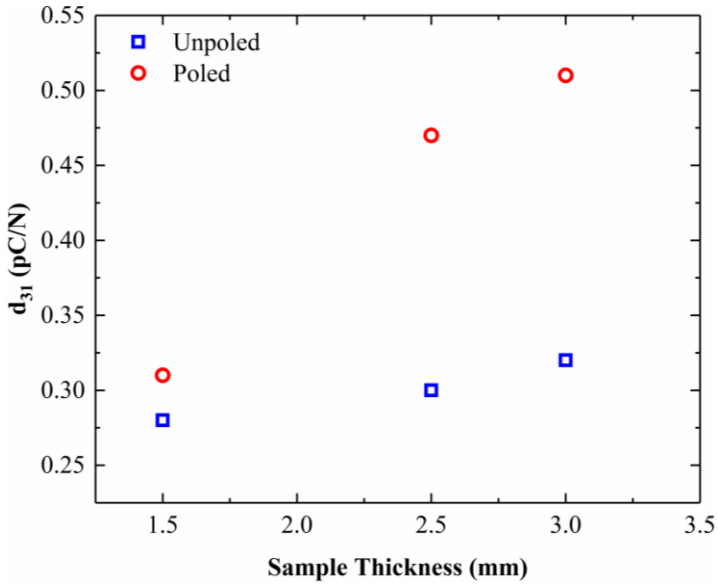

(b)

Figure 2. 19 Piezoelectric coefficients before and after poling for sintered un-cracked samples with thickness of *Z = 1.5 - 3 mm* **(a)** longitudinal piezoelectric coefficient (d_{33}) and **(b)** transverse piezoelectric coefficient (d_{31}). Poling voltage (*11 kV* for sample thickness of *Z = 1.5 mm*, *13 kV* for sample thickness of *Z = 2.5 mm*, *14.5 kV* for sample thickness of *Z = 3 mm).*

2.6 Summary

In summary, drying curves and change in dimensions of Pickering foams (or composite foams) under different drying conditions are measured in this chapter. For all cases, drying curves were performed in the falling rate period. The end of drying time is found for all samples, where thicker samples as well as composite foams take longer time to dry. On the contrary, by increasing the substrate temperature, the end of drying time is decreased exponentially. Also, the wettability of substrate has not a strong effect on the end of drying time. For all samples ($Z_0 = 2.5 - 12.5\ mm$) located on superhydrophobic substrate, the change in sample dimension (*i.e.* diameter and thickness) are seem to happen in a similar rate. While, in the case of samples located on PDMS and glass substrates, the change in sample thickness is dominated. As the initial sample thickness increases it seems that change in sample dimensions have similar trends. We reported that the characterization of dry samples (*e.g.* density and porosity) do not depend on the initial sample size and drying conditions. We calculated the change in volume, porosity, as well as density (*i.e.* relative density and bulk density) of samples during aging based on different drying conditions. We find that sample volume and density decrease over time, while porosity increase during drying. Finally, the piezoelectric coefficient of all sintered un-cracked samples are increased after poling.

Chapter 3

Effective Moisture Diffusivity

3.1 Introduction

To describe the drying process, we calculate the effective moisture diffusivity (D_{eff}) based on the collected drying data. For this, we use the *method of the slope* that is derived based on the solution to the *Fick's second law of diffusion*.

The assumption can be made that mass transfer resistance at the edges of the disk is negligible and that moisture transfer is one dimensional in the *Z-direction*, see Figure 3. 1.

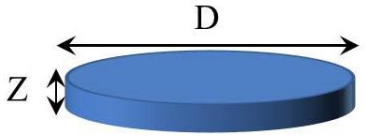

Figure 3. 1 Sample shape (not drawn to scale).

We use the data that we have collected beyond the first hour mark (when the mold is removed) and thus assume that the moisture transfer is one-dimensional across the sample thickness (*Z*-direction). The unsteady state Fick's second law in cylindrical coordinates is [34]:

$$\frac{\partial C_l}{\partial t} = D_{eff}\,\frac{\partial^2 C_l}{\partial Z^2} \qquad (3.\ 1)$$

Where C_l is the moisture concentration (kg/m^3), C_l is the mass (kg) of liquid used to prepare the sample over the sample volume (m^3), t is time (h), D_{eff} is the effective diffusivity (m^2/h), a function of moisture concentration, and Z is the coordinate along the sample thickness.

We can multiply both sides of equation (3. 1) by (1/C_s), where C_s is the solid concentration (kg/m^3):

$$\frac{\partial\left(\frac{C_l}{C_s}\right)}{\partial t} = D_{eff}\ \frac{\partial^2 \frac{C_l}{C_s}}{\partial Z^2} \tag{3. 2}$$

substituting:

$$X = \frac{C_l}{C_s} \tag{3. 3}$$

equation (3. 1) becomes:

$$\frac{\partial X}{\partial t} = D_{eff}\ \frac{\partial^2 X}{\partial Z^2} \tag{3. 4}$$

where X is the average moisture content (g liq./g dry solid). The average moisture content is related to the measured sample mass during drying and can be calculated as

$$X = \frac{m_l}{m_s} = \frac{m}{m_s} - 1 \tag{3. 5}$$

where m_l is liquid mass, m_s is solid mass, and m is the sample mass at any given time.

As mentioned before, two approaches were taken to estimate the D_{eff} of Pickering foams. In the first approach, the influence of sample shrinkage is neglected, while it is included in the second one. In the next sections both approaches are presented in details.

Fundamental Questions

(1) What is the effect of substrate wettability and temperature on the effective moisture diffusivity during drying process?

(2) What is the effect of initial sample thickness and shape on the effective diffusivity?

(3) Do MWCNTs concentration in composite foams (*i.e.* PVDF/MWCNTs) affect the diffusivity over time.

3.2 Neglecteing Shrinkage

In this section, the effect of sample shrinkage on the effective diffusivity calculation is neglected. The details of mathematical simplification of the governing equation and the approach used to estimate the effective moisture diffusivity is presented in the next steps.

3.2.1 Mathematical Simplification

Applying the initial and boundary conditions, equations (3. 6) – (3. 8), the solution to equation (3. 4), assuming constant D_{eff} and ignoring sample shrinkage, is given by equation (3. 9) [34] (see Figure 3. 1, initial thickness is Z_0)

$$t = 0 \qquad 0 \leq Z \leq Z_0 \qquad X = X_0 \tag{3. 6}$$

$$t > 0 \qquad Z = 0 \qquad \frac{\partial X}{\partial Z} = 0 \tag{3. 7}$$

$$t > 0 \qquad Z = Z_0 \qquad X = X_e \tag{3. 8}$$

$$W = \frac{8}{\pi^2} \sum_{n=0}^{\infty} \frac{1}{(2n+1)^2} exp[-\frac{(2n+1)^2 \pi^2 D_{eff} t}{4Z_0^2}] \tag{3. 9}$$

where,

$$W = \frac{X - X_e}{X_0 - X_e} \tag{3. 10}$$

here, *W* is the fractional average moisture content or dimensionless moisture content, *X* is the average moisture content at any time, see equation (3. 5), X_e is the final average moisture content and X_o is the initial average moisture content, both described as:

$$X_e = \frac{m_{l,e}}{m_s} = \frac{m_e}{m_s} - 1 \tag{3. 11}$$

$$X_0 = \frac{m_{l,0}}{m_s} = \frac{m_0}{m_s} - 1 \tag{3. 12}$$

In equation (3. 11) $m_{l,e}$ is the final mass of liquid and m_s is the mass of solid used to prepare the sample (this quantity stays constant during aging). In equation (3. 12) $m_{l,0}$ is the initial mass of liquid, the liquid used to prepare the sample.

In this work, $X_e = 0$, m_e is equal to m_s (we assumed that all liquid is evaporated during drying process) for dry sample, and $0 \leq W \leq 1$.

For long drying times, equation (3. 9) can be simplified by taking $n = 0$ to give:

$$W = \frac{8}{\pi^2} exp[-\frac{\pi^2 D_{eff} t}{4Z_0^2}] \quad (3.\ 13)$$

Taking the logarithm and subsequently the time derivative on both sides of equation (3. 13), we arrive at:

$$\frac{\partial log W}{\partial t} = -\frac{\pi^2 D_{eff}}{4Z_0^2} \quad (3.\ 14)$$

By plotting $logW$ versus time, we then calculate the effective diffusivity, D_{eff}, as:

$$D_{eff} = -\left(\frac{4{Z_0}^2}{\pi^2}\right) * (slope\ of\ line) \quad (3.\ 15)$$

3.2.2 Moisture Transport

For un-cracked samples dried under different drying conditions (substrate wettability, initial sample thiacknes, and substrate temperature), the change in the average moisture content, equation.(3. 5), and fractional average moisture content, equation (3. 10), are plotted over time in Figure 3. 2 and Figure 3. 3. For all investigated drying, fractional moisture content is normalized by the change in the sample moisture content and varies between *one* and *zero* (for fully dried sample with no bound water).

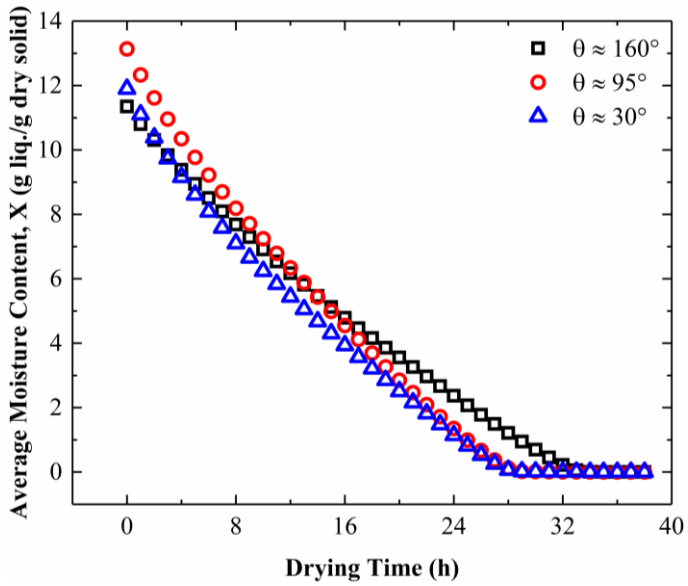

(a)

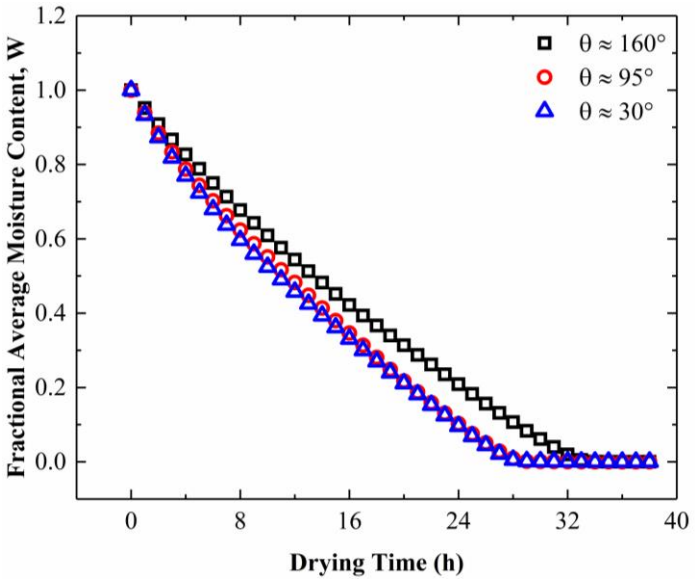

(b)

Figure 3. 2 (a) Average moisture content and **(b)** fractional average moisture content for samples with initial thickness of $Z_0 = 12.5\ mm$ and initial diameter of $D_0 = 52\ mm$ as well as substrates with $\theta \approx 30°, 95°,$ and $160°$.

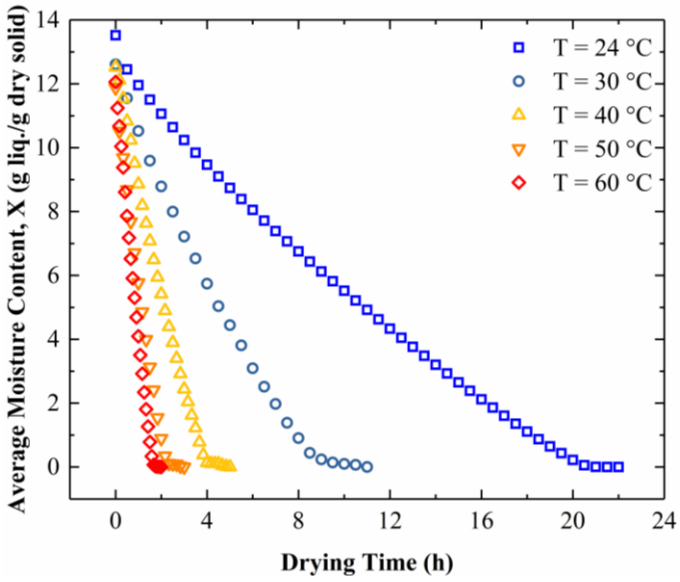

(a)

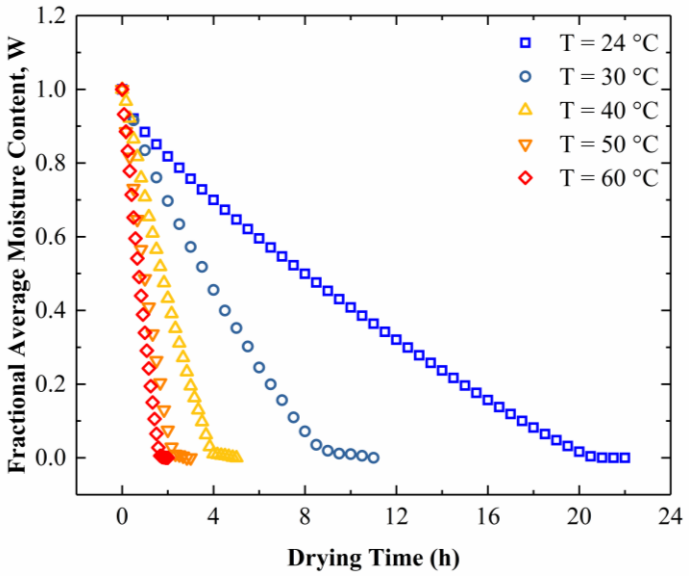

(b)

Figure 3. 3 (a) Average moisture content and **(b)** fractional average moisture content for samples with initial thickness of $Z_0 = 5\ mm$ and initial diameter of $D_0 = 52\ mm$ as well as substrate with $\theta \approx 160°$ and temperature of $T = 24$ to $60\ ℃$.

3.2.3 Effective Moisture Diffusivity

We employ *method of slope* to calculate the effective moisture diffusivities of the drying samples. As expected, we note that the effective moisture diffusivity vary with the average moisture content of the samples as shown in Figure 3. 4.

The effective moisture diffusivity increases with a decrease in average moisture content for all the experimental cases. This maybe due to changes in the sample morphology and structure during drying. For instance, the sample permeability at the beginning is close to *zero* but increases with time as the excess liquid leaves the sample. The increase in permeability may cause to increase in the effective moisture diffusivity during aging. Previous studies with different systems (e.g. some type of food) focused on the effective moisture diffusivity behavior during drying also found similar behaviors of results [30, 85-88].

As substrate temperature increased, the drying time decreased exponentially due to higher evaporation rate. As shown in Figure 3. 4 (b), the substrate temperature playes a role to increase the values of effective moisture diffusivity (or modified effective moisture diffusivity) due to the increase in evaporation rate during drying process. See appendix B for diffusivity curves.

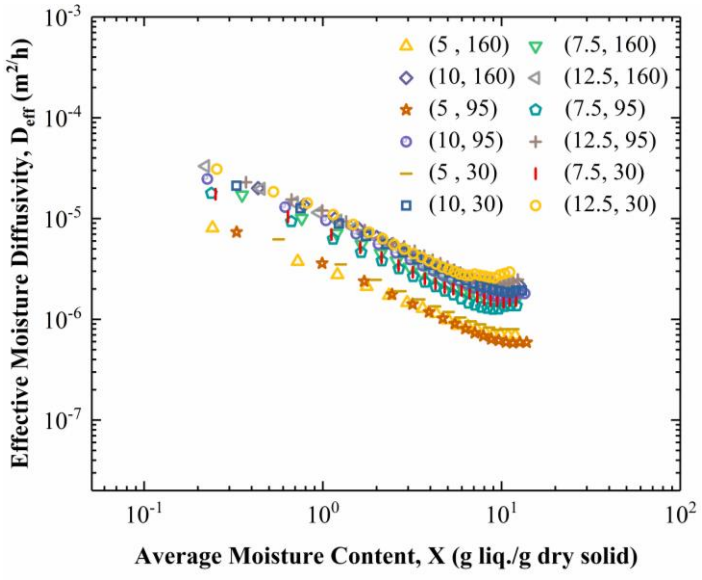

(a)

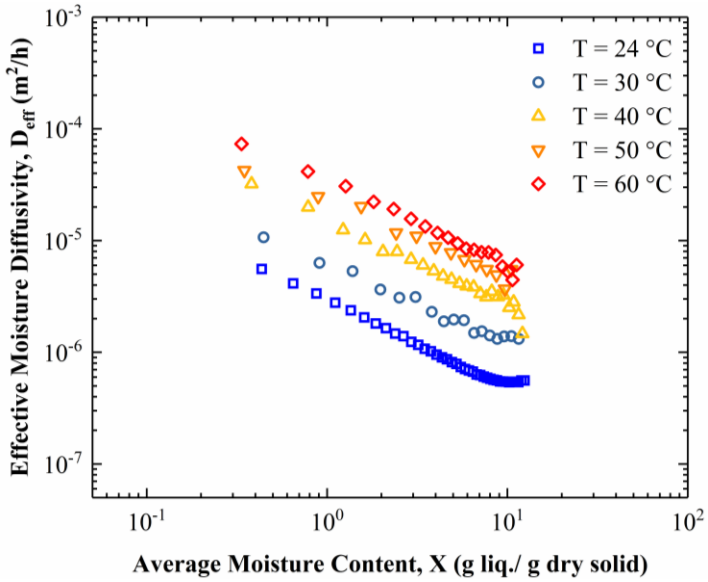

(b)

Figure 3. 4 Effective moisture diffusivity for **(a)** samples with initial thickness of Z_0 = *5.0 to 12.5 mm* and initial diameter of D_0 = *52 mm* as well as substrates with $\theta \approx 30°$, *95 °*, and *160 °* and **(b)** samples with initial thickness of Z_0 = *5 mm* and initial diameter of D_0 = *52 mm* as well as substrates with $\theta \approx 160°$ and temperature of *T = 24* to *60 ℃*. The first number in the parenthesis is initial sample thickness in mm and the second number is substrate contact angle in degree.

3.3 Including Shrinkage

In this section, consider the effect of samples shrinkage on the effective moisture diffusivity during drying processe. In this approach we include the sample volume in real time when estimate effective moisture diffusivity of Pickering foams. The new effective moisture diffusivity is called *modified effective moisture diffusivity*. We compare between the values of effective moisture diffusivity (*i.e.* shrinkage neglected) and modified effective moisture diffusivity (*i.e.* shrinkage included) in the next section.

3.3.1 Mathematical Simplification

To include the effect of sample shrinkage during drying on effective moisture diffusivity, both sides of equation (3. 4) are multiplied by the density of the dry solid (ρ_d) [40-46]:

$$\frac{\partial(\rho_d X)}{\partial t} = D_{eff,m}\nabla^2(\rho_d X) \tag{3. 16}$$

where $D_{eff,m}$ is the modified effective moisture diffusivity. For constant mass of dry solid, ρ_d is replaced by:

$$\rho_d = \frac{m_{ds}}{V} \tag{3. 17}$$

so equation (3. 16) becomes

$$\frac{\partial(m_{ds}/V)X}{\partial t} = D_{eff,m}\nabla^2\big((m_{ds}/V)X\big) \tag{3. 18}$$

In this equation, m_{ds} is the mass of solid material used to prepare the sample and it is constant during the drying process. Eliminate m_{ds} from both sides of equation (3. 18):

$$\frac{\partial(X/V)}{\partial t} = D_{eff,m}\nabla^2(X/V) \tag{3. 19}$$

We show that the change in sample volume (V) is linear over time, see Figure 3. 5, so we can assume:

$$Y = X/V \tag{3. 20}$$

so equation (3. 19) becomes:

$$\frac{\partial Y}{\partial t} = D_{eff,m}(\nabla^2 Y) \tag{3. 21}$$

We defined the following parameters:

$$Y_e = \frac{X_e}{V_e} \tag{3. 22}$$

$$Y_0 = \frac{X_0}{V_0} \tag{3. 23}$$

here, Y is the modified average moisture content (g liquid / g dry solid .m^3) at any time, Y_e is the final average modified moisture content (in this study $Y_e = 0$), Y_0 is the initial modified moisture content, V is the volume of the sample (m^3) at any time, and V_e and V_0 are the final and initial sample volume respectively.

Solve this along with the modified initial and boundary conditions, equations (3. 24) - (3. 26), we get equation (3. 27):

$$t = 0 \qquad 0 \leq Z \leq Z_0 \qquad Y = Y_0 \tag{3. 24}$$

$$t > 0 \qquad \mathrm{Z} = 0 \qquad \frac{\partial Y}{\partial Z} = 0 \tag{3. 25}$$

$$t > 0 \qquad \mathrm{Z} = Z_0 \qquad Y = Y_e \tag{3. 26}$$

$$M = \frac{8}{\pi^2} \sum_{n=0}^{\infty} \frac{1}{(2n+1)^2} exp[-\frac{(2n+1)^2 \pi^2 D_{eff,m} t}{4Z_0^2}] \tag{3. 27}$$

where;

$$M = \frac{Y - Y_e}{Y_0 - Y_e} \tag{3. 28}$$

here, *M* is the modified fractional average moisture content or dimensionless modified average moisture content that varies as $0 \leq M \leq 1$.

To simplify equation (3. 28), for long drying times we can set $n = 0$ and get:

$$M = \frac{8}{\pi^2} exp[-\frac{\pi^2 D_{eff,m} t}{4Z_0^2}] \quad (3.\ 29)$$

By taking the logarithm for the both sides of equation (3. 29), arrive at equation (3. 30)

$$logM = log\frac{8}{\pi^2} - \frac{\pi^2 D_{eff,m} t}{4Z_0^2} \quad (3.\ 30)$$

By taking the time derivative of both sides of equation (3. 30), one finally obtains to equation (3. 31)

$$\frac{\partial logM}{\partial t} = -\frac{\pi^2 D_{eff,m}}{4Z_0^2} \quad (3.\ 31)$$

Once again, by plotting $logM$ versus drying time and by using the *method of slope* $D_{eff,m}$ is calculated as

$$D_{eff,m} = -\left(\frac{4{Z_0}^2}{\pi^2}\right) * (slope\ of\ line) \quad (3.\ 32)$$

3.3.2 Modified Moisture Transport

Figure 3. 5 shows the relation between the foam volume and average moisture content during drying process. As mentioned in chapter two, there are two linear slopes, during the falling rate period, the second linear slope is higher than the first linear slope due to the increase in the capillary stress. This figure shows the validity of the assumption between the foam volume and average moisture content, see equation (3. 20).

By using equation (3. 20) and equation (3. 28), the modified average moisture content and modified fractional average moisture content values are calculated and plotted against the drying time as shown in Figure 3. 6 and Figure 3. 7.

We can see from these figures that both the modified average moisture content and modified fractional average moisture content are decreased linearly under all drying conditions (i.e initial sample thickness, substrate wettability, and substrate temperature)..

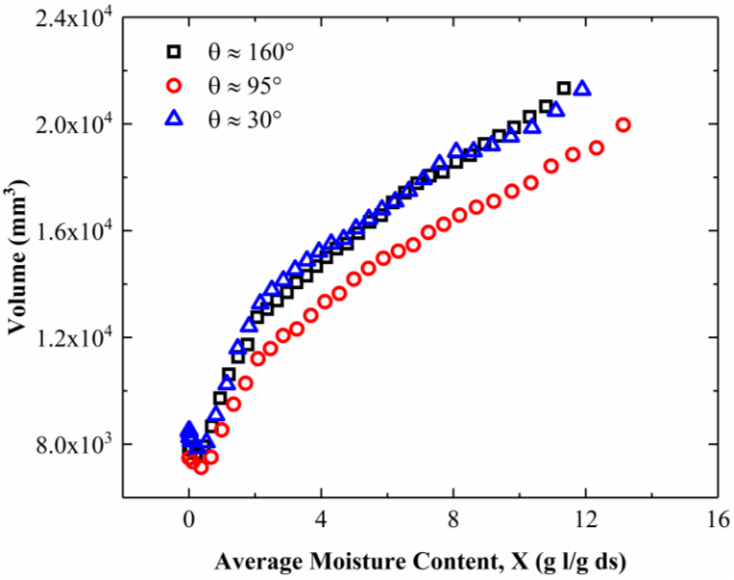

(a)

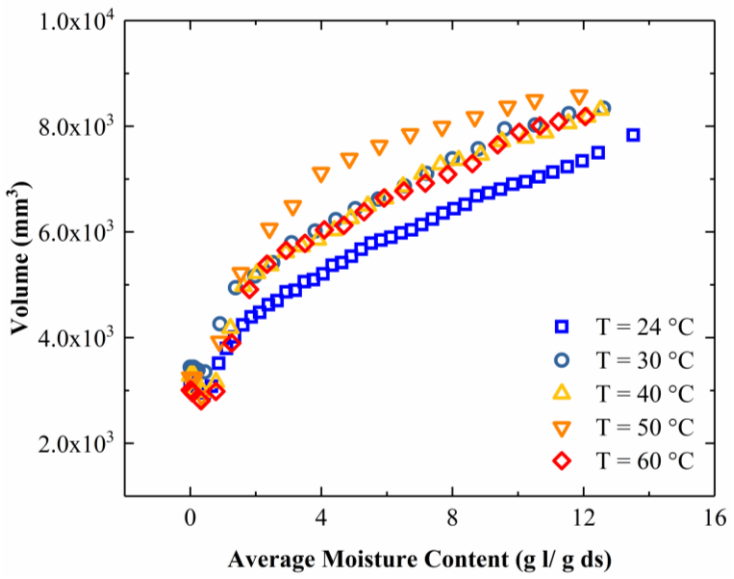

(b)

Figure 3. 5 Volume change versus average moisture content during drying for **(a)** samples with initial thickness of $Z_0 = 12.5\ mm$ and initial diameter of $D_0 = 52\ mm$ as well as substrates with $\theta \approx 160°$, $95°$, and $30°$ and **(b)** samples with initial thickness of $Z_0 = 5\ mm$ and initial diameter of $D_0 = 52\ mm$ as well as substrates with $\theta \approx 160°$ and temperature of $T = 24$ to $60\ ℃$.

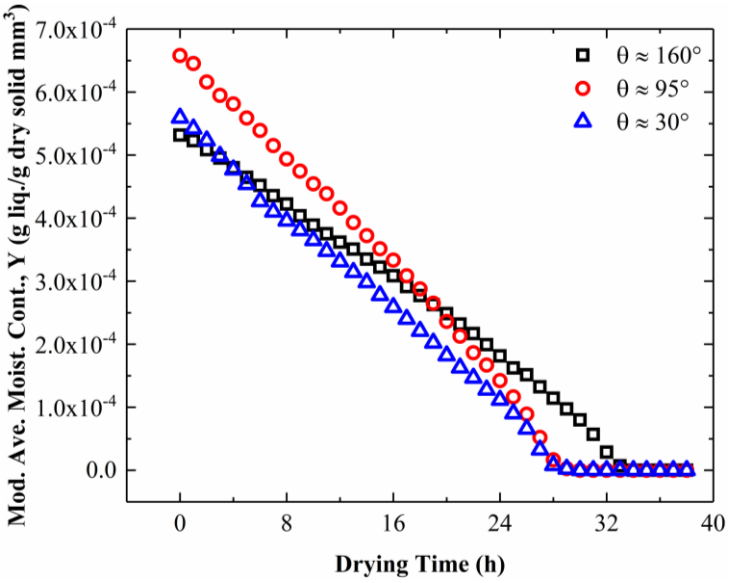

(a)

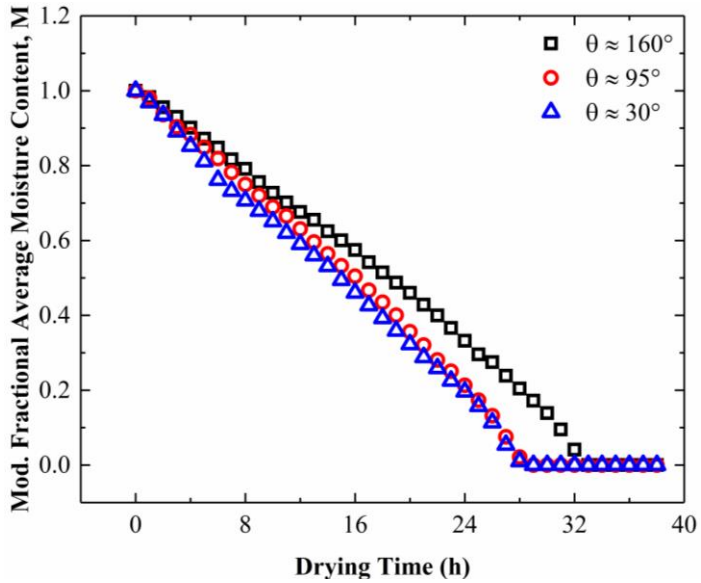

(b)

Figure 3. 6 (a) Modified average moisture content and **(b)** modified fractional average moisture content for samples with initial thickness of $Z_0 = 12.5\ mm$ and initial diameter of $D_0 = 52\ mm$ as well as substrates with $\theta \approx 30°, 95°,$ and $160°$.

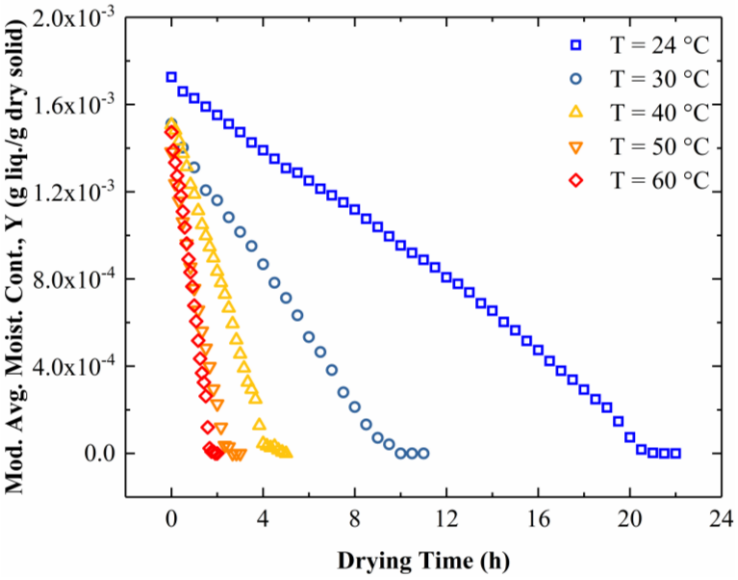

(a)

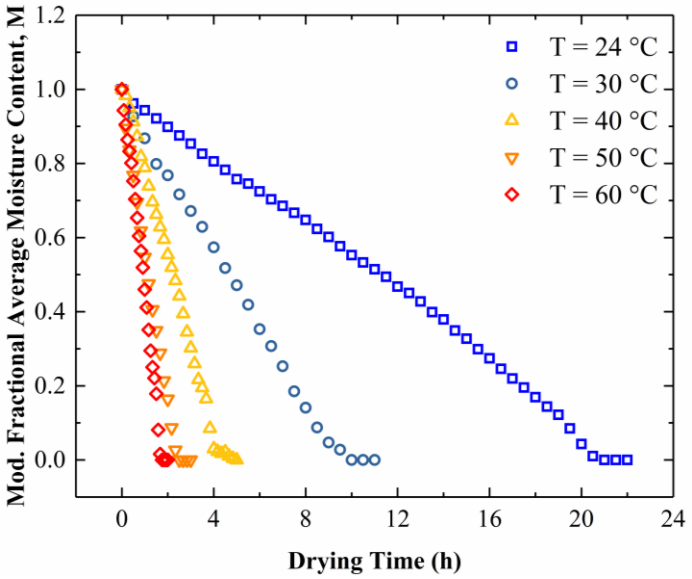

(b)

Figure 3. 7 (a) Modified average moisture content and **(b)** modified fractional average moisture content for samples with initial thickness of $Z_0 = 5\ mm$ and initial diameter of $D_0 = 52\ mm$ as well as substrates with $\theta \approx 160°$ and temperature of $T = 24 - 60\ ℃$.

3.3.3 Modified Effective Moisture Diffusivity

As illuminated in Figure 3. 8, for samples with initial sample thickness of Z_0 = 5 - 12.5, substrate wettability of $\theta \approx 30^\circ$ *to* 160°, *and substarte temperature of T = 24 – 60* ℃, the modified effective moisture diffusivity increases with a decrease in the average moisture content. The change in mofified effective diffusivity is seems similar to the change in effective moisture diffusivity during drying process. In the next section. We calculate the difference between these values over time so we can study the effect of including on neglecting the foam shrinkage on the effective diffusivity during the drying process. See appendix B for diffusivity curves.

3.4 Effective Moisture Diffusivity Behavior

In this section, the effect of sample shrinkage, initial sample thickness as well as substrate wettability and temperature on the effective moisture diffusivity over time are presented in details. Also, the non-dimensional parameters are found and plotted for different cases of drying.

3.4.1 Shrinkage Influence

To study the effect of sample shrinkage on the effective moisture diffusivity during drying, the difference between the effective moisture diffusivity (D_{eff}) and modified effective moisture diffusivity ($D_{eff,m}$) is calculated as shown in Figure 3. 9. At the first period of drying, the difference between D_{eff} and $D_{eff,m}$ is negligible, but increases at the second period. The reason for this increase is the higher shrinkage in sample volume during this period, see Figure 2. 14 (a). Based on this plot, shrinkage should be considered towards the end of drying curve.

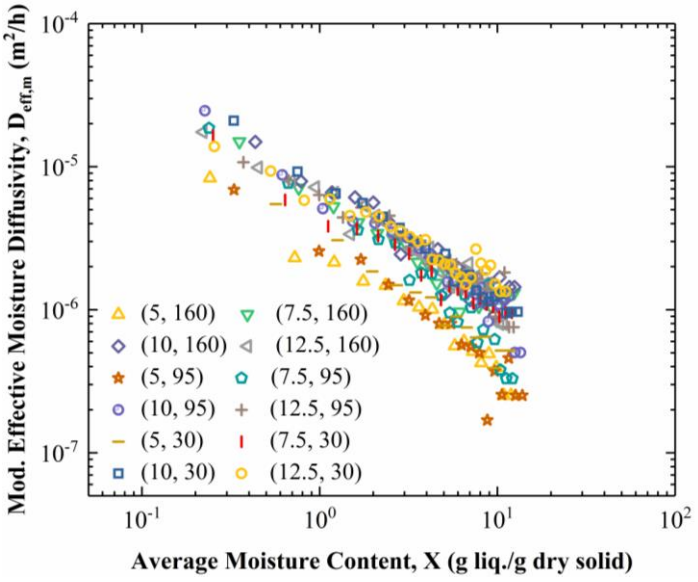

(a)

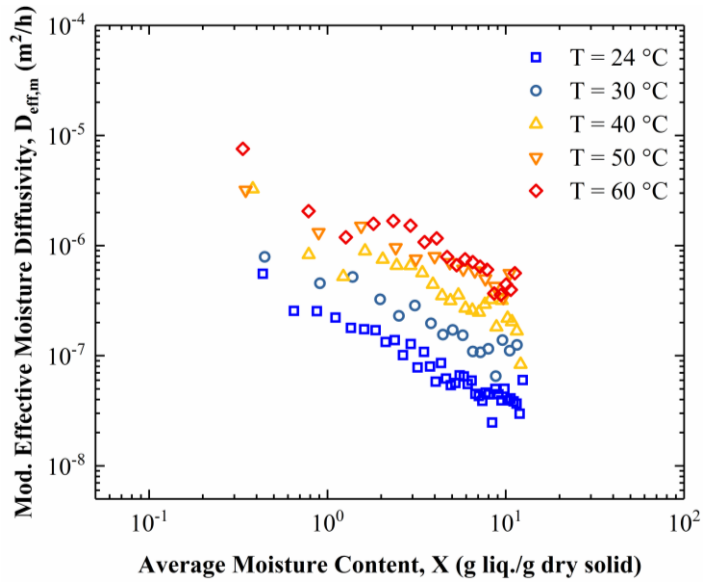

(b)

Figure 3. 8 Modified effective moisture diffusivity for **(a)** samples with initial thickness of $Z_0 = 5.0$ to *12.5 mm* and initial diameter of $D_0 = 52$ *mm* as well as substrates with $\theta \approx 30°, 95°$, and *160°* and **(b)** samples with initial thickness of $Z_0 = 5$ *mm* and initial diameter of $D_0 = 52$ *mm* as well as substrates with θ ≈ 160° and temperature of $T = 24 – 60$ *℃*. The first number in the parenthesis is initial sample thickness in mm and the second number is substrate contact angle in degree.

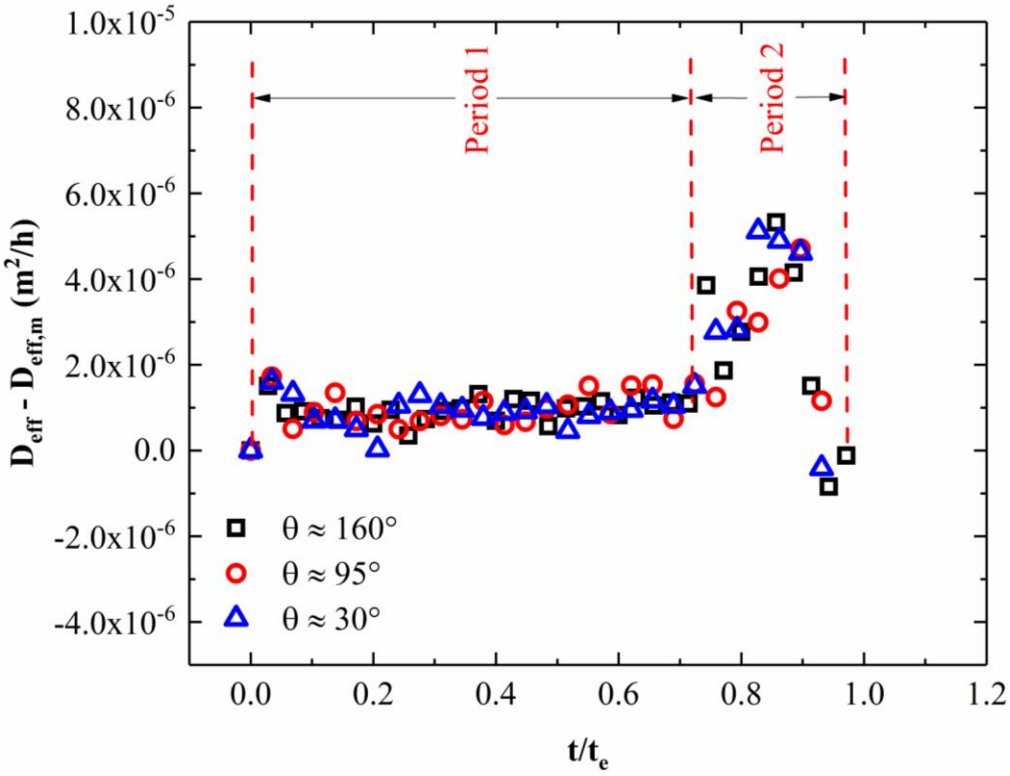

Figure 3. 9 The difference between effective moisture diffusivity and modified effective moisture diffusivity during drying for samples with initial thickness of Z_0 = *12.5 mm* and initial diameter of D_0 = *52 mm* as well as substrates with $\theta \approx 30°$, *95 °*, and *160 °*. t_e is the end of drying time.

3.4.2 Sample Thickness as well as Substrate Wettability and Temperature

From equation (3. 15), we can note that effective moisture diffusivity is depended on two parameters:

(1) The size of sample (*i.e.* thickness);

(2) Slope of drying curve (*i.e.* drying conditions).

To show the effect of substrate wettability on the effective moisture diffusivity values, the average effective moisture diffusivity $(D_{eff})_{avg}$ is calculated by taking the mathematical mean of D_{eff}. As shown in Figure 3. 10 (a), for different wettability of substrates, the difference between the average effective moisture diffusivity values is not clear. For low initial sample thickness, average effective moisture diffusivity for all cases are close. While for higher initial thickness, there is some difference between the values of the average effective moisture diffusivities.

Generally, we can conclude from this figure that the value of average effective moisture diffusivity for Pickering foams system do not depend strongly on the substrate wettability, especially for smaller sample size (*i.e.* Z_0 = 5 mm).

Figure 3. 10 (b) showed that $(D_{eff})_{avg}$ increases linearly as substrate temperature increases.

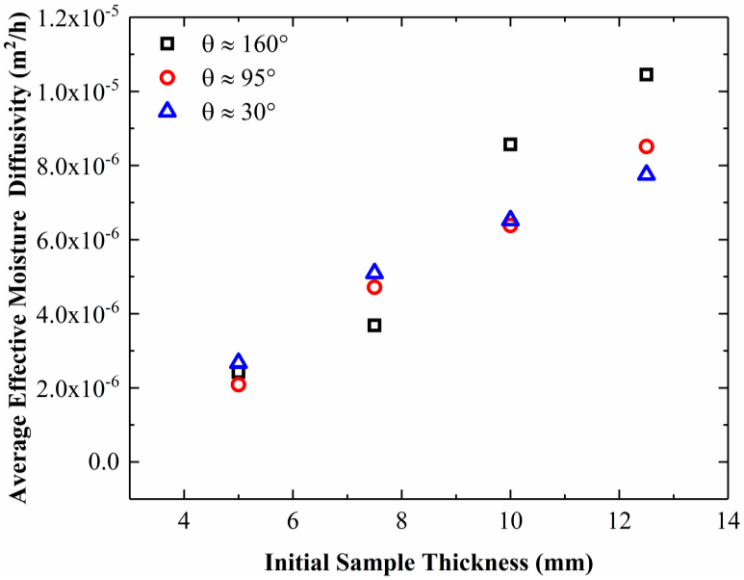

(a)

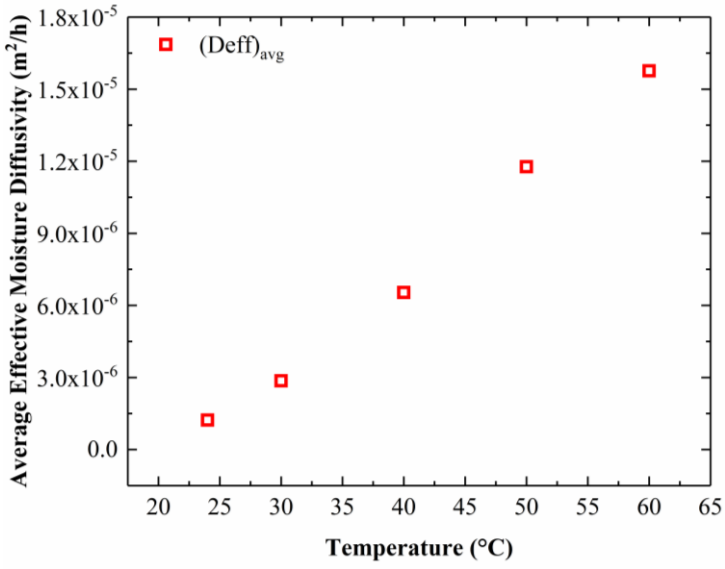

(b)

Figure 3. 10 Average effective moisture diffusivity (a) for samples with initial thickness of $Z_0 = 5.0$ to *12.5 mm* and initial diameter of $D_0 = 52$ *mm* as well as substrates with $\theta \approx 30°, 95°$, and $160°$ and (b) for samples with initial thickness of $Z_0 = 5$ *mm* and initial diameter of $D_0 = 52$ *mm* as well as substrates with $\theta \approx 160°$ and temperature of $T = 24$ - *60 ℃*.

3.4.3 Non Dimensional Form

We non-dimensionalized the effective moisture diffusivities for all samples under different drying conditions by noting the available groups in equations (3. 10) and (3. 28). We define the Fourier number of diffusion (F) and modified Fourier number of diffusion (F_m) as [89, 90]:

$$F = \frac{D_{eff}t}{Z^2} \tag{3. 33}$$

$$F_m = \frac{D_{eff,m}t}{Z^2} \tag{3. 34}$$

here Z is sample thickness at any time. As demonstrated in Figure 3.11and Figure 3.12, for all the trial under different drying conditions, we see that the diffusivity curves collapse on a *master curve*. Also, we note from these figures that the value of Fourier number of diffusion is increased as fractional average moisture content/modified fractional average moisture content decrease. See appendix B for more cases of non-dimensional diffusivities.

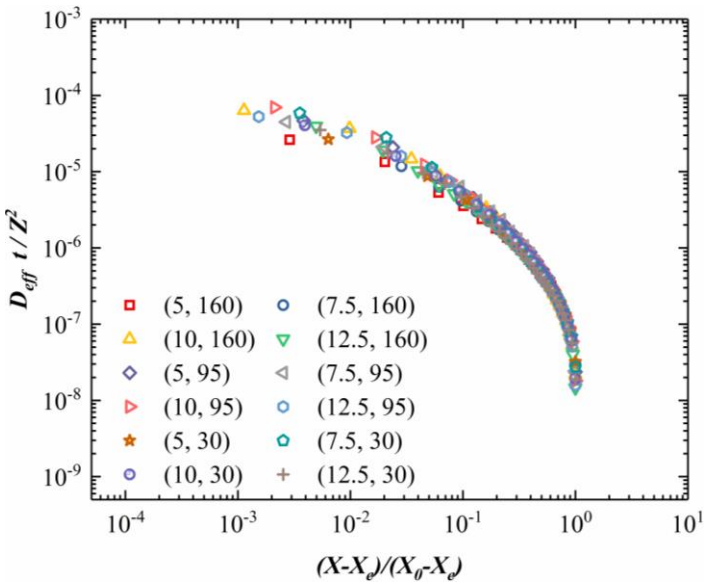

(a)

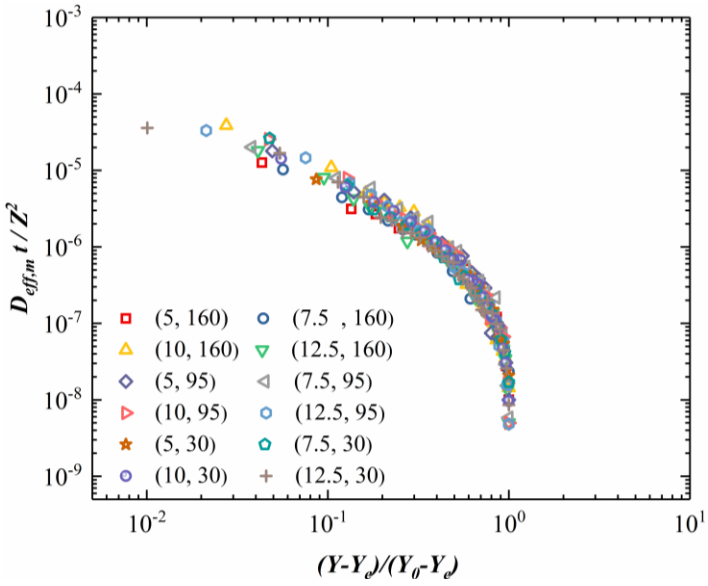

(b)

Figure 3.11 Non-dimensionalized form for liquid diffusion in Pickering foam for samples with initial thickness of Z_0 = *5.0 - 12.5 mm* and initial diameter of D_0 = *52 mm* as well as substrates with $\theta \approx$ *30 °, 95 °,* and *160 °* **(a)** Fourier number of diffusion vs. fractional average moisture content and **(b)** Modified Fourier number of diffusion vs. modified fractional average moisture content. The first number in the parenthesis is initial sample thickness in mm and the second number is substrate contact angle in degree.

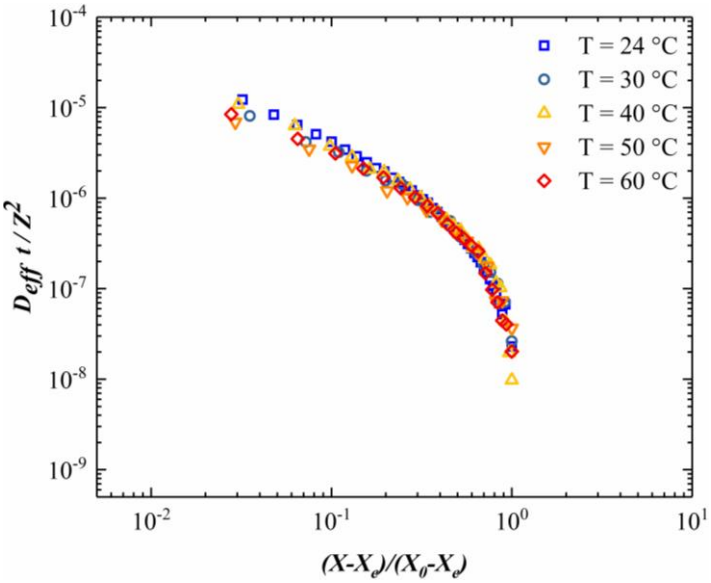

(a)

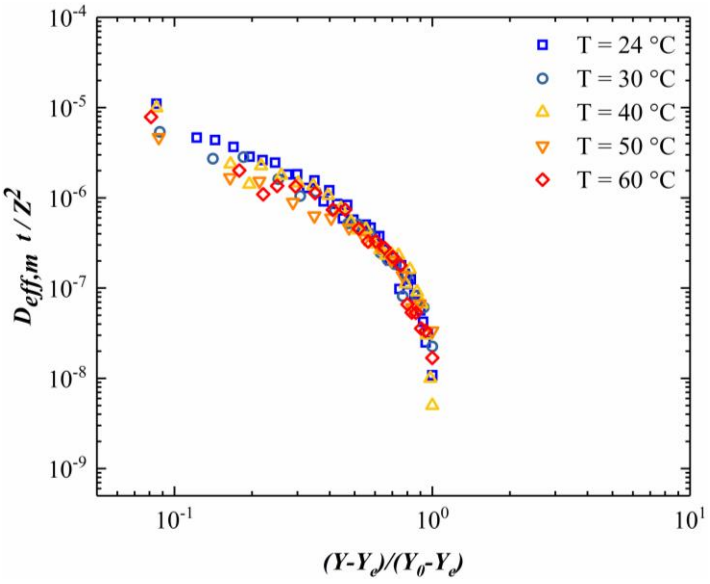

(b)

Figure 3.12 Non-dimensionalized form for liquid diffusion in Pickering foam for samples with initial thickness of $Z_0 = 5\ mm$ and initial diameter of $D_0 = 52\ mm$ as well as substrates with $\theta \approx 160°$ and temperature of $T = 24 - 60\ ℃$ **(a)** Fourier number of diffusion vs. fractional average moisture content and **(b)** Modified Fourier number of diffusion vs. modified fractional average moisture content.

3.5 Summary

In conclusions, using the drying curves and by employing the *method of slope*, the effective moisture diffusivity and modified effective moisture diffusivity are estimated as a function of average moisture content. The difference between these diffusivities is calculated then discussed in this chapter. We recommend to include the effect of sample shrinkage on the effective moisture diffusivity calculation of Pickering foams during the drying process under all drying conditions. The value of effective moisture diffusivity is decreased as average moisture content increase due to the change in sample morphology (porosity). Both initial sample thickness and substrate temperature influence the values of average effective moisture diffusivity. As initial sample thickness and substrate temperature increase, the effective moisture diffusivity and modified effective moisture diffusivity are increased too. In other hand, neither sample shape nor MWCNTs concentration are not effected strongly on the effective moisture diffusivity or modified effective moisture diffusivity. Finally, we non-dimensionalized the diffusivities and showed that diffusivities collapsed on a master curve under all drying conditions.

Chapter 4

Crack Formation

4.1 Introduction

Pickering foams, as well as most of multiphase porous materials, are likely to deform (or shrink) during drying process. This phenomenon sometime leads to samples crack (or fragment) over time. The probability of crack formation depends on the drying conditions (*i.e.* drying rate), substrate wettability, and on the mechanical properties of sample. In Pickering foams system, the change in sample volume during drying is depended on the values of adhesive force and cohesive force, which force is dominate. These forces can be viewed in more detail.

Adhesive force is an interface characteristic between external substrate and sample particles [61]. This force prevents samples shrinkage through drying processes (resist capillary stress). The value of adhesive force is depended on the contact area between sample and substrate. Lower substrate wettability value (higher contact area between sample and substrate) leads to higher adhesion force value and vice versa. However, cohesive force is an interior characteristic between sample particles. This force causes sample shrinkage during drying processes. To get dry sample with no crack, the adhesive force should be less than the cohesive force as shown in Figure 4. 1.

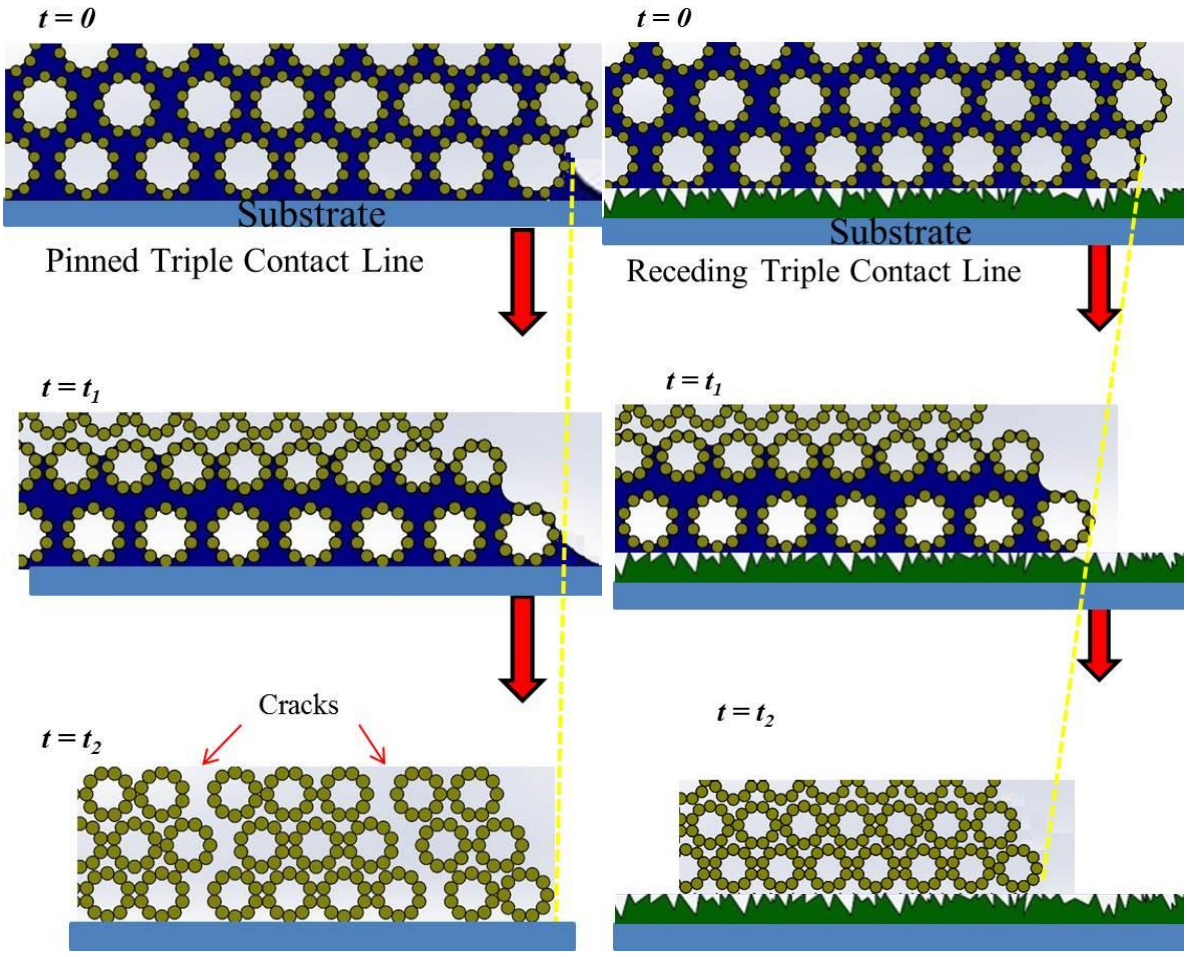

Wenzel State **Cassie State**

(a) **(b)**

Figure 4. 1 Schematic illustration of Pickering foam aging at **(a)** high adhesive force hydrophilic substrate (glass), in this case the value of adhesive force is greater than the cohesive force and **(b)** low adhesive force super hydrophobic substrate (modified glass), in this case the adhesive force is less than the cohesive force.

As shown in Figure 4. 1 (a), the *liquid-solid-gas triple contact line* is pinned so the adhesive force between sample and substrate, which is glass in this case, is higher than the cohesive force. As aresults, the crack is appeared on the upper surface. Obviously, it is noted that sample edge is hold/stacked with the substrate over time. On the contrary, the *liquid-solid-gas triple contact line* is receding, see Figure 4. 1 (b), so the adhesive force between sample and substrate (which is modified glass in this case) is less than the cohesive force. As a result, no crack occurs on the upper surface of sample. We can note how the edge is hold/stacked and substrate (which is modified glass in this case) is less than the cohesive force. This case called *Cassie state* [91]. As a result, no crack is occurs on the upper surface of sample. Obviously, we can note how the edge of sample is moves freely over time. The value of cohesive force depends on the capillary pressure between the particles inside the sample. One can calculate the magnitude of capillary pressure between any two particles by using the following equation [66, 92, 93]:

$$p_{cap} = -\frac{2 * \gamma_{LG}}{r_m} \qquad (4.\ 1)$$

In equation (4. 1) p_{cap} is the capillary pressure γ_{LG} is the surface tension between the liquid and gas, and r_m is the radius of nanomenisci curvature between solid particles. We can calculate the minimum radius of nanomenisci through drying from the following equation [94]:

$$r_m = 0.15 * r_p \qquad (4.\ 2)$$

In above equation r_p is the radius of particle. By using the previous equations, we can calculate the maximum value of capillary pressure to be around *-77 atm.*, particle diameter of *250 nm*. The negative sign means the direction of capillary pressure is inward, this causing shrinkage.

Figure 4. 2 shows the nanomenisci radius evolution during drying, where it decreases as drying time increases. At the beginning, the nanomenisci shape looks flat, low capillary pressure, but after short period it starts to deform due to evaporation, capillary stress starts increase due to the decrease in the radius of menisci. Furthermore, the of initial sample thickness influences the volume change of aqueous foam. Capillary force depends on the sample thickness (cross section area) [64, 95, 96] so thicker samples give higher capillary forces.

Fundamental Questions

(1) What is the effect of substrate wettability and temperature on the crack formation in samples during drying process?

(2) What is the effect of initial sample thickness and shape on crack pattern?

(3) Do MWCNTs prevent crack formation in composite foams (*i.e.* PVDF/MWCNTs).

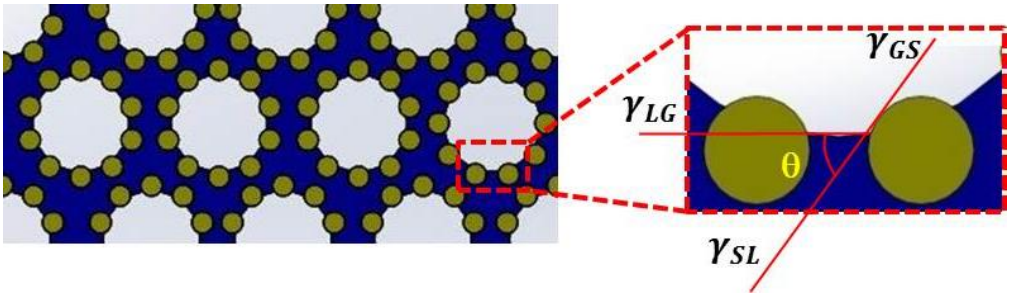

(a)

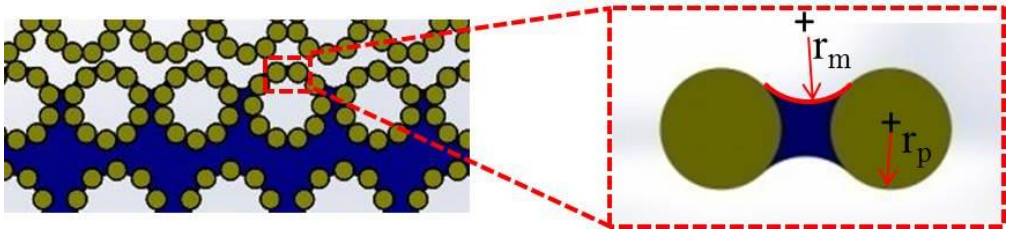

(b)

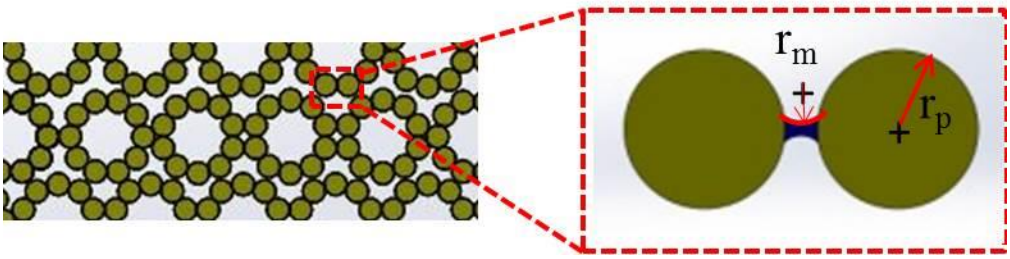

(c)

Figure 4. 2 The evolution in nanomenisci shape during drying of Pickering foam: **(a)** fully wet, **(b)** partially wet, and **(c)** almost dry.

4.2 Crack Formation

The effects of initial sample thickness and shape, substrate wettability and temperature, and MWCNTs concentration on crack formation is presented in this section.

4.2.1 Substrate Wettability

Figure 4. 3 demonstrates the sequence of drying for an initial sample thickness of 5 mm on three different substrates. As drying proceeds, cracks began to appear in some samples and spread outward to the edge. We note that as substrate wettability decreases, crack formation is prohibited. This means that samples drying on superhydrophobic substrates remain crack-free; an important feature from a manufacturing point of view. A superhydrophobic substrate has low surface energy (*i.e.* weak adhesive interactions) and as such can relax the capillary-induced stresses as they form during the drying. On the contrary, a hydrophilic substrate facilitates adhesion between the sample and the substrate; the resulting capillary-induced stresses therefore cannot get relaxed. When such stresses overcome the mechanical integrity of the samples, cracks are formed and propagate.

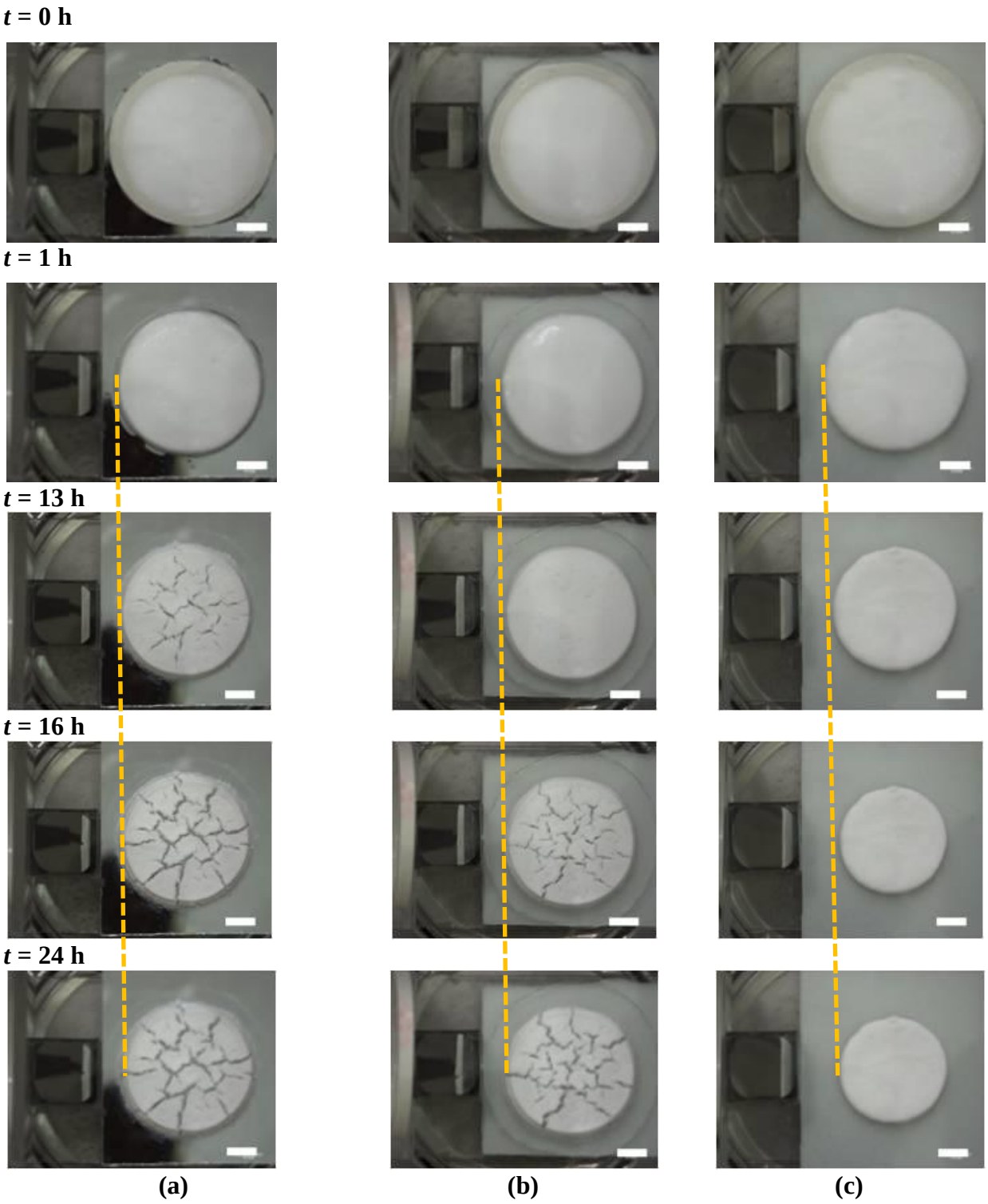

Figure 4. 3 The effect of substrate wettability on the crack formation behavior of sample with initial thickness of $Z_0 = 5\ mm$ and initial diameter of $D_0 = 52\ mm$ as well as substrates with: **(a)** $\theta \approx 30°$, **(b)** $\theta \approx 95°$, and **(c)** $\theta \approx 160°$. Each point contains a portion of the side-view (left) and top-view (right) of the sample. Scale bar is 10 mm.

4.2.2 Substrate Temperature

To examine the effect of drying rate on the probability of cracking during drying process, five different temperatures were tested in this study as shown in Figure 4. 4, see appendix B. Increasing the substrate temperature reduces crack density as well as the required time for samples to reach the end of drying.

Figure 4. 5 (a) shows the final crack pattern for *5 mm* initial thick sample and *52 mm* initial diameter for five different temperaturs. Coresponding drying curves are shown in Figure 4. 5 (b). An interesting observation is that the point where cracks occurs begin to form happens at the same value of fractional average moisture content for all cases irresptive of substrate temperature.

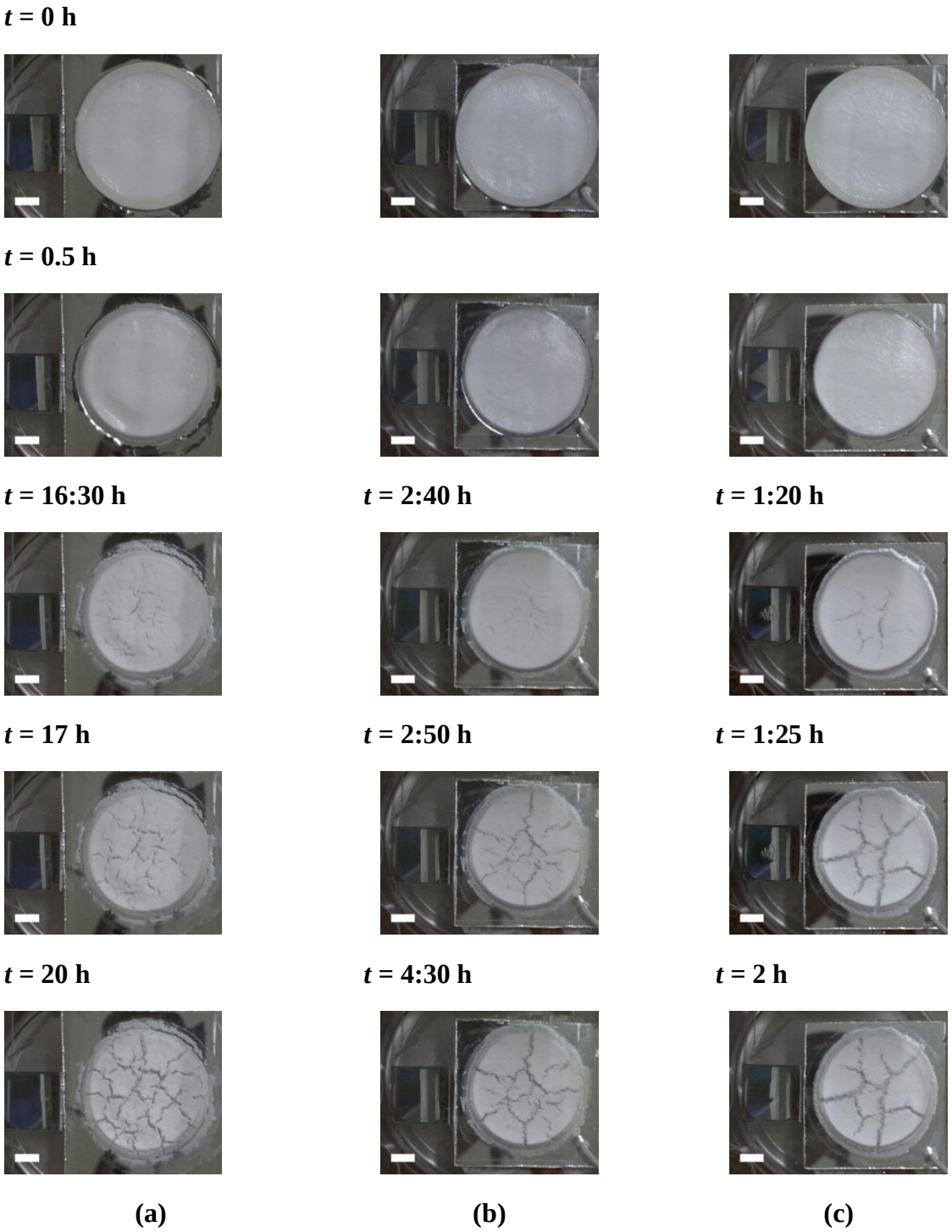

Figure 4. 4 The effect of substrate temperature on the crack formation behavior of sample with initial thickness of $Z_0 = 5\ mm$ and initial diameter of $D_0 = 52\ mm$ as well as substrate with $\theta \approx 30°$ and temperature of: **(a)** $T = 24\ ℃$, **(b)** $T = 40\ ℃$, and **(c)** $T = 60\ ℃$. Each picture contains a portion of the side-view (left) and top-view (right) of the sample. Scale bar is 10 mm.

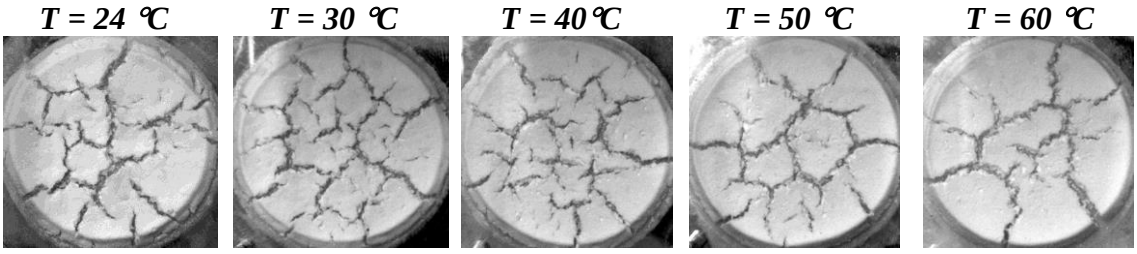

(a)

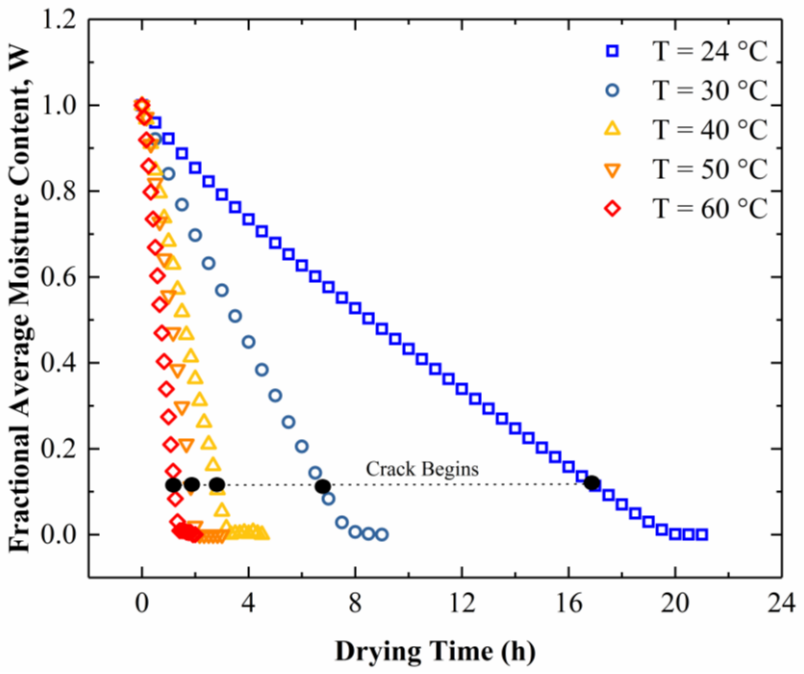

(b)

Figure 4. 5 (a) Final crack patterns for sample with initial thickness of $Z_0 = 5\ mm$ and initial diameter of $D_0 = 52\ mm$ as well as substrate with $\theta \approx 95°$ (*i.e.* PDMS) and temperature of $T = 24 - 60\ ℃$ and **(b)** drying curves for samples on five different temperaures. As shown, crack begins at same fractional averge moisture content.

4.2.3 Sample Thickness

For three substrates types and six initial sample thicknesses, crack formation depends on the substrate wettability and the initial sample thickness as demonstrated in Figure 4. 6. Under the given drying conditions (chamber temperature of 22 ± 1 ℃ and relative humidity of 46 ± 5 %), there seems to be an initial sample thickness after which visible cracks are not formed. In addition, like those shown in Figure 4. 7, cracked samples become fragmented on hydrophilic and partially hydrophobic substrates, resulting in faster drying times.

We also note that there exists a deposition of unbounded particles on some substrates (see Figure 4. 3 $\theta \approx 30°$) due to gravity-induced drainage. Simply put, not all the particles may find the opportunity to adsorb at the liquid-gas interfaces during the foaming process. The un-adsorbed particles remain suspended in the liquid film between neighboring bubbles and in Plateau borders and get deposited on the substrate as they leave the foam along with the excess drained liquid. Such particle deposited residue is absent for the superhydrophobic substrate, since drained liquid is forced to remain contained inside the sample.

As a predictive tool, we have determined the time when the initial crack begins to appear as a function of sample thickness as shown in Figure 4. 7. The data shows a linear trend for the hydrophilic and partially hydrophobic substrates, which may suggest (given possible measurement errors) that the crack initiation time is independent of the substrate type.

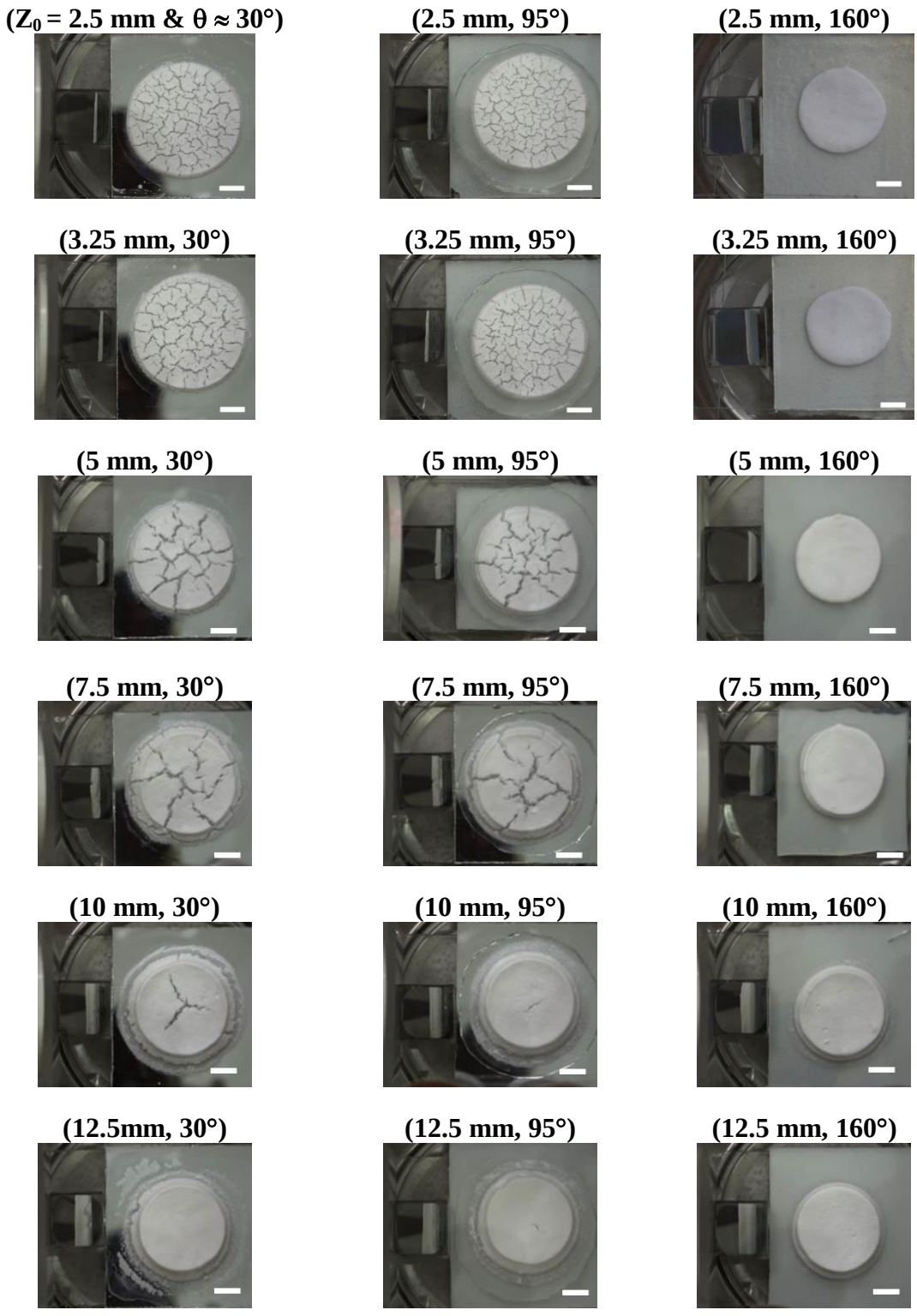

Figure 4. 6 The effect of contact angle and initial sample thickness on the crack behavior of samples at the end of drying. Each picture contains a portion of the side-view (left) and top-view (right) of the sample. Scale bar is 10 mm.

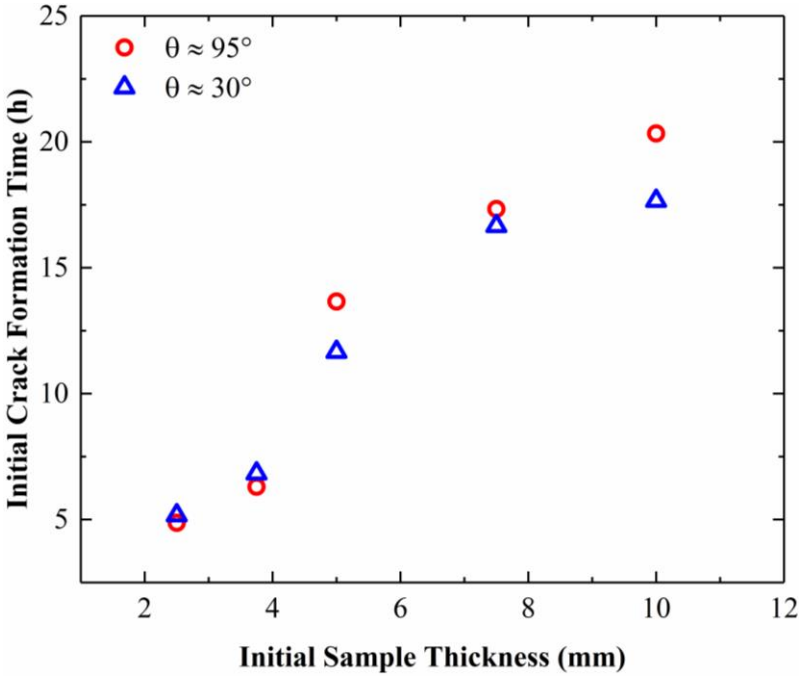

Figure 4. 7 Initial crack formation time versus initial sample thickness of Z_0 = *2.5 - 10 mm* and initial diameter of D_0 = *52 mm* as well as substrates with $\theta \approx 30°$ and $95°$.

4.2.4 Sample Shape

To examine the effect of sample shape on crack formation during drying process, three different shapes were examined in this study as shown in Figure 4. 8. The surface area of all samples is equal. The dimension of samples are: circle with thickness of $Z_0 = 5$ *mm and* diameter of $D_0 = 34$ *mm*, square with thickness of $Z_0 = 5$ *mm and* length of $L_0 = 30.13$ *mm*, and triangle with thickness of $Z_0 = 5$ *mm and* base of $B_0 = 45.79$ *mm* and height of $H_0 = 39.66$ *mm*. all samples are dried at laborotary conditions.

Our observations show that cracks in square and triangle extend to the sides. This is surprising as sharp corners are usually the source of stress concentrations. We also note that cracks in square sample begin sooner than other shapes.

Two points of interest are marked in Figure 4. 9. The first point shows where the crack begins for samples with different shapes. The second point of interest shows that crack starts around at the same value of fractional average moisture content for all tests. That means the probability of sample cracking does not depend on the sample shape. See Appendix C for more cases of drying conditions.

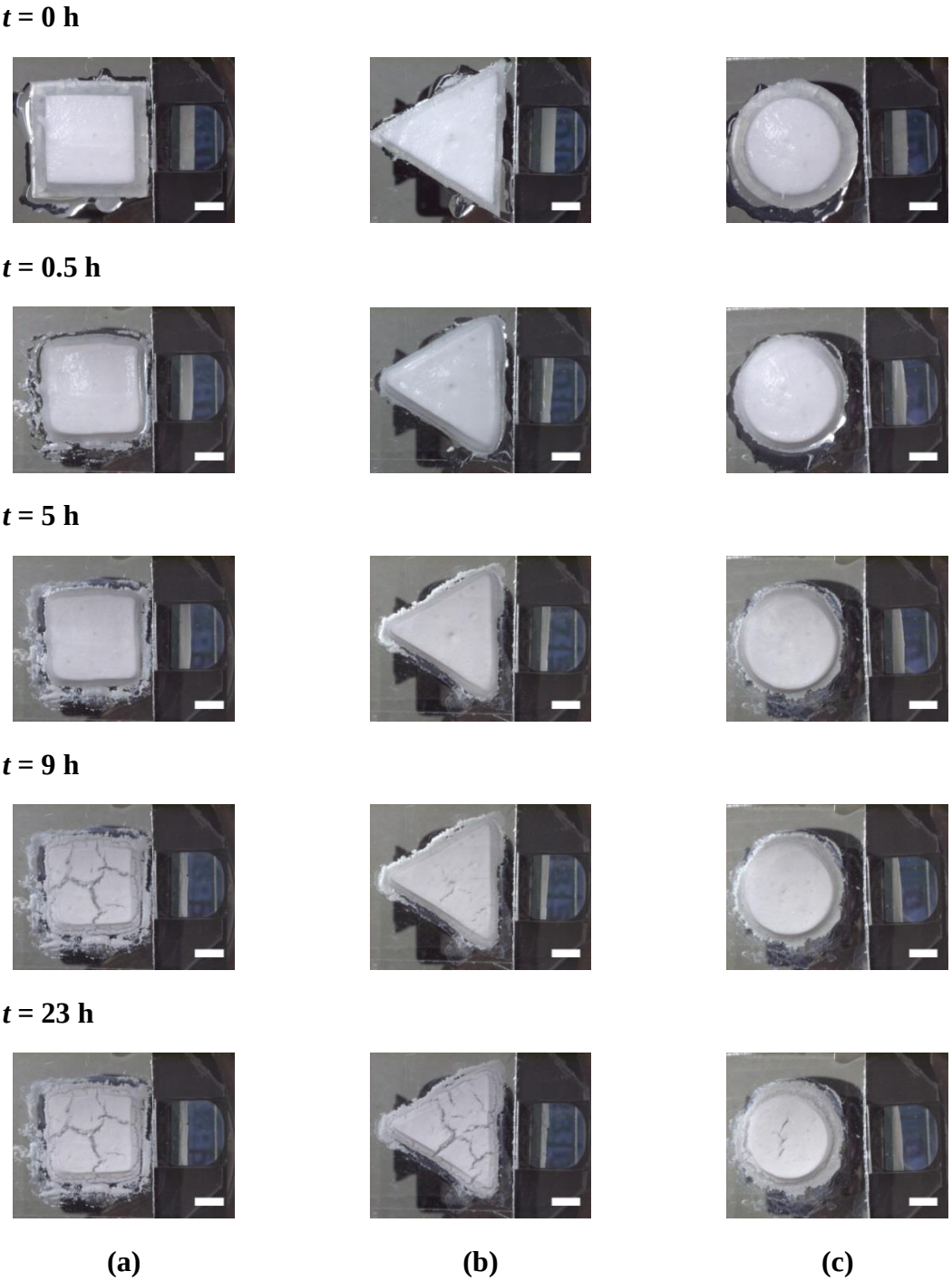

Figure 4. 8 The effect of sample shapes on the crack formation behavior of sample with initial thickness of $Z_0 = 5.0\ mm$ and substrates with $\theta \approx 30°$ and temperature of: **(a)** *square*, **(b)** *triangle*, and **(c)** *circle*. Each picture contains a portion of the side-view (right) and top-view (lift) of the sample. The surface area of all samples is equal. The initial dimension of samples are: circle with diameter of $D_0 = 34\ mm$, square with length of $L_0 = 30.13\ mm$, and triangle with base of $B_0 = 45.79\ mm$ and height of $H_0 = 39.66\ mm$. Scale bar is 10 mm.

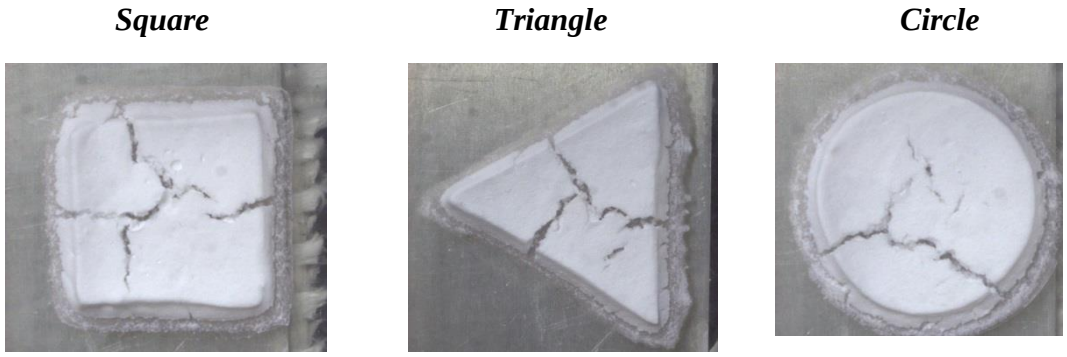

(a)

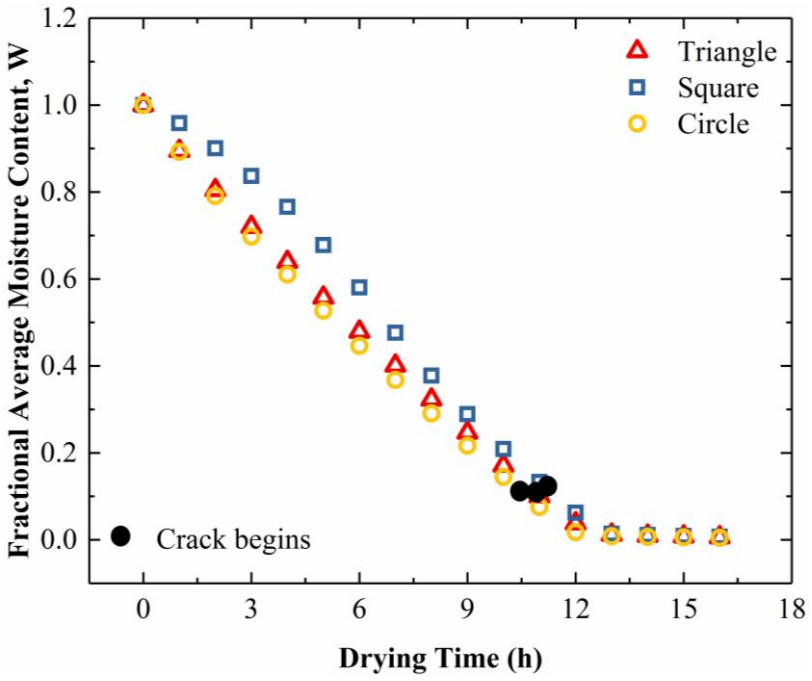

(b)

Figure 4. 9 (a) Final crack patterns in sample of initial thickness $Z_0 = 5\ mm$ with different shape located over PDMS substrate (*i.e.* $\theta \approx 95°$) and **(b)** drying curves for three different shapes. Note that cracks initiaton happens at the same fractional average moisture content for all three shapes.

4.2.5 Composite PVDF/MWCNTs Foams

To examine the effect of multi-walled carbon nanotubes concentration (C_{MWCNTs}) on the probability of crack density (or pattern) during drying process, three different concentrations of MWCNTs are selected in this study. As shown in Figure 4. 10, the crack density is increased as MWCMTs concentration increase. The increase in crack density maybe due to the increase in the viscosity of the suspension. The increase in the suspension viscosity results in increase of the adhesion between the sample and substrate so the probability of the crack is increased. That means the probability of sample cracking depends strongly on the concentration of the MWCNTs. Also, a previous studies found that increasing the concentration of MWCNTs decreases the mechanical strength of the sample due to the lack of adequate PVDF-MWCNTs bonding [71].

Two points of interest are marked in Figure 4. 11. The first point shows where crack begins for samples with different concentration of multi walled carbon nano tubes. The second point shows as MWCNTs concentration increase the crack initiate early during drying process. The crack begins at fractional average moisture content around 0.1 in the case of lower concentration (*i.e.* $C_{MWCNTs} = 0\ \%\ v/v$), while the crack begins at fractional average moisture content around 0.2 in the case of higher concentration (*i.e.* $C_{MWCNTs} = 0.5\ \%\ v/v$). See Appendix C for more experiments.

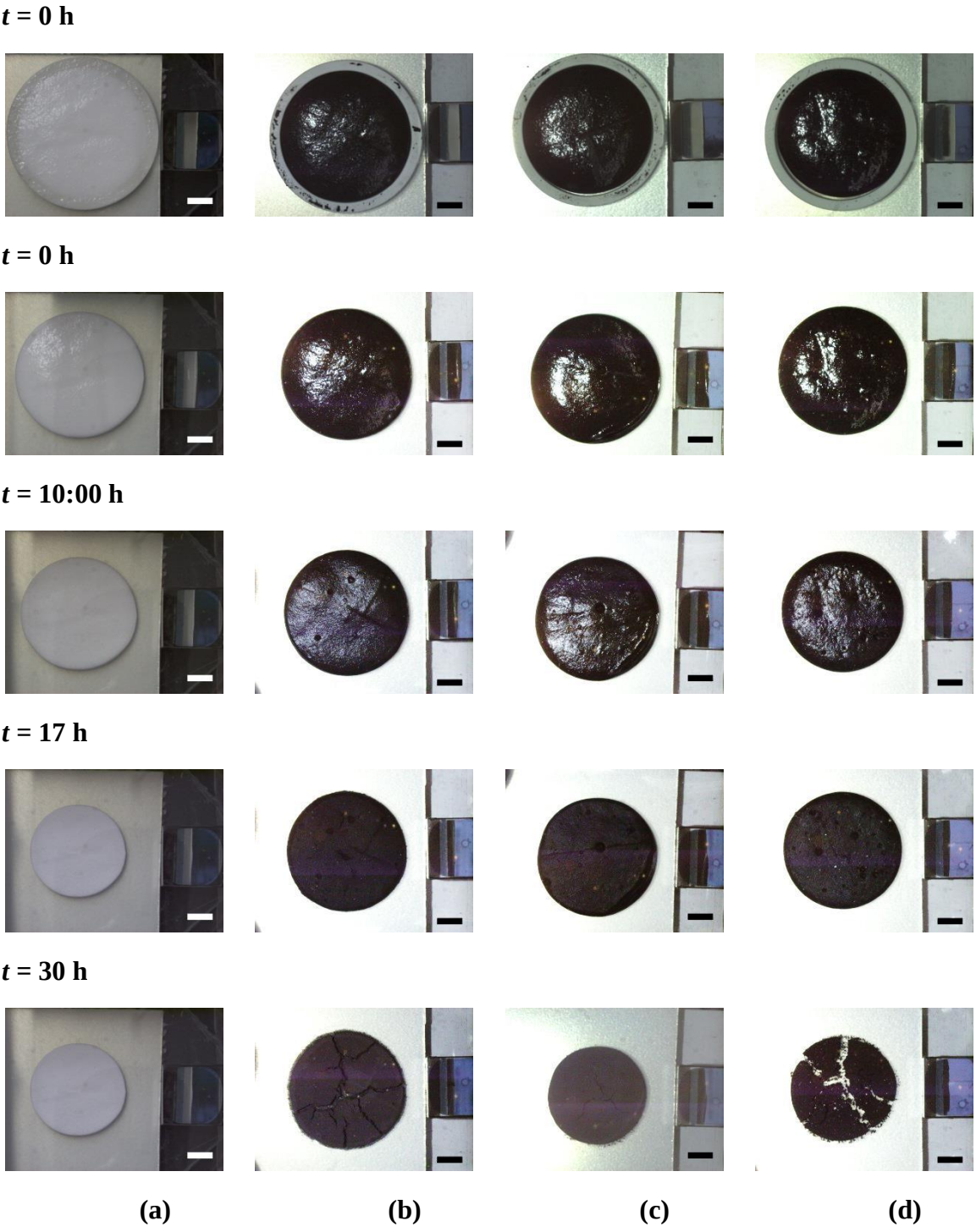

Figure 4. 10 The effect of MWCNTs concentration on the crack formation behavior of sample with initial thickness of $Z_0 = 5\ mm$ and initial diameter of $D_0 = 52\ mm$ as well as substrates with $\theta \approx 160°$ at: **(a)** $C_{MWCNTs} = 0\ \%\ v/v$, **(b)** $C_{MWCNTs} = 0.1\ \%\ v/v$, **(c)** $C_{MWCNTs} = 0.3\ \%\ v/v$, and **(d)** $C_{MWCNTs} = 0.5\ \%\ v/v$. Each picture contains a portion of the side-view (right) and top-view (left) of the sample. Scale bar is 10 mm.

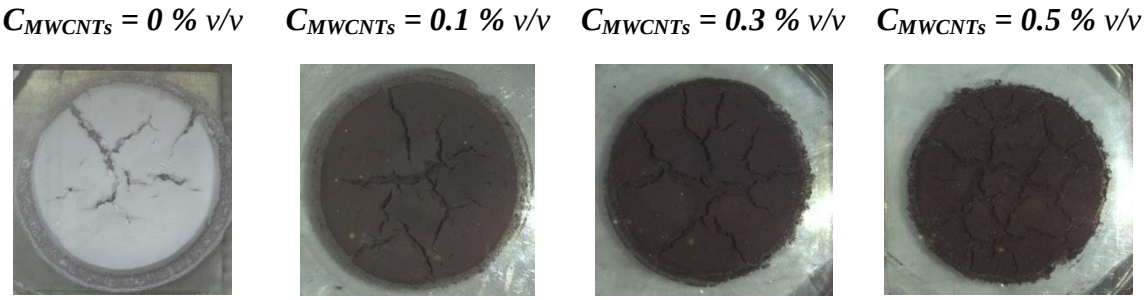

(a)

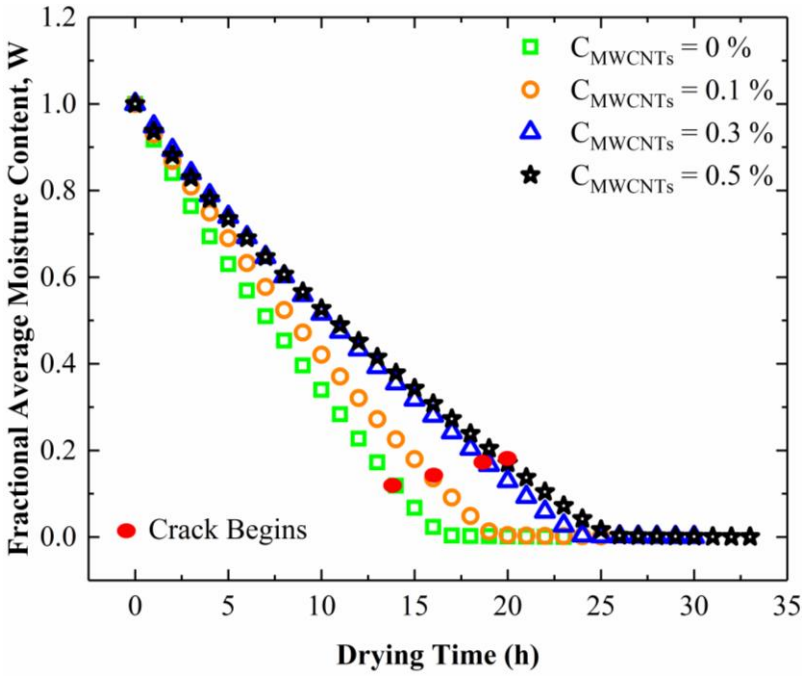

(b)

Figure 4. 11 (a) Final crack patterns in sample with initial thickness of $Z_0 = 5\ mm$ and initial diameter of $D_0 = 52\ mm$ as well as substrate with $\theta \approx 95°$ (*i.e.* PDMS) and various MWCNTs concentration of $C_{MWCNTs} = 0 - 0.5\ \%$ **(b)** drying curves for four different concentration of MWCNTs. Note that cracks initiaton happens at the different fractional average moisture content.

Scanning electron microgarph (SEM) images for PVDF foams and PVDF/MWCNTs composite foams are shown in Figure 4. 12. The effect of MWCNTs on the morphology of the sample is evident. Firstly, adding MWCNTs cause defects on the walls of the bubbles. Secondly, they result in change in bubble size. Average bubble diameter goes from around 80 μm for samples with no MWCNTs (*i.e.* PVDF foams)to around 40 μm for those with MWCNTs (*i.e.* PVDF/MWCNTs composite foams).

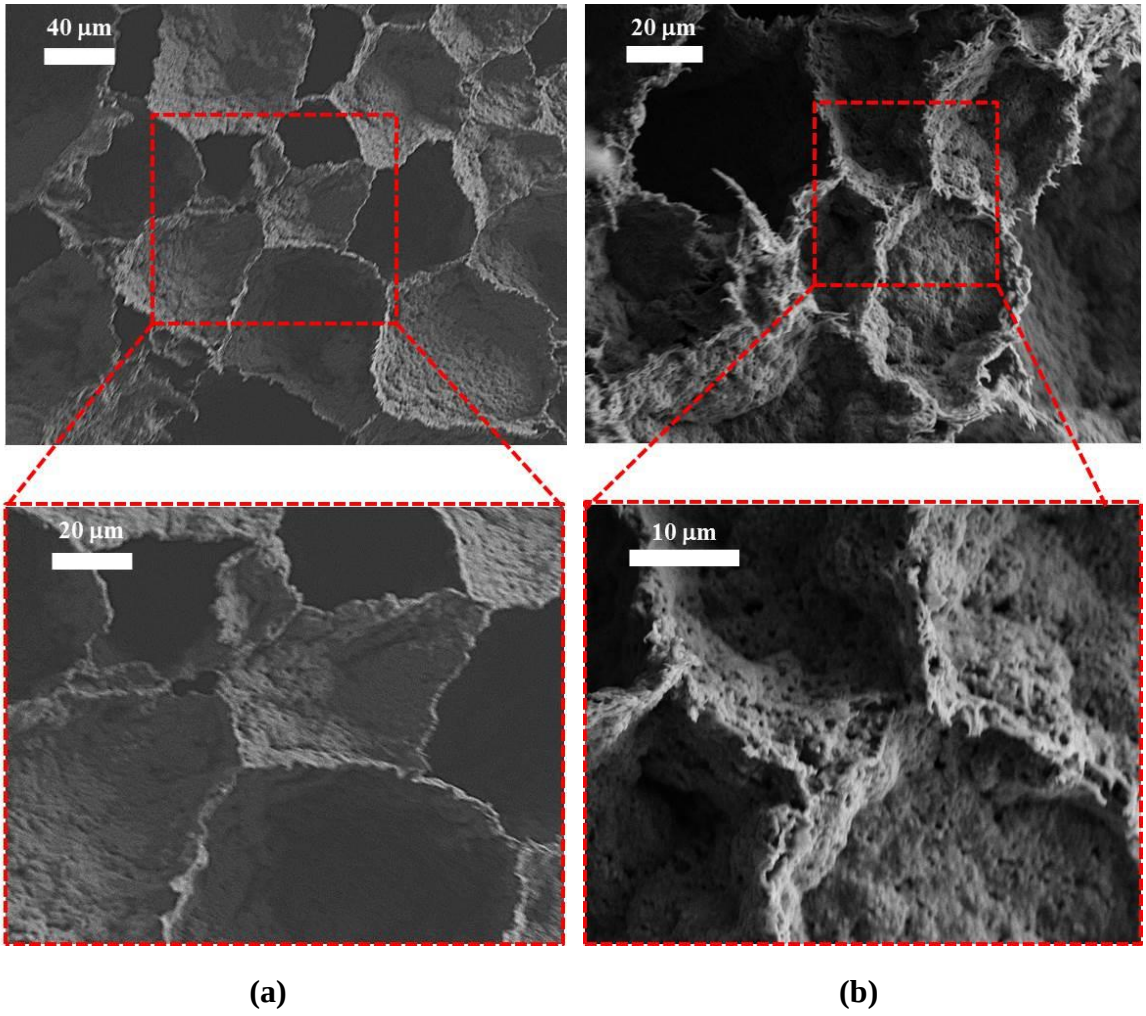

Figure 4. 12 Scanning electron micrograph (SEM) images taken of the sintered **(a)** un-cracked solid foams and **(b)** cracked solid composite foams with MWCNTs (C_{MWCNTs} = *0.3 % v/v*). These samples are dried over superhydrophobic substrate (*i.e.* $\theta \approx 160°$).

4.3 Summary

Dry porous PVDF particle stabilized foams with no cracks (or defect) have been produced by tuning the hydrophobicity of substrate, initial sample thickness, and controlling drying conditions (or drying rate). By keeping the cohesion force of Pickering foam samples greater than the adhesion force, the creation of crack (or defects) in samples are decrease. In this work also, we have been reported that dry samples with no crack can produce by using low-adhesive superhydrophobic substrate (*i.e.* modified glass). The critical cracking thickness (CCT) for samples located on both PDMS and glass substrates have been found (*CCT = 12.5 mm*). Loading MWCNTs with different concentration increase the crack formation for all types of substrates. Where, the crack formation increases as MWCNTs concentrations increase, as well. Finally both sample shape and substrate temperature have not prevented crack formation during drying drocess but they influence crack pattern.

Chapter 5

Conclusions

5.1 Conclusions

The drying curves as well as the required drying time (*i.e.* end of drying point) are determined for Pickering foams samples under all drying conditions. In addition, the evaluation in Pickering foams size during drying is investigated. Generally, the Pickering foams have three steps during drying: reduction, expansion, and no change. By utilizing from the drying curves and sample volume, the effective moisture diffusivity and modified effective moisture diffusivity were estimated as a function of average moisture content (*method of slope* is used in this work). Where, the values of effective moisture diffusivity and modified effective moisture diffusivity are increased as average moisture content decrease due to the change in sample morphology such as porosity. Both initial sample thickness and substrate temperature result to increase the values of effective moisture diffusivity. While sample shape and multi-walled carbon nanotubes have not srong effect on the effective moisture diffusivity. We have been recommended include the sample shrinkage effect on the effective moisture diffusivity calculation during drying for Pickering foams system under all drying conditions. In conclusions, highly porous (*i.e.* low weight) PVDF particle stabilized foams with no crack (or defects) have been produced by tuning the hydrophobicity of substrate (*i.e.* contact angle), on one hand and controlling drying rates (*i.e.* substrate temperature) and adding MWCNTs have not

prevented this problem, on the other hand. By keeping the strength of Pickering foam samples less than the drying stress, the creation of crack in samples is decreased. Finally, we have been reported that dry samples with no crack can be manufacturing by using low-adhesive superhydrophobic substrate.

The research presented in this thesis is unique in that for the first time, to the best of our knowledge, effective moisture diffusivity is reported for drying of particle-stabilized foams. Such data can be used to numerically model this process which is currently unavailable in the literature. Combination of predictive models along with experimental values will enable design and fabrication of low-density/high-porosity porous materials using Pickering foam as precursor. This manufacturing approach is environmentally friendly, cost-effective, and does not require complex equipment and trained personnel.

Crack formation is a by-product of drying in many systems including the one we have investigated here, and they are detrimental to the integrity of the final product. In this thesis, we have presented a detailed investigation to understand and prevent crack-formation in dried Pickering foams. We show that substrate wettability plays an important role in relaxing the capillary-induced stresses that are responsible for crack formation. A superhydrophobic substrate prevents crack formation for a wide range of of initial foam thickness but causes the samples to undergo largest radial shrinkage. Other investigated parameters, such as substrate temperature and including nanofillers, influenced crack

pattern (density) but could not prohibit their formation.This dissertation shed some light on the complex transport phenomena during drying of Pickering foams. We hope that our findings ignite an interest in the scientific community to continue investigating the fascinating physics of drying and aging in relevant systems.

5.2 Future Work

- Exploring the influence of initial sample porosity on drying kinetics as well as crack formation behavior.
- Studying the effect of introducing functional multi-walled carbon nanotubes (FMWCNTs) on the drying kinetics and crack formation in Pickering foams.
- Predict numerically the concentration of moisture content inside the foams during the drying process by utilizing from the exist results (*e.g.* effective moisture diffusivity, average moisture content.

Appendix A

Drying Conditions

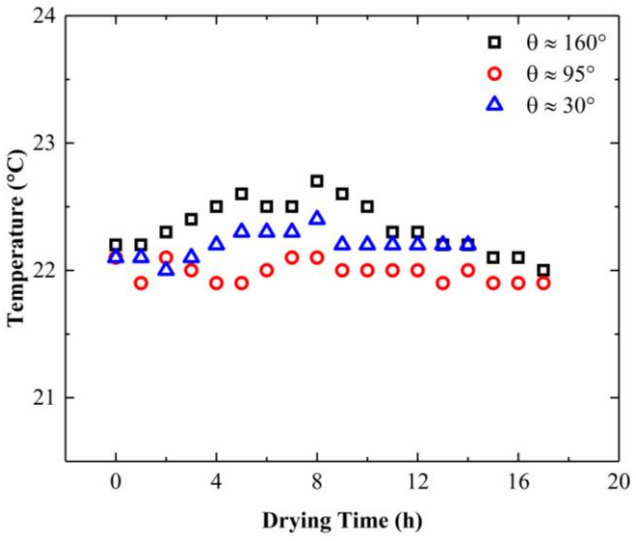

(a)

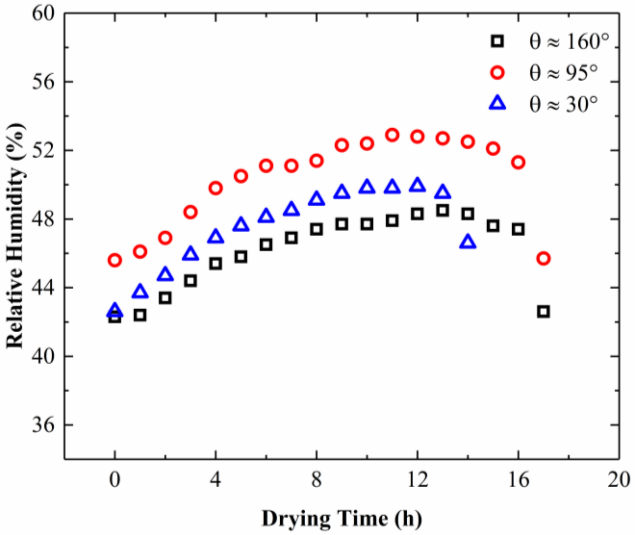

(b)

Figure A. 1 The drying conditions for samples with initial thickness of $Z_0 = 5\ mm$ and initial diameter of $D_0 = 52\ mm$ as well as substrates with $\theta \approx 160°, 95°,$ and $30°$ **(a)** temperature (T) and **(b)** relative humidity (Φ).

Appendix B

Diffusivity Curves

1. Average Moisture Content and Fractional Average Moisture Content

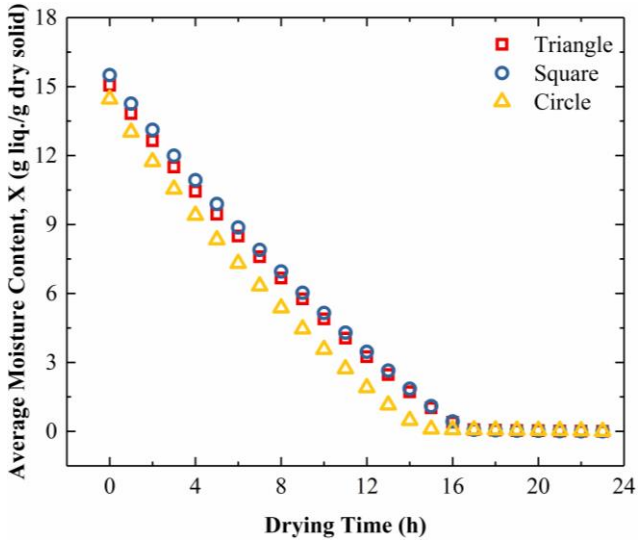

(a)

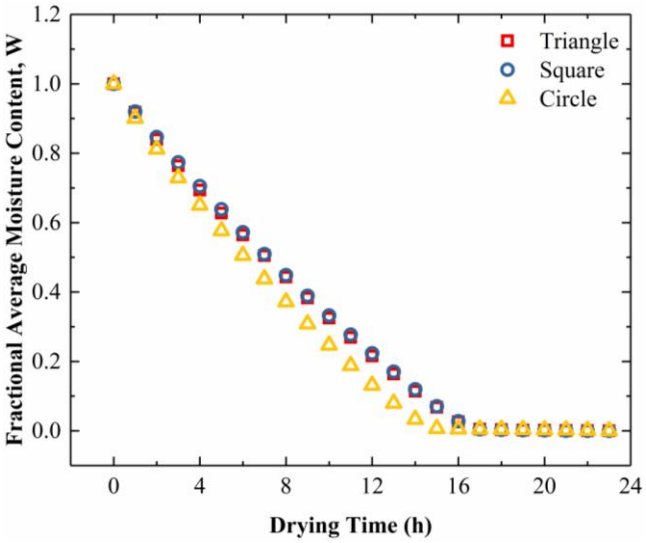

(b)

Figure B. 1 (a) Average moisture content and **(b)** fractional average moisture content for sample with three different shapes of samples and initial thickness of $Z_0 = 5\ mm$ and substrate with $\theta \approx 160°$.

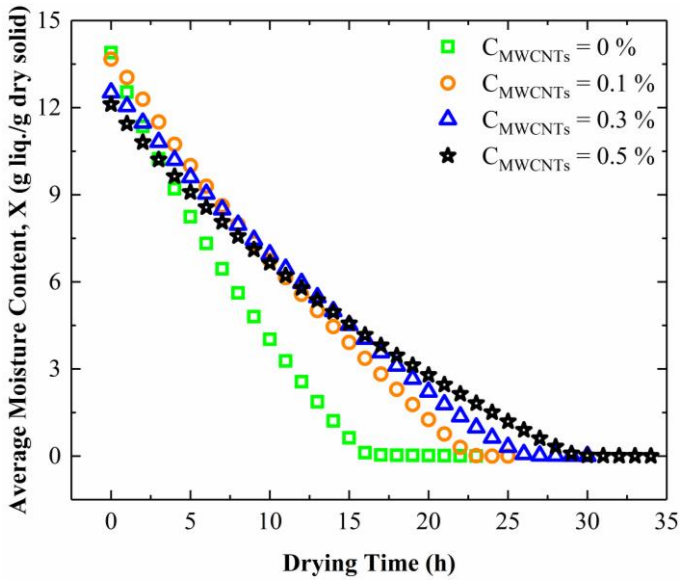

(a)

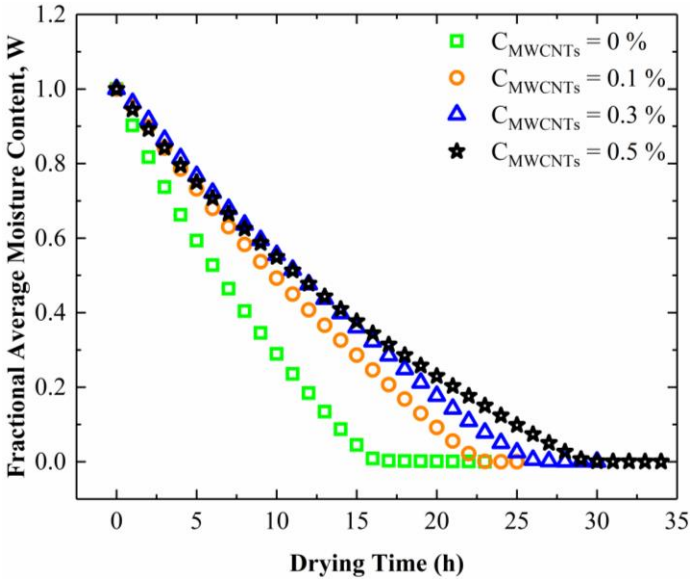

(b)

Figure B. 2 (a) Average moisture content and **(b)** fractional average moisture content for samples with initial thickness of $Z_0 = 5\ mm$ and initial diameter of $D_0 = 52\ mm$ as well as MWCNTs concentration of $C_{MWCNTs} = 0 - 0.5\ \%\ v/v$ on substrates with $\theta \approx 160°$.

2. Effective Moisture Diffusivity

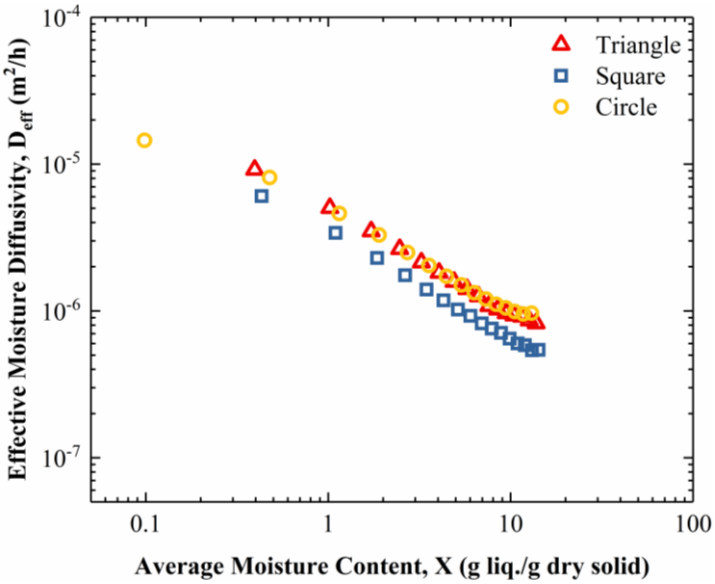

(a)

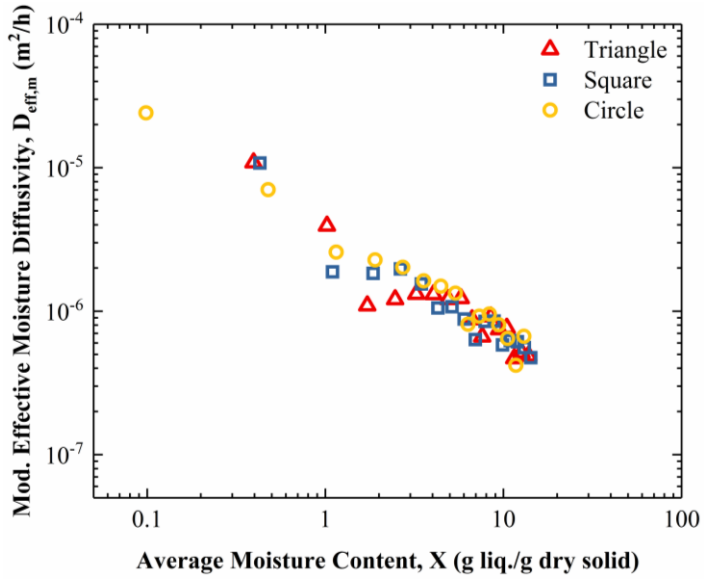

(b)

Figure B. 3 (a) Effective moisture diffusivity and **(b)** modified effective moisture diffusivity for samples with initial thickness of $Z_0 = 5.0\ mm$ and three different shapes and substrates with $\theta \approx 160°$.

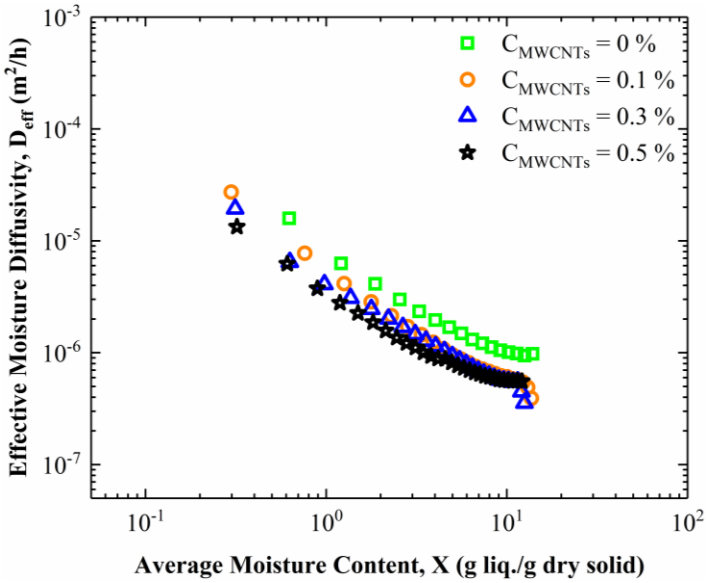

(a)

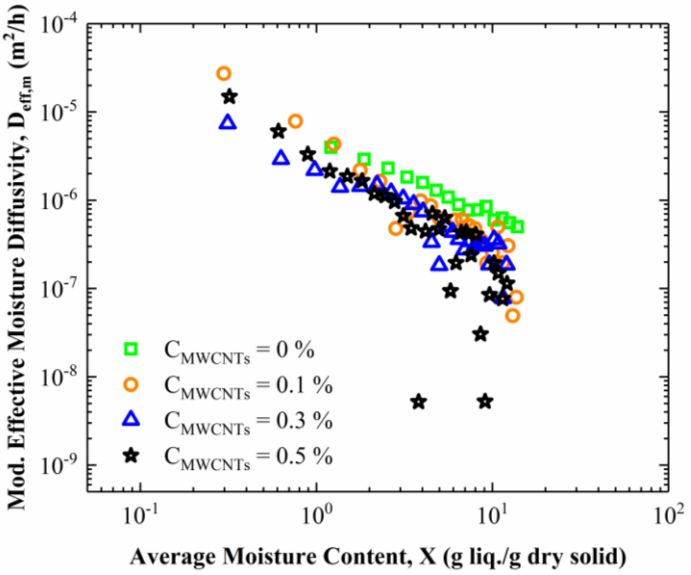

(b)

Figure B. 4 (a) Effective moisture diffusivity and **(b)** modified effective moisture diffusivity for samples with initial thickness of $Z_0 = 5$ *mm* and initial diameter of $D_0 = 52$ *mm* as well as different MWCNTs concentration of $C_{MWCNTs} = 0.0 - 0.5$ *% v/v* and substrates with $\theta \approx 160°$.

3. Non-Dimensional Curves

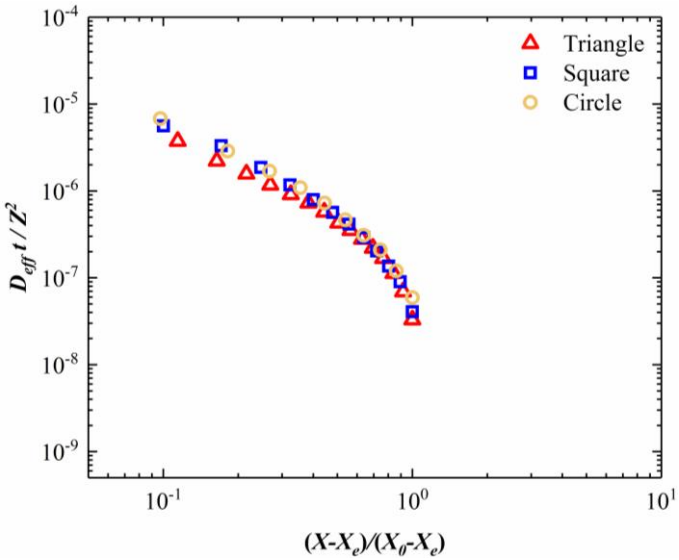

(a)

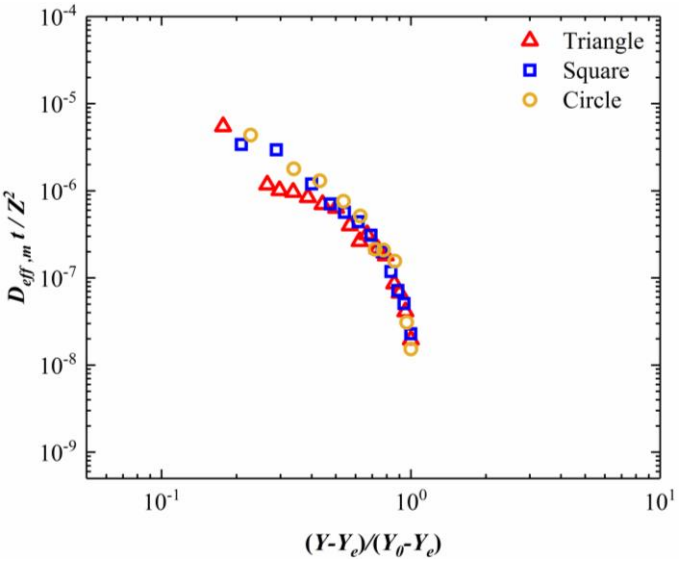

(b)

Figure B. 5 Non-dimensionalized form for liquid diffusion in Pickering foam for samples with initial thickness of $Z_0 = 5\ mm$ and initial diameter of $D_0 = 52\ mm$ as well as three shapes and substrates with $\theta \approx 160°$,. **(a)** Fourier number of diffusion vs. modified fractional average moisture content and **(b)** Modified Fourier number of diffusion vs. modified fractional average moisture content. The surface area of all sample are equal. The initial dimension of samples are: circle with diameter of $D_0 = 34\ mm$, square with length of $L_0 = 30.13\ mm$, and triangle with base of $B_0 = 45.79\ mm$ and height of $H_0 = 39.66\ mm$.

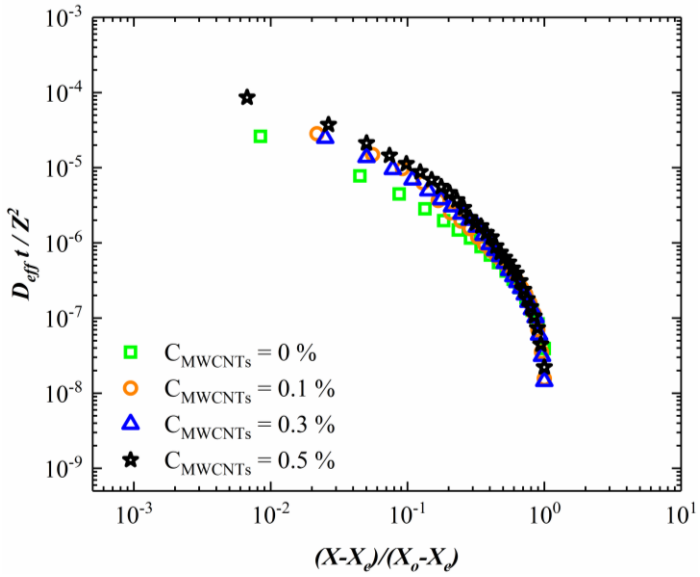

N nn(a)

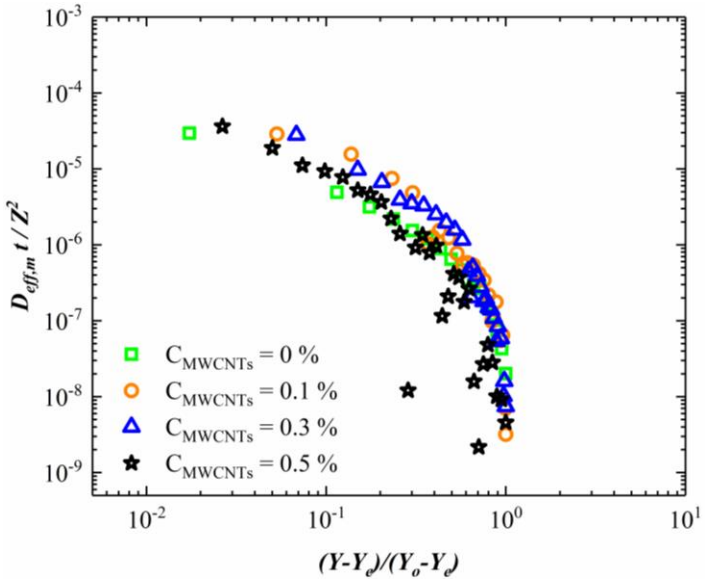

(b)

Figure B. 6 Non-dimensionalized form for liquid diffusion in Pickering foam for samples with initial thickness of $Z_0 = 5\ mm$ and initial diameter of $D_0 = 52\ mm$ as well as MWCNTs concentration of $C_{MWCNTs} = 0 - 0.5\ \%\ v/v$ and substrates with $\theta \approx 160°$,. **(a)** Fourier number of diffusion vs. fractional average moisture content and **(b)** Modified Fourier number of diffusion vs. modified fractional average moisture content.

Appendix C

Crack Formation

1. Initial Sample Thickness

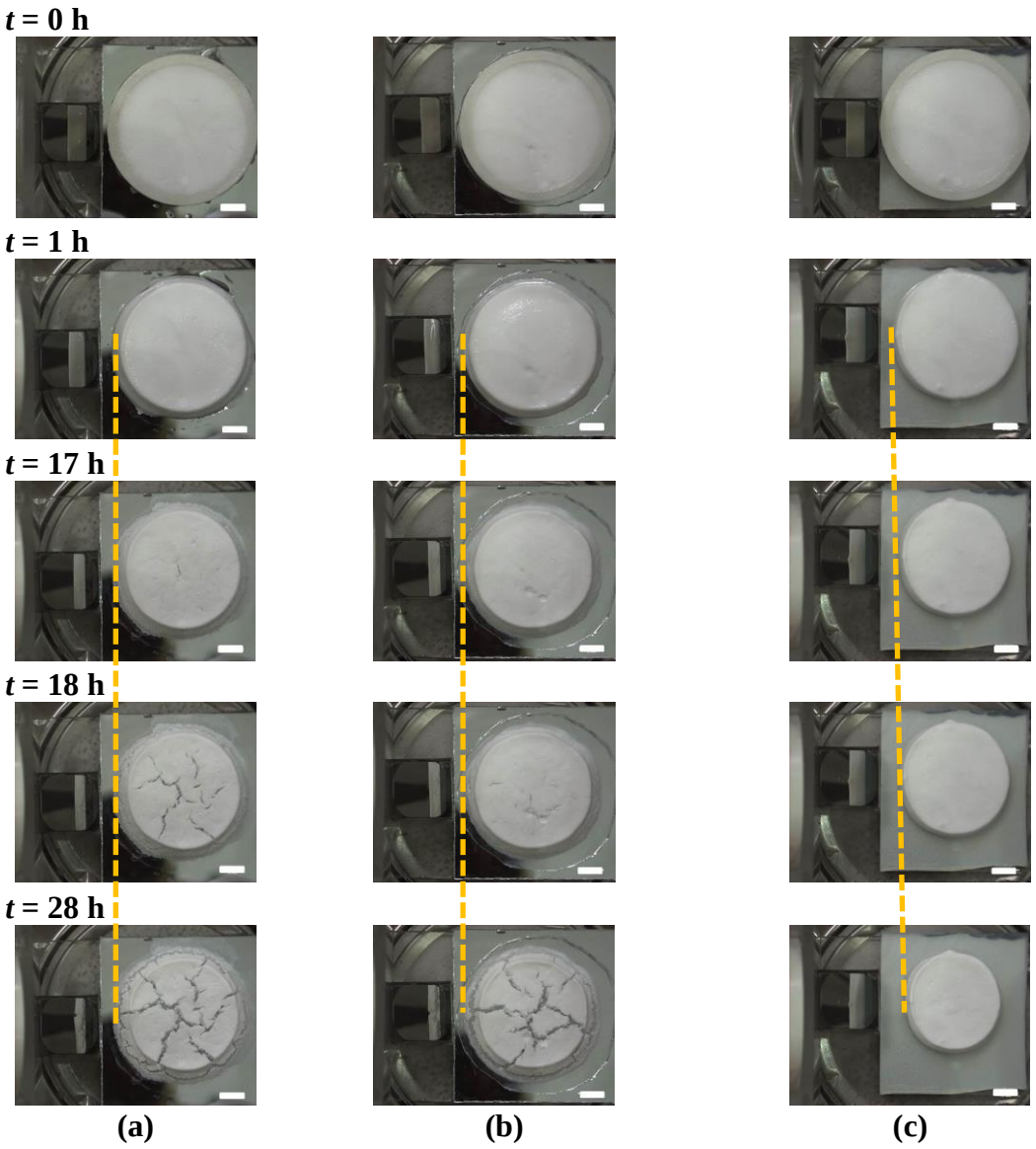

Figure C. 1 The effect of substrate wettability on the crack formation behavior of samples with initial thickness of $Z_0 = 7.5\ mm$ and substrate of: **(a)** $\theta \approx 30°$, **(b)** $\theta \approx 95°$, and **(c)** $\theta \approx 160°$. Each picture contains a portion of the side-view (left) and top-view (right) of the sample. Scale bar is 10 mm.

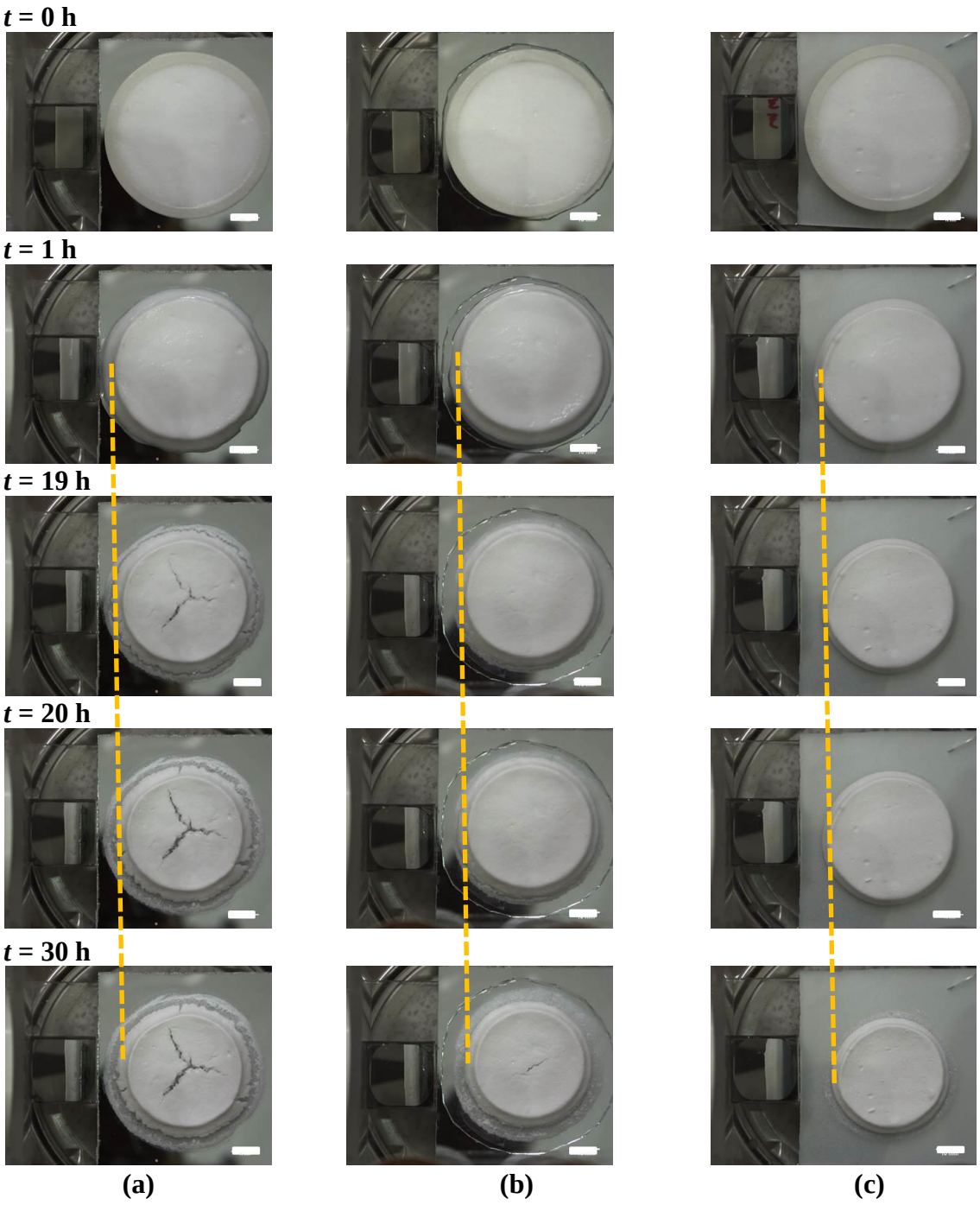

Figure C. 2 The effect of substrate wettability on the crack formation behavior of samples with initial thickness of $Z_0 = 10\ mm$ and initial diameter of $D_0 = 52\ mm$ as well as substrate of: **(a)** $\theta \approx 30°$, **(b)** $\theta \approx 95°$, and **(c)** $\theta \approx 160°$. Each picture contains a portion of the side-view (left) and top-view (right) of the sample. Scale bar is 10 mm.

t = 0 h

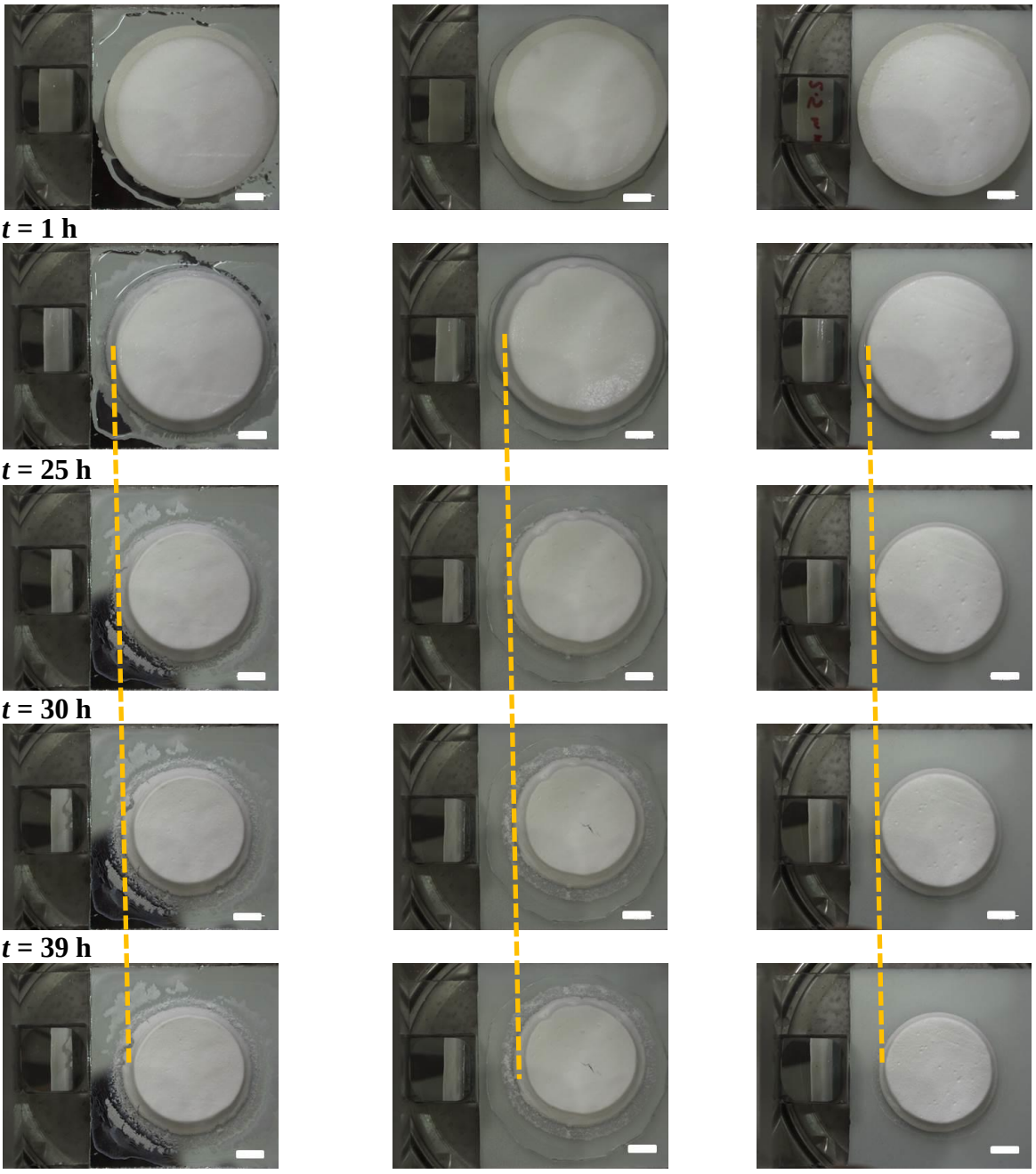

Figure C. 3 The effect of substrate wettability on the crack formation behavior of samples with initial thickness of $Z_0 = 12.5\ mm$ and initial diameter of $D_0 = 52\ mm$ as well as substrate of: **(a)** $\theta \approx 30°$, **(b)** $\theta \approx 95°$, and **(c)** $\theta \approx 160°$. Each picture contains a portion of the side-view (left) and top-view (right) of the sample. Scale bar is 10 mm.

2. Substrate Temperature

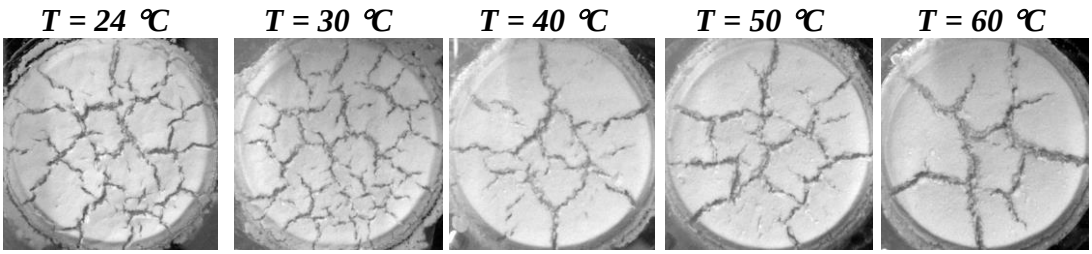

(a)

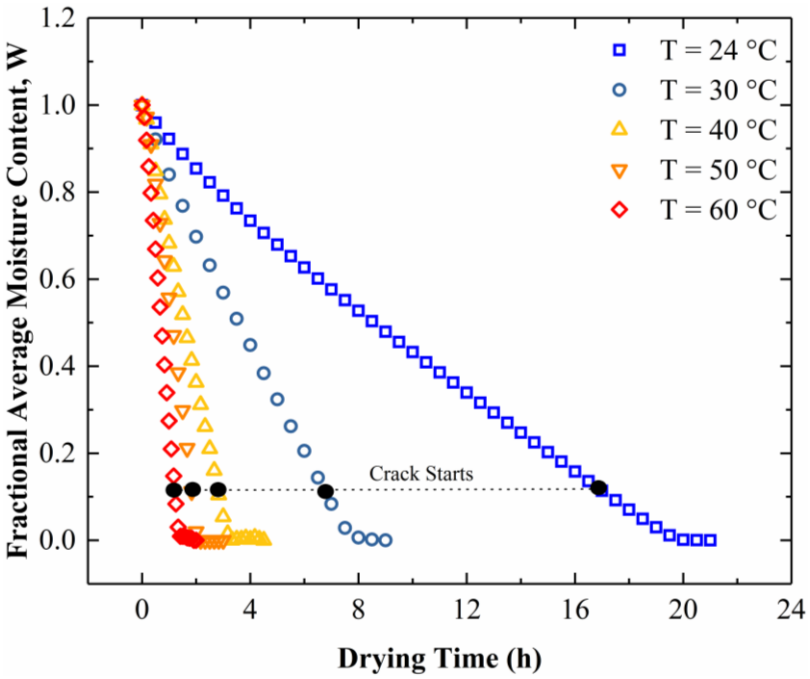

(b)

Figure C. 4 (a) Final crack patterns in samples of initial thickness of $Z_0 = 5\ mm$ and initial diameter of $D_0 = 52\ mm$ as well as substrate with $\theta \approx 30°$ and temperature of $T = 24 - 60$ ℃ and. **(b)** crack begins at same fractional moisture content value with different temperature of substrate.

3. Sample Shape

Square ***Triangle*** ***Circle***

(a)

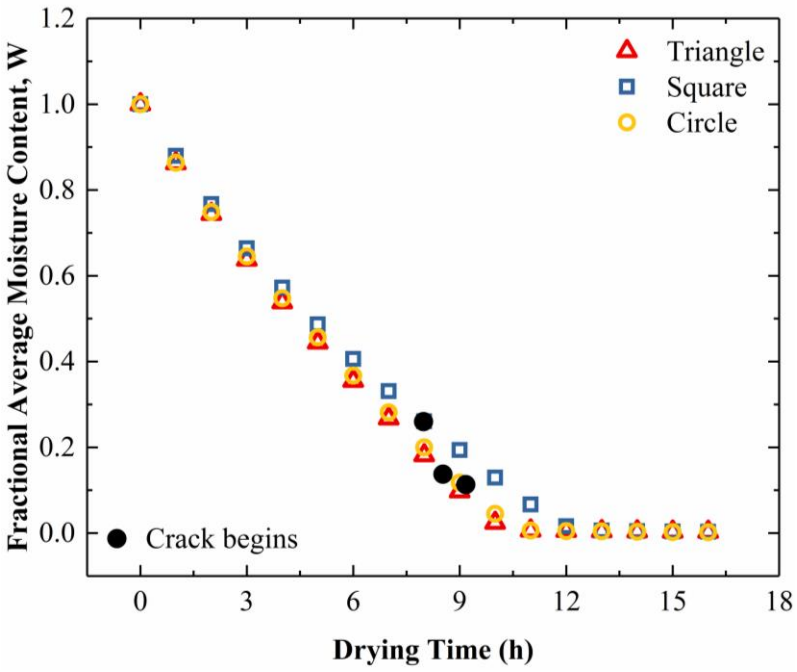

(b)

Figure C. 5 (a) Final crack patterns in samples with initial thickness of $Z = 5\ mm$ and different shapes and substrate with $\theta \approx 30°$ and **(b)** crack begins at different fractional average moisture content value for samples with different shapes. The surface area of all samples is equal. The initial dimension of samples are: circle with diameter of $D_0 = 34\ mm$, square with length of $L_0 = 30.13\ mm$, and triangle with base of $B_0 = 45.79\ mm$ and height of $H_0 = 39.66\ mm$.

4. Composite PVDF/MWCNTs Foam

C_{MWCNTs} = 0 % v/v C_{MWCNTs} = 0.1 % v/v C_{MWCNTs} = 0.3 % v/v C_{MWCNTs} = 0.5 % v/v

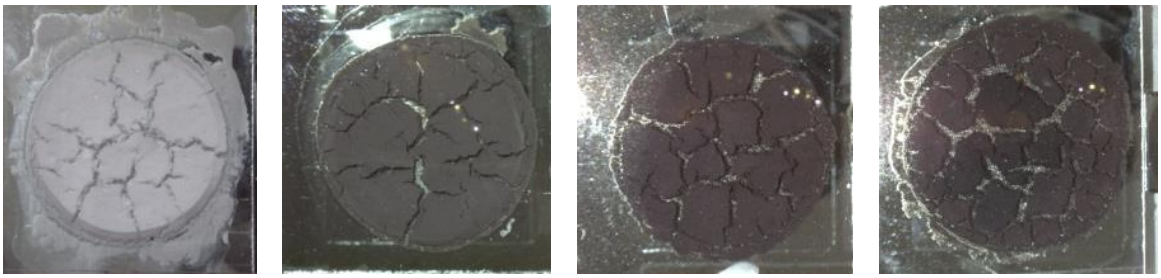

(a)

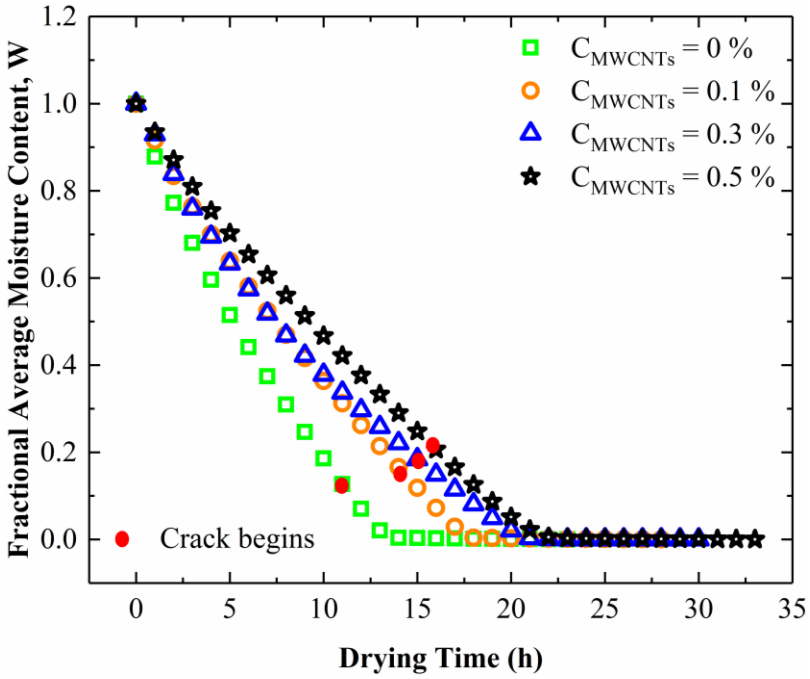

(b)

Figure C. 6 (a) Final crack patterns in samples with initial thickness of $Z_0 = 5\ mm$ and initial diameter of $D_0 = 52\ mm$ as well as different concentration of MWCNTs of $C_{MWCNTs} = 0.0 - 0.5\ \%\ v/v$ and substrates with $\theta \approx 30°$ and **(b)** crack begins at different fractional average moisture content value in samples with initial thickness of $Z_0 = 5\ mm$ and initial diameter of $D_0 = 52\ mm$ as well as different concentration of MWCNTs of $C_{MWCNTs} = 0.0 - 0.5\ \%\ v/v$ and substrates with $\theta \approx 30°$.

***t* = 0 h**

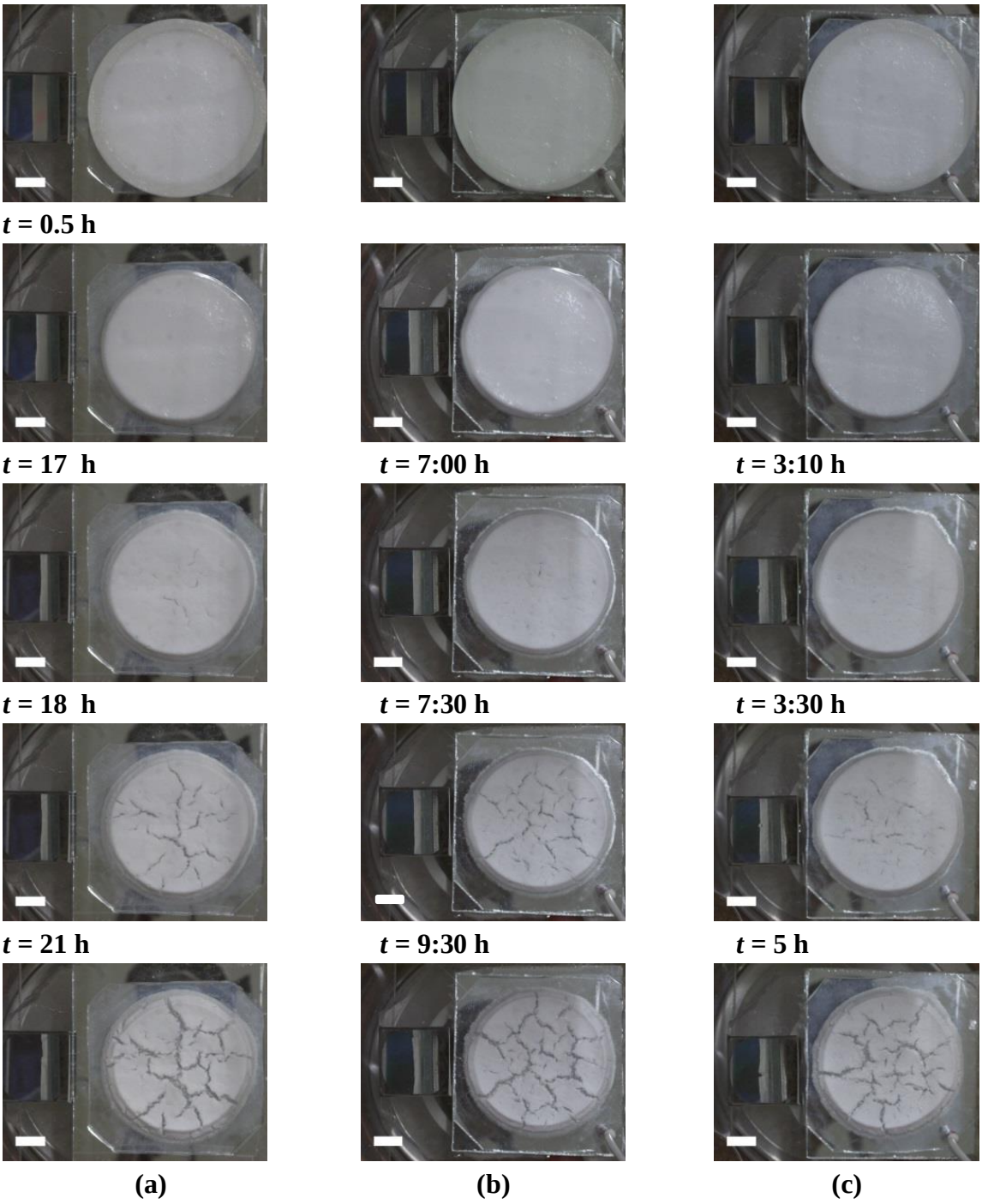

Figure C. 7 The effect of substrate temperature on the crack formation behavior of samples with initial thickness of $Z_0 = 5\ mm$ and initial diameter of $D_0 = 52\ mm$ as well as substrate with $\theta \approx 95°$ and temperature of: **(a)** $T = 24\ ℃$, **(b)** $T = 30\ ℃$, and **(c)** $T = 40\ ℃$. Each picture contains a portion of the side-view (left) and top-view (right) of the sample. Scale bar is 10 mm.

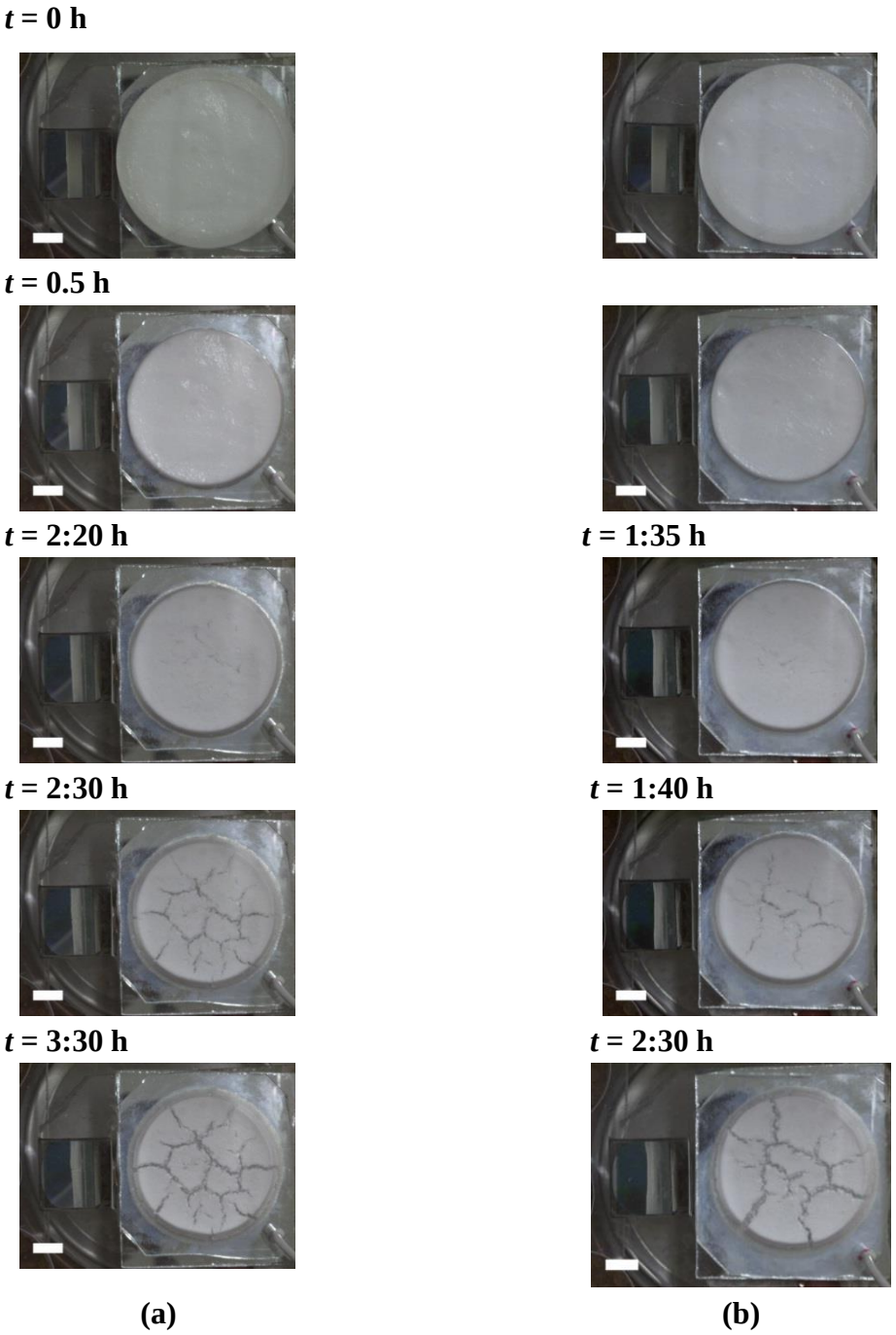

Figure C. 8 The effect of substrate temperature on the crack formation behavior of sample with initial thickness of $Z_0 = 5\ mm$ and initial diameter of $D_0 = 52\ mm$ as well as substrate with $\theta \approx 95°$ and temperature of: **(a)** $T = 50\ ℃$ and **(b)** $T = 60\ ℃$. Each picture contains a portion of the side-view (left) and top-view (right) of the sample. Scale bar is 10 mm.

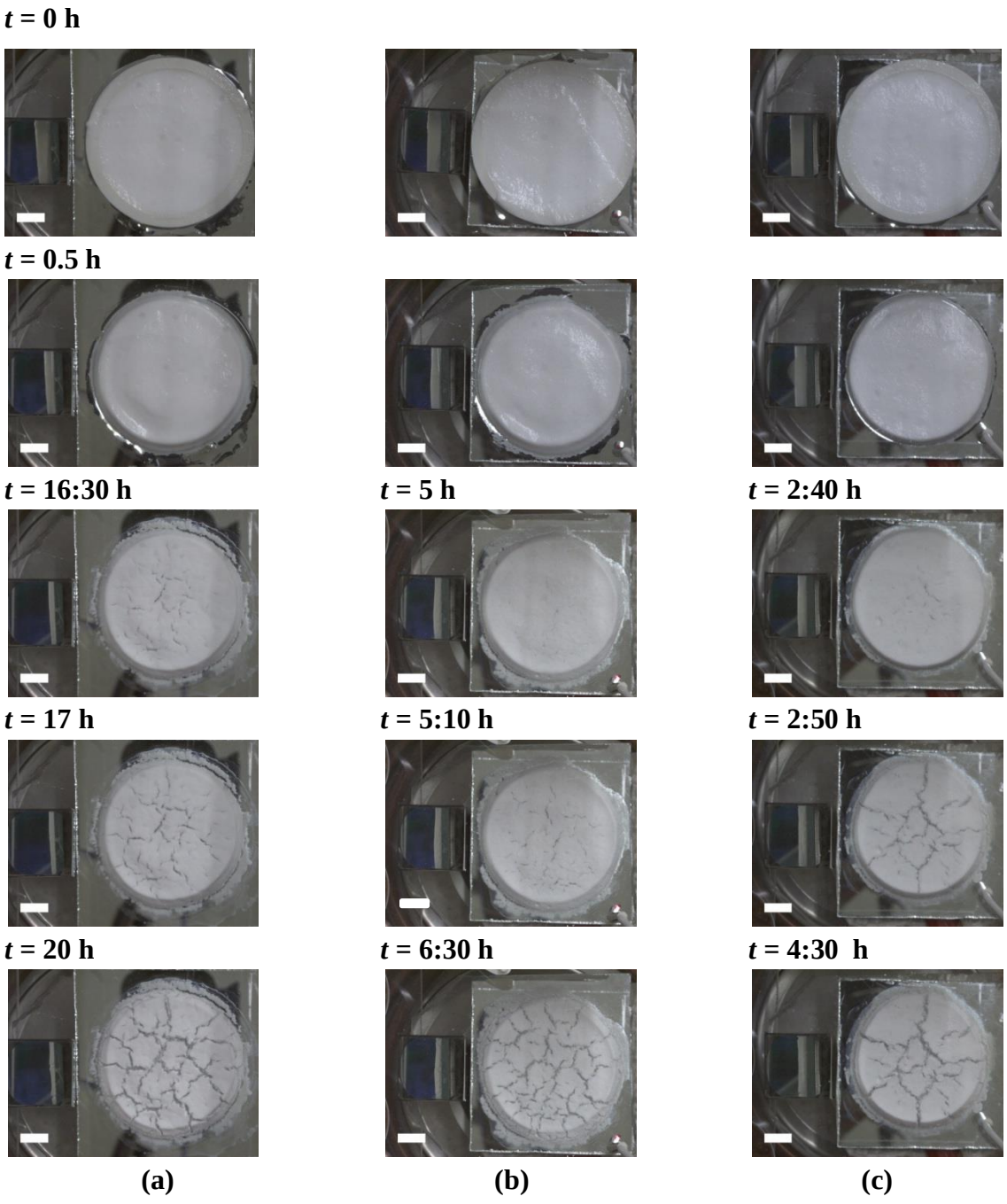

Figure C. 9 The effect of substrate temperature on the crack formation behavior of sample with initial thickness of $Z_0 = 5\ mm$ and initial diameter of $D_0 = 52\ mm$ as well as substrate with $\theta \approx 30°$ and temperature of: **(a)** $T = 24\ ℃$, **(b)** $T = 30\ ℃$, and **(c)** $T = 40\ ℃$. Each picture contains a portion of the side-view (left) and top-view (right) of the sample. Scale bar is 10 mm.

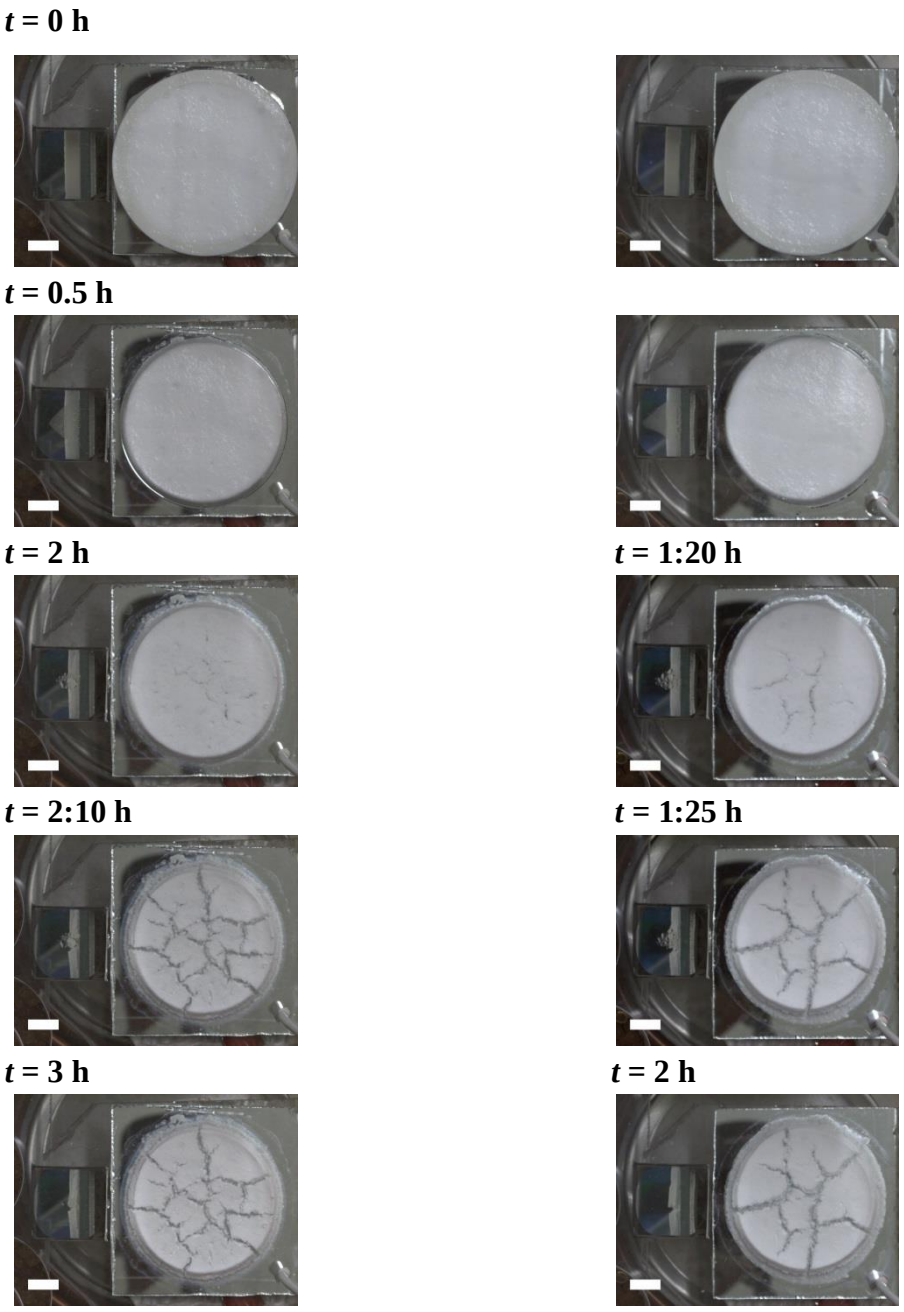

Figure C. 10 The effect of substrate wettability on the crack formation behavior of sample with initial thickness of $Z_0 = 5\ mm$ and initial diameter of $D_0 = 52\ mm$ as well as substrate with $\theta \approx 30°$ and temperature of: **(a)** $T = 50\ ℃$ and **(b)** $T = 60\ ℃$. Each picture contains a portion of the side-view (left) and top-view (right) of the sample. Scale bar is 10 mm.

***t* = 0 h**

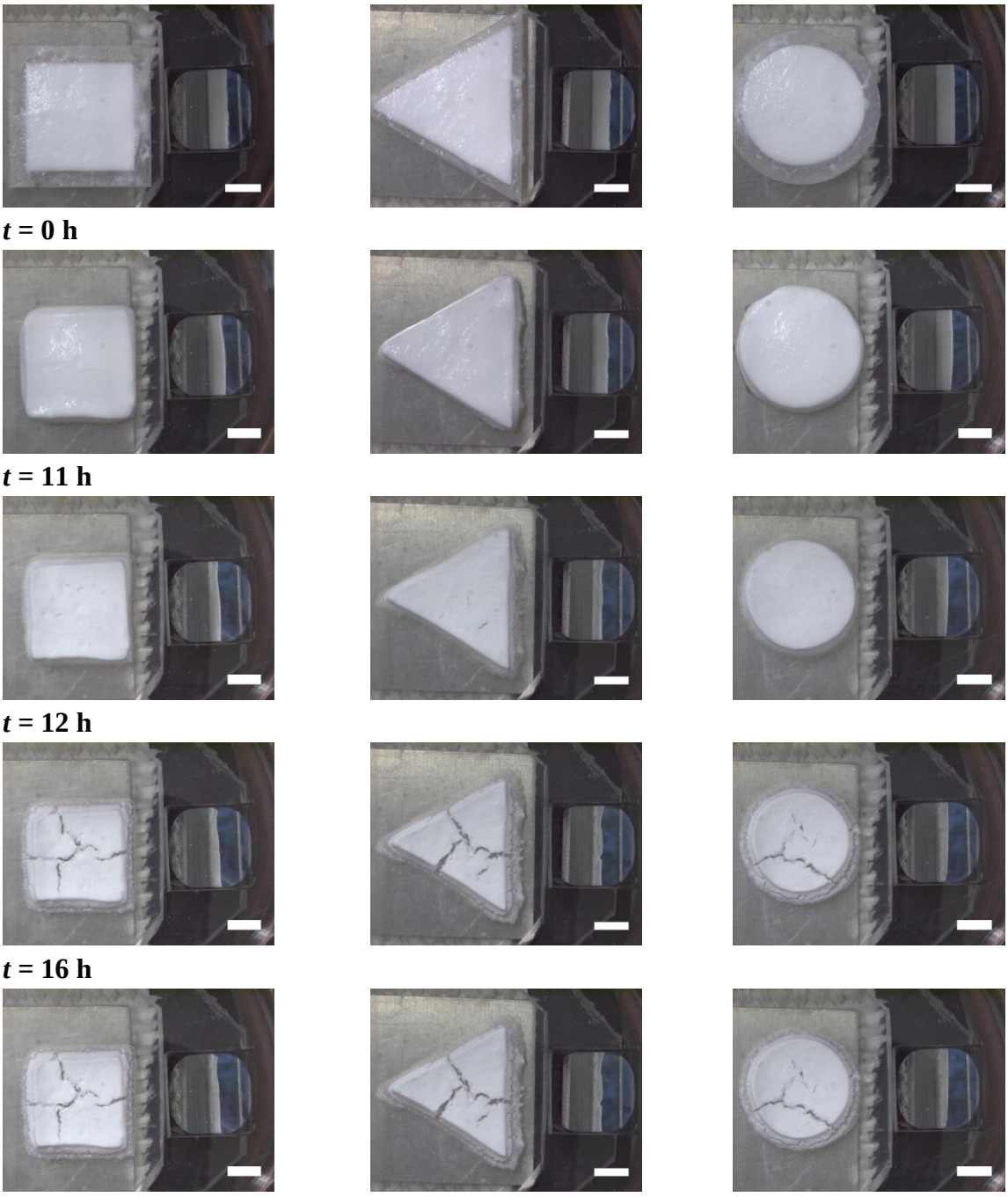

Figure C. 11 The effect of sample shape on the crack formation behavior of samples with initial thickness of $Z_0 = 5\ mm$ as well as substrate with $\theta \approx 95$: **(a)** square, **(b)** triangle, and **(c)** circle. Each picture contains a portion of the side-view (right) and top-view (left) of the sample. The surface area of all samples is equal. The initial dimension of samples are: circle with diameter of $D_0 = 34\ mm$, square with length of $L_0 = 30.13\ mm$, and triangle with base of $B_0 = 45.79\ mm$ and height of $H_0 = 39.66\ mm$. Scale bar is 10 mm.

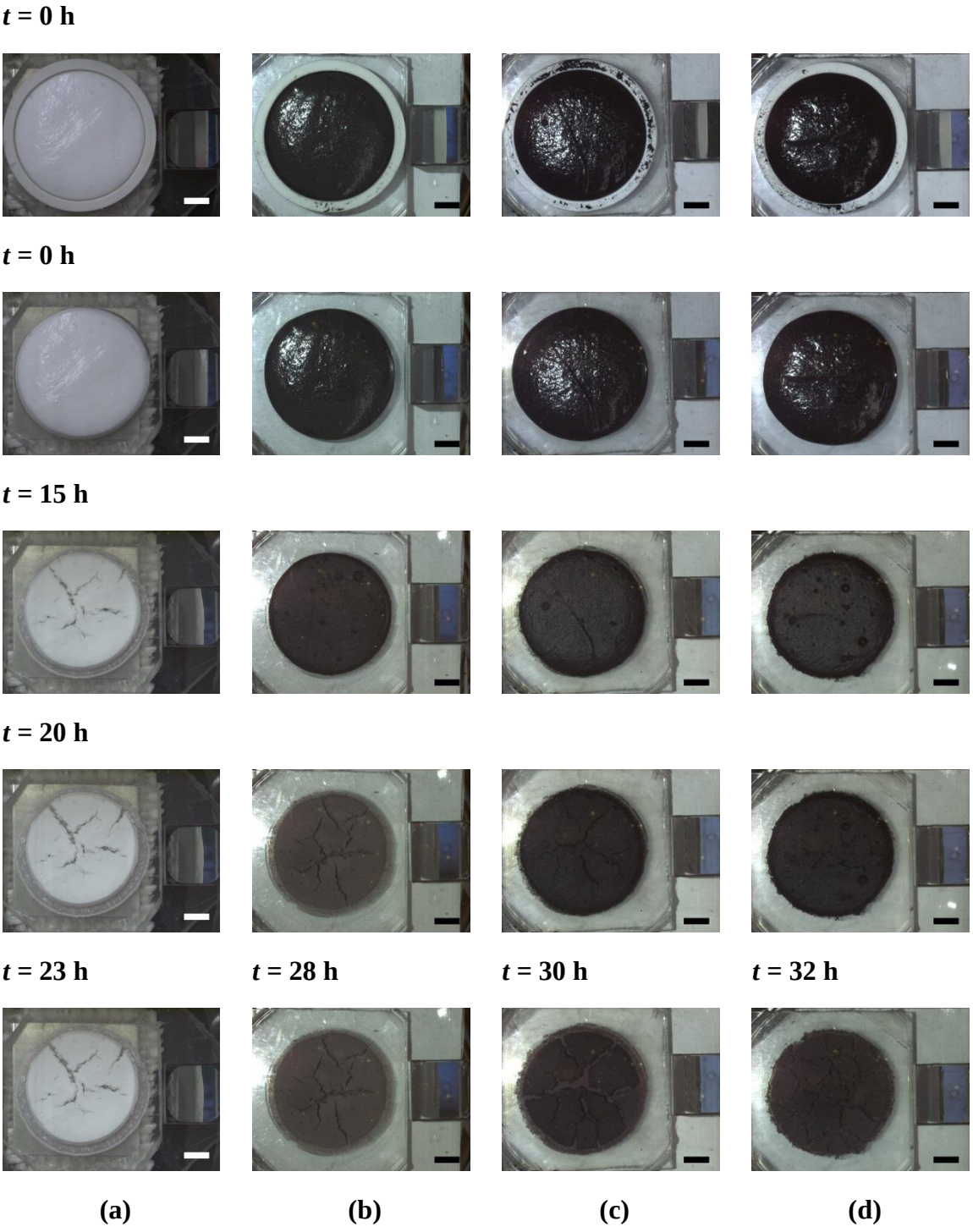

Figure C. 12 The effect of MWCNTs concentration on the crack formation behavior of samples with initial thickness of $Z_0 = 5\ mm$ and initial diameter of $D_0 = 52\ mm$ as well as substrate with $\theta \approx 95°$ at: **(a)** $C_{MWCNTs} = 0\ \%\ v/v$, **(b)** $C_{MWCNTs} = 0.1\ \%\ v/v$, **(c)** $C_{MWCNTs} = 0.3\ \%\ v/v$, and **(d)** $C_{MWCNTs} = 0.5\ \%\ v/v$. Each picture contains a portion of the side-view (right) and top-view (left) of the sample. Scale bar is 10 mm.

References

1. Binks, B.P., *Particles as surfactants—similarities and differences.* Current opinion in colloid & interface science, 2002. **7**(1): p. 21-41.

2. Kim, I., A.J. Worthen, K.P. Johnston, D.A. DiCarlo, and C. Huh, *Size-dependent properties of silica nanoparticles for Pickering stabilization of emulsions and foams.* Journal of Nanoparticle Research, 2016. **18**(4): p. 82.

3. Nakayama, S., S. Hamasaki, K. Ueno, M. Mochizuki, S. Yusa, Y. Nakamura, and S. Fujii, *Foams stabilized with solid particles carrying stimuli-responsive polymer hairs.* Soft matter, 2016. **12**(21): p. 4794-4804.

4. Binks, B.P., K. Muijlwijk, H. Koman, and A.T. Poortinga, *Food-grade Pickering stabilisation of foams by in situ hydrophobisation of calcium carbonate particles.* Food Hydrocolloids, 2017. **63**: p. 585-592.

5. Gonzenbach, U.T., A.R. Studart, E. Tervoort, and L.J. Gauckler, *Stabilization of foams with inorganic colloidal particles.* Langmuir, 2006. **22**(26): p. 10983-10988.

6. Lesov, I., S. Tcholakova, and N. Denkov, *Factors controlling the formation and stability of foams used as precursors of porous materials.* Journal of Colloid and Interface Science, 2014. **426**: p. 9-21.

7. Bournival, G., S. Ata, and E.J. Wanless, *The roles of particles in multiphase processes: Particles on bubble surfaces.* Advances in colloid and interface science, 2015. **225**: p. 114-133.

8. Chevalier, Y. and M.-A. Bolzinger, *Emulsions stabilized with solid nanoparticles: Pickering emulsions.* Colloids and Surfaces A: Physicochemical and Engineering Aspects, 2013. **439**: p. 23-34.

9. Joanna C. H. Wong, E.T., Stephan Busato, Urs T. Gonzenbach, Andre R. Studart, Paolo Ermanni and Ludwig J. Gauckler, *Macroporous polymers from particle-stabilized foams.* Journal of Materials Chemistry, 2009. **19**: p. 5129-5133.

10. Wong, J.C., E. Tervoort, S. Busato, U.T. Gonzenbach, A.R. Studart, P. Ermanni, and L.J. Gauckler, *Designing macroporous polymers from particle-stabilized foams.* Journal of Materials Chemistry, 2010. **20**(27): p. 5628-5640.

11. Callen, H.B., *Thermodynamics and An Introduction to Thermostatics*, ed. 2nd. 2014: Wiley.

12. Binks, B.P., *Colloidal particles at liquid interfaces.* Physical Chemistry Chemical Physics, 2007. **9**(48): p. 6298-6299.

13. Wang, J. and A. Nguyen, *Foam drainage in the presence of solid particles.* Soft matter, 2016. **12**(12): p. 3004-3012.

14. Studart, A.R., U.T. Gonzenbach, I. Akartuna, E. Tervoort, and L.J. Gauckler, *Materials from foams and emulsions stabilized by colloidal particles.* Journal of Materials Chemistry, 2007. **17**(31): p. 3283-3289.

15. McHale, G. and M. Newton, *Liquid marbles: topical context within soft matter and recent progress.* Soft Matter, 2015. **11**(13): p. 2530-2546.

16. K., L., B. A., S.D. Simeon, and P.N. V., *Colloidal and nanocellulose-stabilized emulsions.* In HANDBOOK OF GREEN MATERIALS: 3 Self-and direct-assembling of bionanomaterials, 2014: p. 185-196.

17. Hunter, T.N., R.J. Pugh, G.V. Franks, and G.J. Jameson, *The role of particles in stabilising foams and emulsions.* Advances in Colloid and Interface Science, 2008. **137**(2): p. 57-81.

18. Gonzenbach, U.T., A.R. Studart, T. E., and G.J. L., *Ultrastable Particle-Stabilized Foams* Angew, Chem. Int. Ed., 2006. **45**: p. 3526-3530.

19. Gonzenbach, U.T., A.R. Studart, E. Tervoort, and L.J. Gauckler, *Tailoring the microstructure of particle-stabilized wet foams.* Langmuir, 2007. **23**(3): p. 1025-1032.

20. Zabiegaj, D., E. Santini, M. Ferrari, L. Liggieri, and F. Ravera, *Carbon based porous materials from particle stabilized wet foams.* Colloids and Surfaces A: Physicochemical and Engineering Aspects, 2015. **473**: p. 24-31.

21. D., F., S.E. G., M.-L. M., and G.S. G., *Crack-Free Drying of Ceramic Foams by the Use of Viscous Cosolvents.* Am. Soc., 2010. **93**: p. 3632-3636.

22. Lesov, I., S. Tcholakova, and N. Denkov, *Drying of particle-loaded foams for production of porous materials: mechanism and theoretical modeling.* Rsc Advances, 2014. **4**(2): p. 811-823.

23. Wong, J.C., E. Tervoort, S. Busato, U.T. Gonzenbach, A.R. Studart, P. Ermanni, and L.J. Gauckler, *Macroporous polymers from particle-stabilized foams.* Journal of Materials Chemistry, 2009. **19**(29): p. 5129-5133.

24. Dhall, A. and A.K. Datta, *Transport in deformable food materials: A poromechanics approach.* Chemical Engineering Science, 2011. **66**(24): p. 6482-6497.

25. Onwude, D.I., N. Hashim, R.B. Janius, N. Nawi, and K. Abdan, *Modelling Effective Moisture Diffusivity of Pumpkin (Cucurbita moschata) Slices under Convective Hot Air Drying Condition.* International Journal of Food Engineering, 2016. **12**(5): p. 481-489.

26. Torki-Harchegani, M., D. Ghanbarian, A.G. Pirbalouti, and M. Sadeghi, *Dehydration behaviour, mathematical modelling, energy efficiency and essential oil yield of peppermint leaves undergoing microwave and hot air treatments.* Renewable & Sustainable Energy Reviews, 2016. **58**: p. 407-418.

27. Hathan, B.S., *Studies on Mass Transfer and Diffusion Coefficients in Elephant Foot Yam (Amorphophallus spp.) during Osmotic Dehydration in Sodium Chloride Solution.* Journal of Food Processing and Preservation, 2015.

28. Cao, Z.z., L.y. Zhou, J.f. Bi, J.y. Yi, Q.q. Chen, X.y. Wu, J.k. Zheng, and S.r. Li, *Effect of different drying technologies on drying characteristics and quality of red pepper (Capsicum frutescens L.): a comparative study.* Journal of the Science of Food and Agriculture, 2016.

29. Gulati, T. and A.K. Datta, *Mechanistic understanding of case-hardening and texture development during drying of food materials.* Journal of Food Engineering, 2015. **166**: p. 119-138.

30. Batista, L.M., C.A. da Rosa, and L.A. Pinto, *Diffusive model with variable effective diffusivity considering shrinkage in thin layer drying of chitosan.* Journal of Food Engineering, 2007. **81**(1): p. 127-132.

31. Karim, M.A. and M. Hawlader, *Mathematical modelling and experimental investigation of tropical fruits drying.* International Journal of Heat and Mass Transfer, 2005. **48**(23): p. 4914-4925.

32. Mohan, V.C. and P. Talukdar, *Three dimensional numerical modeling of simultaneous heat and moisture transfer in a moist object subjected to convective drying.* International Journal of Heat and Mass Transfer, 2010. **53**(21): p. 4638-4650.

33. Katekawa, M. and M. Silva, *A review of drying models including shrinkage effects.* Drying technology, 2006. **24**(1): p. 5-20.

34. Crank, J., *The Mathematics of Diffusion*. 2nd ed. 1975, Oxford: Oxford University Press.

35. Beigi, M., *Hot air drying of apple slices: dehydration characteristics and quality assessment.* Heat and Mass Transfer, 2016. **52**(8): p. 1435-1442.

36. Babalis, S.J. and V.G. Belessiotis, *Influence of the drying conditions on the drying constants and moisture diffusivity during the thin-layer drying of figs.* Journal of Food Engineering, 2004. **65**(3): p. 449-458.

37. Batista, L.M., C.A. da Rosa, and L.A.A. Pinto, *Diffusive model with variable effective diffusivity considering shrinkage in thin layer drying of chitosan.* Journal of Food Engineering, 2007. **81**(1): p. 127-132.

38. Perry R, G.D., *Perry's chemical engineers' handbook*. 6th edn. ed. 1984, New York: McGraw-Hill International.

39. Saravacos, G. and G. Raouzeos, *Diffusivity of moisture in air drying of starch gels.* Engineering and food, 1984. **1**: p. 499-507.

40. Aral, S. and A.V. Bese, *Convective drying of hawthorn fruit (Crataegus spp.): Effect of experimental parameters on drying kinetics, color, shrinkage, and rehydration capacity.* Food Chemistry, 2016. **210**: p. 577-584.

41. Sharma, G. and S. Prasad, *Effective moisture diffusivity of garlic cloves undergoing microwave-convective drying.* Journal of Food Engineering, 2004. **65**(4): p. 609-617.

42. Schossler, K., H. Jager, and D. Knorr, *Effect of continuous and intermittent ultrasound on drying time and effective diffusivity during convective drying of apple and red bell pepper.* Journal of Food Engineering, 2012. **108**(1): p. 103-110.

43. Hanson, T., W. Cramer, W. Abraham, and E. Lancaster. *Rates of water-vapor absorption in granular corn starch*. in *Chemical Engineering Progress Symposium Series*. 1971.

44. Arevalo-Pinedo, A. and F.E.X. Murr, *Kinetics of vacuum drying of pumpkin (Cucurbita maxima): Modeling with shrinkage.* Journal of Food Engineering, 2006. **76**(4): p. 562-567.

45. Park, K.J., *Diffusional model with and without shrinkage during salted fish muscle drying.* Drying Technology, 1998. **16**(3-5): p. 889-905.

46. Sahin, U. and H.K. Ouml;zturk, *Effects of pulsed vacuum osmotic dehydration (PVOD) on drying kinetics of figs (Ficus carica L).* Innovative Food Science & Emerging Technologies, 2016. **36**: p. 104-111.

47. Ketelaars, A.A.J., *Drying Deformable Media Kinetics, Shrinkage and Stresses.* Drying Technology, 1994. **12**(4): p. 983-987.

48. Osman, A., L. Goehring, A. Patti, H. Stitt, and N. Shokri, *Fundamental investigation of the drying of solid suspensions.* Industrial & Engineering Chemistry Research, 2017. **56**(37): p. 10506-10513.

49. Fuks, D., G.E. Shter, M. Mann–Lahav, and G.S. Grader, *Crack-free drying of ceramic foams by the use of viscous cosolvents.* Journal of the American Ceramic Society, 2010. **93**(11): p. 3632-3636.

50. Gonzenbach, U.T., A.R. Studart, D. Steinlin, E. Tervoort, and L.J. Gauckler, *Processing of particle-stabilized wet foams into porous ceramics.* Journal of the American Ceramic Society, 2007. **90**(11): p. 3407-3414.

51. Tirumkudulu, M.S. and W.B. Russel, *Cracking in drying latex films.* Langmuir, 2005. **21**(11): p. 4938-4948.

52. Singh, K.B. and M.S. Tirumkudulu, *Cracking in drying colloidal films.* Physical review letters, 2007. **98**(21): p. 218302.

53. Gan, S.-H. and C.-L. Law, *Conventional and Intermittent Food Drying Processes and the Effect on Food Quality*. Intermittent and Nonstationary Drying Technologies: Principles and Applications, 2017.

54. Khalloufi, S., C. Almeida-Rivera, and P. Bongers, *A theoretical model and its experimental validation to predict the porosity as a function of shrinkage and collapse phenomena during drying.* Food Research International, 2009. **42**(8): p. 1122-1130.

55. Govani, K.J. and J.K.S. , *Study of Cold Chain Status at Mamta Session of Each Urban Health Centres(UHCs) of Ahmedabad Municipal Corporation (AMC) Area.* International Journal of Health Sciences & Research, 2014. **4**(6): p. 15-19.

56. Oltean, L., A. Teischinger, and C. Hansmann, *Influence of temperature on cracking and mechanical properties of wood during wood drying–A review.* BioResources, 2007. **2**(4): p. 789-811.

57. Scherer, G.W., *Theory of drying.* Journal of the American Ceramic Society, 1990. **73**(1): p. 3-14.

58. Russel, W.B., *Mechanics of Drying Colloidal Dispersions: Fluid/Solid Transitions, Skinning, Crystallization, Cracking, and Peeling.* Aiche Journal, 2011. **57**(6): p. 1378-1385.

59. Hu, X., Z. Shi, C. Shi, Z. Wu, B. Tong, Z. Ou, and G. de Schutter, *Drying shrinkage and cracking resistance of concrete made with ternary cementitious components.* Construction and Building Materials, 2017. **149**: p. 406-415.

60. Rumpf, H., *The Strength of Granules and Agglomerates, chap, W. Knepper (),* . 1962.

61. Papadakis, S.E. and R.E. Bahu, *The sticky issues of drying.* Drying Technology, 1992. **10**(4): p. 817-837.

62. Quéré, D., A. Lafuma, and J. Bico, *Slippy and sticky microtextured solids.* Nanotechnology, 2003. **14**(10): p. 1109.

63. Ghosh, U.U., C. M., B.B. A., C. S., and D.G. S., *Effect of Surface Wettability on Crack Dynamics and Morphology of Colloidal Films.* Langmuir, 2015. **31**: p. 6001-6010.

64. Lazarus, V. and L. Pauchard, *From craquelures to spiral crack patterns: influence of layer thickness on the crack patterns induced by desiccation.* Soft Matter, 2011. **7**(6): p. 2552-2559.

65. Wallace, S. and L. Hench, *The processing and characterization of DCCA modified gel-derived silica.* MRS Online Proceedings Library Archive, 1984. **32**.

66. Cervin, N.T., L.a. Andersson, J.B.S. Ng, P. Olin, L. Bergström, and L. Wågberg, *Lightweight and strong cellulose materials made from aqueous foams stabilized by nanofibrillated cellulose.* Biomacromolecules, 2013. **14**(2): p. 503-511.

67. Huang, Y., J. Zhou, B. Su, L. Shi, J. Wang, S. Chen, L. Wang, J. Zi, Y. Song, and L. Jiang, *Colloidal photonic crystals with narrow stopbands assembled from low-adhesive superhydrophobic substrates.* Journal of the American Chemical Society, 2012. **134**(41): p. 17053-17058.

68. Zhou, J., J. Wang, Y. Huang, G. Liu, L. Wang, S. Chen, X. Li, D. Wang, Y. Song, and L. Jiang, *Large-area crack-free single-crystal photonic crystals via combined effects of polymerization-assisted assembly and flexible substrate.* NPG Asia Materials, 2012. **4**(8): p. e21.

69. Chiu, R.C., T. Garino, and M. Cima, *Drying of granular ceramic films: I, effect of processing variables on cracking behavior.* Journal of the American Ceramic Society, 1993. **76**(9): p. 2257-2264.

70. Chiu, R.C. and M.J. Cima, *Drying of granular ceramic films: II, drying stress and saturation uniformity.* Journal of the American Ceramic Society, 1993. **76**(11): p. 2769-2777.

71. Rezvantalab, H., N. Ghazi, M.J. Ambrusch, J. Infante, and S. Shojaei-Zadeh, *An Aqueous-Based Approach for Fabrication of PVDF/MWCNT Porous Composites.* Scientific Reports, 2017. **7**.

72. Khedkar, M.A., P.R. Nimbalkar, S.G. Gaikwad, P.V. Chavan, and S.B. Bankar, *Sustainable biobutanol production from pineapple waste by using Clostridium acetobutylicum B 527: Drying kinetics study.* Bioresource technology, 2017. **225**: p. 359-366.

73. Goehring, L., W.J. Clegg, and A.F. Routh, *Solidification and ordering during directional drying of a colloidal dispersion.* Langmuir, 2010. **26**(12): p. 9269-9275.

74. Peron, H., L. Laloui, L.-B. Hu, and T. Hueckel, *Formation of drying crack patterns in soils: a deterministic approach.* Acta Geotechnica, 2013. **8**(2): p. 215-221.

75. Madiouli, J., J. Sghaier, D. Lecomte, and H. Sammouda, *Determination of porosity change from shrinkage curves during drying of food material.* Food and bioproducts processing, 2012. **90**(1): p. 43-51.

76. Mayor, L. and A. Sereno, *Modelling shrinkage during convective drying of food materials: a review.* Journal of Food Engineering, 2004. **61**(3): p. 373-386.

77. Wong, J.C., S. Busato, E. Tervoort, U.T. Gonzenbach, A.R. Studart, L.J. Gauckler, and P. Ermanni, *PVDF Particle-stabilized Polymeric Foams as Piezoelectric Space-charge Electrets.* 2008.

78. Chen, D. and J.X. Zhang, *Microporous polyvinylidene fluoride film with dense surface enables efficient piezoelectric conversion.* Applied Physics Letters, 2015. **106**(19): p. 193901.

79. Dmitriev, I.Y., I. Kuryndin, V. Lavrentyev, and G. Elyashevich, *Structure and piezoelectric properties of microporous polyvinylidene fluoride films.* Physics of the Solid State, 2017. **59**(5): p. 1041-1046.

80. Begum, S., A. Kausar, H. Ullah, and M. Siddiq, *Potential of Polyvinylidene Fluoride/Carbon Nanotube Composite in Energy, Electronics, and Membrane Technology: An Overview.* Polymer-Plastics Technology and Engineering, 2016. **55**(18): p. 1949-1970.

81. Singh, H.H., S. Singh, and N. Khare, *Enhanced β-phase in PVDF polymer nanocomposite and its application for nanogenerator.* Polymers for Advanced Technologies, 2017.

82. Sharifi Olyaei, N., M.M. Mohebi, and R. Kaveh, *Directional properties of ordered 3-3 piezocomposites fabricated by sacrificial template.* Journal of the American Ceramic Society, 2017. **100**(4): p. 1432-1439.

83. Begum, S., A. Kausar, H. Ullah, and M. Siddiq, *Exploitation of carbon nanotubes in high performance polyvinylidene fluoride matrix composite: A review.* Polymer-Plastics Technology and Engineering, 2016. **55**(2): p. 199-222.

84. Kausar, A., *Mechanical, thermal, and electrical properties of epoxy matrix composites reinforced with polyamide-grafted-MWCNT/poly (azo-pyridine-benzophenone-imide)/polyaniline nanofibers.* International Journal of Polymeric Materials and Polymeric Biomaterials, 2014. **63**(16): p. 831-839.

85. Carrín, M.E. and G.H. Crapiste, *Convective drying of foods.* Advances in food dehydration. CRC Press, Boca Raton, 2008: p. 123-151.

86. Ramesh, M.N., W. Wolf, D. Tevini, and G. Jung, *Influence of processing parameters on the drying of spice paprika.* Journal of Food Engineering, 2001. **49**(1): p. 63-72.

87. Kim, S.S. and S.R. Bhowmik, *Effective Moisture Diffusivity of Plain Yogurt Undergoing Microwave Vacuum Drying.* Journal of Food Engineering, 1995. **24**(1): p. 137-148.

88. Marousis, S.N., V.T. Karathanos, and G.D. Saravacos, *Effect of Physical Structure of Starch Materials on Water Diffusivity.* Journal of Food Processing and Preservation, 1991. **15**(3): p. 183-195.

89. Karathanos, V., G. Villalobos, and G. Saravacos, *Comparison of two methods of estimation of the effective moisture diffusivity from drying data.* Journal of Food Science, 19 90. **55**(1): p. 218-223.

90. Fusco, A., J. Avanza, R. Aguerre, and J. Gabitto, *A diffusional model for drying with volume change.* Drying Technology, 1991. **9**(2): p. 397-417.

91. Cassie, A. and S. Baxter, *Wettability of porous surfaces.* Transactions of the Faraday society, 1944. **40**: p. 546-551.

92. Holmes, D.M., R. Vasant Kumar, and W.J. Clegg, *Cracking during lateral drying of alumina suspensions.* Journal of the American Ceramic Society, 2006. **89**(6): p. 1908-1913.

93. Strauch, S. and S. Herminghaus, *Wet granular matter: a truly complex fluid.* Soft Matter, 2012. **8**(32): p. 8271-8280.

94. Dufresne, E., D. Stark, N. Greenblatt, J. Cheng, J. Hutchinson, L. Mahadevan, and D. Weitz, *Dynamics of fracture in drying suspensions.* Langmuir, 2006. **22**(17): p. 7144-7147.

95. Smith, M. and J. Sharp, *Effects of substrate constraint on crack pattern formation in thin films of colloidal polystyrene particles.* Langmuir, 2011. **27**(13): p. 8009-8017.

96. Boulogne, F., F. Giorgiutti-Dauphiné, and L. Pauchard, *How to reduce the crack density in drying colloidal material?* Oil & Gas Science and Technology–Revue d'IFP Energies nouvelles, 2014. **69**(3): p. 397-404.